Journal of Medicinal Chemistry

pubs.acs.org/jmc Article

Glucosylpolyphenols as Inhibitors of Aβ-Induced Fyn Kinase Activation and Tau Phosphorylation: Synthesis, Membrane Permeability, and Exploratory Target Assessment within the Scope of Type 2 Diabetes and Alzheimer's Disease

Ana M. de Matos,[¶] M. Teresa Blázquez-Sánchez,[¶] Andreia Bento-Oliveira, Rodrigo F. M. de Almeida, Rafael Nunes, Pedro E. M. Lopes, Miguel Machuqueiro, Joana S. Cristóvão, Cláudio M. Gomes, Cleide S. Souza, Imane G. El Idrissi, Nicola A. Colabufo, Ana Diniz, Filipa Marcelo, M. Conceição Oliveira, Óscar López, José G. Fernandez-Bolaños, Philipp Dätwyler, Beat Ernst, Ke Ning, Claire Garwood, Beining Chen,* and Amélia P. Rauter*

Cite This: *J. Med. Chem.* 2020, 63, 11663−11690 Read Online

ACCESS | Metrics & More | Article Recommendations | Supporting Information

ABSTRACT: Despite the rapidly increasing number of patients suffering from type 2 diabetes, Alzheimer's disease, and diabetes-induced dementia, there are no disease-modifying therapies that are able to prevent or block disease progress. In this work, we investigate the potential of nature-inspired glucosylpolyphenols against relevant targets, including islet amyloid polypeptide, glucosidases, and cholinesterases. Moreover, with the premise of Fyn kinase as a paradigm-shifting target in Alzheimer's drug discovery, we explore glucosylpolyphenols as blockers of Aβ-induced Fyn kinase activation while looking into downstream effects leading to Tau hyperphosphorylation. Several compounds inhibit Aβ-induced Fyn kinase activation and decrease pTau levels at 10 μM concentration, particularly the per-*O*-methylated glucosylacetophloroglucinol and the 4-glucosylcatechol dibenzoate, the latter inhibiting also butyrylcholinesterase and β-glucosidase. Both compounds are nontoxic with ideal pharmacokinetic properties for further development. This work ultimately highlights the multitarget nature, fine structural tuning capacity, and valuable therapeutic significance of glucosylpolyphenols in the context of these metabolic and neurodegenerative disorders.

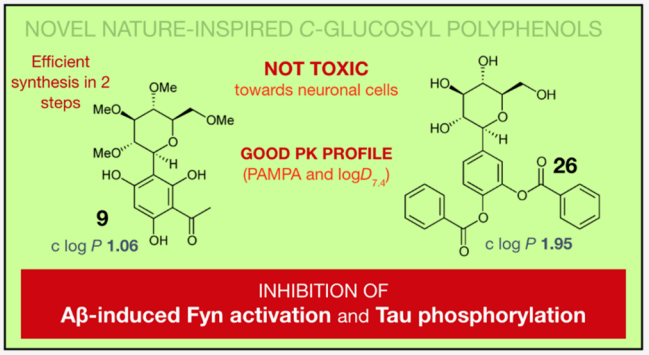

INTRODUCTION

More than 463 million adults are currently suffering from type 2 diabetes (T2D) worldwide,[1] and up to 73% of them are likely to be diagnosed with dementia, including Alzheimer's disease (AD). T2D, the non-insulin-dependent type of diabetes, primarily arises from the ingestion of high-fat diets and lack of physical exercise, which leads to hyperinsulinemia, dyslipidemia, insulin resistance, and ultimately, hyperglycemia. In turn, AD is characterized for the presence of extracellular deposits of amyloid beta (Aβ) in the senile plaques and for intracellular neurofibrillary tangles induced by deposits of hyperphosphorylated Tau protein, accompanied by synaptic dysfunction resulting in neuronal death.[2] A recent report indicates that the cellular prion protein (PrP^C) located in the neuronal cell surface works as a high-affinity binding partner of Aβ oligomers (Aβos), leading to the activation of Fyn kinase, which triggers a cell signaling pathway culminating in Tau hyperphosphorylation.[3] Indeed, Fyn activity was found to be increased in the AD brain by exposure of neurons to Aβos *via* PrP^C.[4,5] Moreover, genetic deletion of Fyn prevents Aβos-induced cell death in the hippocampus and Fyn inhibition restores synapse density and memory function in transgenic mice.[6,7] Interestingly, Fyn inhibition, deficiency, or genetic knockout was found to have increased glucose disposal due to increased insulin sensitivity and improved fatty acid oxidation, with decreased visceral adipose tissue inflammation.[8−10] Hence, the inhibition of Fyn activity is also a relevant approach in the treatment of diabetes-induced dementia (DID), the so-called "type 3 diabetes".

Received: May 17, 2020
Published: September 22, 2020

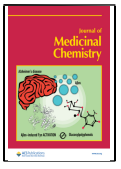

https://dx.doi.org/10.1021/acs.jmedchem.0c00841
J. Med. Chem. 2020, 63, 11663−11690

Other pathophysiological mechanisms are known to be present in both T2D and AD, namely, peripheral and brain insulin resistance and insulin-degrading enzyme (IDE) down-regulation, leading to increased brain Aβ levels.[2] Furthermore, cross-seeding events between the brain-penetrant islet amyloid polypeptide (IAPP) and Aβ have also been reported, being likely to exacerbate the cognitive decline observed in patients suffering from both conditions.[11,12] With the lack of therapeutic alternatives that are able to block disease progression in both cases, we were interested in finding new molecular entities able to tackle several molecular targets common to AD and DID with disease-modifying effects. For this purpose, we turned to nature for inspiration. Polyphenols have been widely reported in the literature for their vast therapeutic potential, with described antidiabetic, anti-inflammatory, and neuroprotective effects.[2,13−16] Polyphenol glucosides (*O*-glucosyl polyphenols) and glucosylpolyphenols[17] (*C*-glucosyl polyphenols, frequently named as polyphenol *C*-glucosides), however, have improved palatability, oral bioavailability due to increased solubility, and enhanced biological activity when compared to the corresponding aglycones, including improved amyloid-remodeling effects.[16,18−21] Importantly, *C*-glucosyl polyphenols are not liable to chemical and enzymatic hydrolysis, as sugar is linked to the polyphenol by a C−C bond, and have been described to show higher antidiabetic effects with improved target selectivity; for instance, the glucosyldihydrochalcone analogue of the glucoside phlorizin is selective toward SGLT-2 *vs* SGLT-1 transporters, while phlorizin is not.[22−24]

For all the above-mentioned reasons, we were interested in exploring the potential multitarget bioactivity of glucosylpolyphenols based on the structure of 8-β-D-glucosylgenistein (**1**, Figure 1), a natural glucosylisoflavone previously reported by our group as a new and potent antidiabetic compound with potential against Aβ(1−42)-induced neurotoxicity.[25] This compound was found to inhibit IAPP aggregation and to interact with Aβ(1−42) polypeptide through the same binding mode, involving the sugar moiety, H-6 of ring A, and the aromatic protons of ring B. Yet, we did not have information as to whether one or more phenol moieties were beneficial for activity or even if the molecular planarity of the aglycone was a crucial feature for the binding epitope and antiaggregating activity of this compound. Moreover, *C*-glucosyl polyphenols derived from acetophloroglucinol or hydroquinone have been reported in the literature for having antidiabetic effects.[26,27] On the basis of this information, we were interested in synthesizing simplified analogues of **1** with a different hydroxylation pattern in ring A, maintaining the sugar β-C linkage found in the original compound (Figure 1). To keep rings A and B linked by a three-bond spacer moiety for mimicking **1**, we planned on inserting benzoate moieties in glucosylhydroquinone (a) and glucosylcatechol derivatives (b) or ketone moieties in glucosylphloroglucinol derivatives (c). Moreover, due to the extremely polar nature of the lead compound, we were also interested in generating more lipophilic analogues of the natural scaffold with higher chances of crossing the blood−brain barrier (BBB), namely, by *O*-methyl protection of sugar hydroxy groups. The major goal was to explore the therapeutic potential and physicochemical properties of compound **1** while comparing them to those of the newly synthesized analogues and elucidating, whenever possible, structural requirements for bioactivity against multiple targets involved in T2D and AD, including IAPP, Fyn kinase activation, Tau hyperphosphorylation, and glucosidase and cholinesterase enzymes. Ultimately,

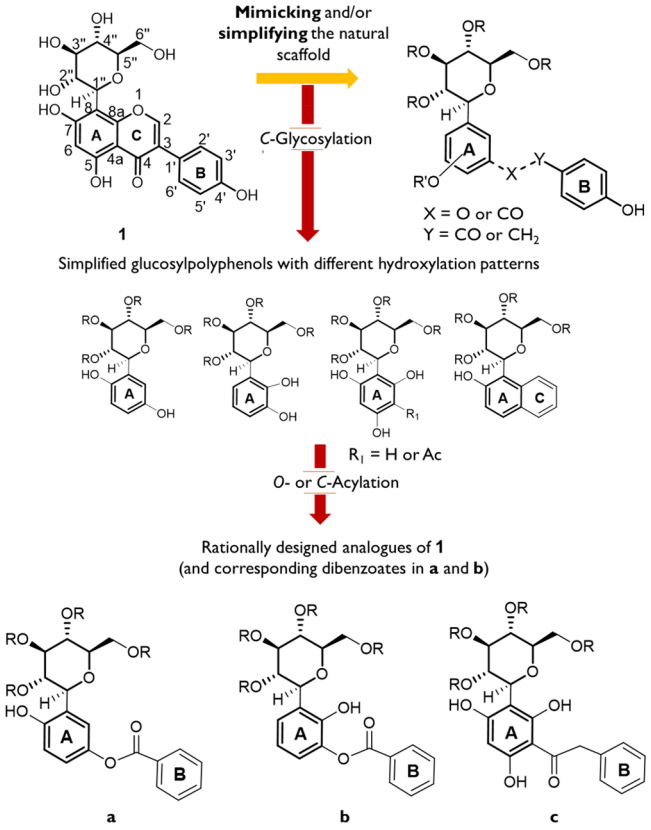

Figure 1. Rationale behind the synthesis of simplified analogues of 8-β-D-glucosylgenistein (**1**). R = H or Me; R′ = H or Bz.

we were interested in investigating the therapeutic potential of glucosylpolyphenols against T2D and AD while identifying new lead molecules for further pharmaceutical development in the context of these pathologies.

C-glycosylation is a key and particularly challenging synthetic step in our strategy. Several methods for *C*-glycosylation are currently known, including nucleophilic attack of aromatic Grignard reagents to glycosyl halides,[28] the use of lactones and lithiated compounds,[29] catalysis by transition metals or samarium diiodide,[30,31] intermolecular free radical reactions,[32] and intramolecular aglycone delivery through the Fries-type rearrangement.[33] The latter approach covers the strategy first developed by Suzuki *et al.*[34] and Kometani *et al.*,[35] and consists of a Lewis acid-catalyzed rearrangement of a phenol glycoside to a *C*-glucosyl derivative, known as the Fries-type rearrangement. It has been exploited by various authors up to the present days and successfully applied to the synthesis of flavonoid *C*-glycosides and of other complex natural products.[25,36−38] In this sense, another goal for this work was to explore the feasibility of *C*-glucosylation by using different glucosyl donors and acceptors while studying their impact in the efficacy of the Fries-type rearrangement.

RESULTS

Chemistry. *C-Glucosylation.* For the generation of glucosylpolyphenols, we employed either a permethylated glucopyranoside[39] (**3**, Scheme 1) or per-benzylated glucosyl donors[25,40] (**4**−**6**). Polyphenols containing their hydroxy groups in *meta*, *para*, and *ortho* orientations were used as acceptors in a series of *C*-glucosylation reactions, and the differences in their reactivity were attentively explored. 2-

https://dx.doi.org/10.1021/acs.jmedchem.0c00841
J. Med. Chem. 2020, 63, 11663−11690

Scheme 1. Preparation of Glucosyl Donors and Protected *C*-Glucosyl Phenols[a]

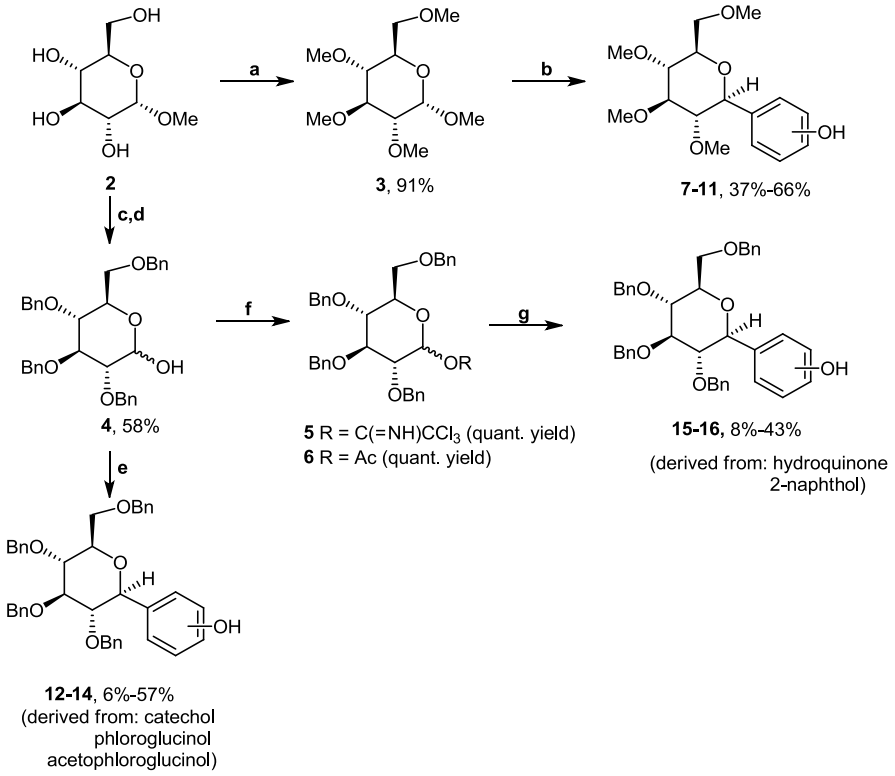

[a]Reagents and conditions: (a) DMF, NaH, MeI, 0 °C, 3 h; (b) dry MeCN, polyphenol, drierite, −78 °C → r.t., TMSOTf, 18−48 h; (c) DMF, NaH, BnBr, 0 °C → r.t., 20 h; (d) AcOH, H_2SO_4, reflux, 36 h; (e) dichloromethane/MeCN, drierite, −78 °C → r.t. or 40 °C, TMSOTf, 8−64 h; (f) for compound **5**: dichloromethane, 3 Å molecular sieves, CCl_3CN, 0 °C, 1 h; for compound **6**: pyridine, DMAP, 0 °C → r.t., Ac_2O, 2.5 h; (g) for compound **15**: dichloromethane/MeCN, drierite, −78 °C → r.t., $BF_3{\cdot}Et_2O$, 40 h; for compound **16**: dichloromethane, 3 Å molecular sieves, 0 °C → r.t., TMSOTf, 20 h.

Naphthol was also used to generate a *C*-glucosyl analogue with two fused planar rings to mimic rings A and C in the original structure.

Precursors and conditions leading to the higher yields are presented in Tables 1 and 2. In the case of catechol and hydroquinone, when using benzyl-protected sugar donors, glucosylation yields were drastically lower when compared to reactions with either phloroglucinol or trihydroxyacetophenone as a sugar acceptor. In the first two cases, different solvent proportions, anomeric protecting groups, and promoter equivalents were tried, attempting to optimize the reaction efficacy; yet, after much experimentation, no significant improvements could be observed. Moreover, no significant differences were found when trying to improve the efficacy of hydroquinone and catechol *C*-glucosylation using either TMSOTf or $BF_3{\cdot}Et_2O$. Notwithstanding, for the first time, per-*O*-methyl-*β*-glucosylated polyphenols have been accessed in good yields by using TMSOTf as the promoter and fully *O*-methylated methyl glucoside as the glucosyl donor. This methodology constitutes an advantage when compared to other approaches by saving reaction steps in the generation of donors with good leaving groups.

Methyl-protected glucosyl donor gave, by reaction with all the acceptors tested, *C*-glucosyl polyphenols as the major products (**7**−**11**, Table 1). Interestingly, with benzyl-protected glucosyl donors, only glucosylphloroglucinol **13**, 3-glucosyl-2,4,6-trihydroxyacetophenone **14**, and 1-glucosylnaphthalen-2-ol **16** were formed in moderate yields as the electron-donating effects of their aglycones were strong enough to promote *C*-glucosylation. On the other hand, catechol and hydroquinone gave *C*-glucosyl derivatives in very low yield (Table 1), even after increasing the reaction time and changing the solvent proportion, promoter and/or polyphenol molar proportion, and temperature (Table 2).

Notably, after careful analysis of the NMR spectra, we observed that the *para*-isomers are formed in the synthesis of catechol *C*-glucosides **7** and **12**, thus indicating that the Lewis acid-promoted Friedel−Crafts-type *C*-glucosylation is the favored reaction mechanism, prevalent over the Fries-type rearrangement described for unprotected phenols. While the synthesis of D-rhamnosyl[41] and D-glucosyl[42,43] aromatic derivatives has been previously described with protected phenols, to the best of our knowledge, this is the first report of exceptions to the Fries-type rearrangement in the *C*-glycosylation of unprotected phenols.

O-Acylation. A benzoyl group was regioselectively introduced in glucosylhydroquinone derivatives **10** and **15** to afford analogues of **1** on the basis of a *para* hydroxylation pattern (a, Figure 1). Using imidazole, DMAP, and benzoyl chloride, the desired ester derivatives **17** and **19** were obtained as the major products in good yield, together with their dibenzoate analogues **18** and **20** (Scheme 2). Further deprotection of benzyl-protected derivatives through catalytic hydrogenation gave the corresponding deprotected compounds **21** and **22**. For comparison purposes, compounds **14** and **16** were also debenzylated to afford compounds **23** and **24**, respectively (*vd.* Experimental Section).

https://dx.doi.org/10.1021/acs.jmedchem.0c00841
J. Med. Chem. 2020, 63, 11663−11690

Table 1. *C*-Glucosylation of Polyphenols Carried Out with TMSOTf as the Promoter

Phenol	Glycosyl donor 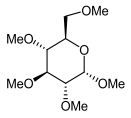	Isolated Yield (%)	Glycosyl donor 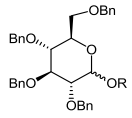	Isolated Yield (%)
Catechol *ortho- Hydroxylation pattern*	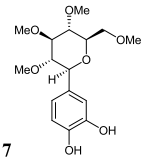 **7**	63	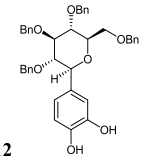 **12**	6 (R = H)
Phloroglucinol *meta- Hydroxylation pattern*	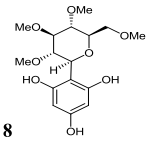 **8**	53	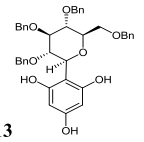 **13**	42 (R = H)
Trihydroxyacetophenone *meta- Hydroxylation pattern*	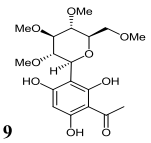 **9**	45	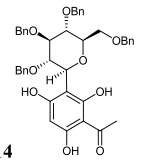 **14**	57 (R = H)
Hydroquinone *para- Hydroxylation pattern*	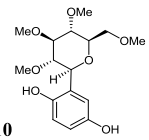 **10**	37	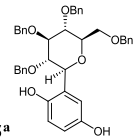 **15**[a]	8 (R = Ac)
2-Naphthol	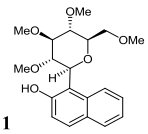 **11**	66	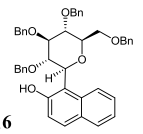 **16**	43 [R = C(=NH)CCl$_3$]

[a]Compound **15** was obtained using $BF_3{\cdot}Et_2O$ as the promoter.

Table 2. Comparison of Experimental Conditions Used in the *C*-Glucosylation of Hydroquinone and Catechol with Benzyl-Protected Sugar Donors[a]

compound no.	sugar donor no.	polyphenol	solvent	promoter	temperature	time	isolated yield
12	**4**	catechol (150 mol %)	DCM/MeCN (5:1)	TMSOTf (100 mol %)	−78 °C → 40 °C	64 h	6%
12	**6**	catechol (150 mmol %)	DCM/MeCN (5:1)	$BF_3{\cdot}Et_2O$ (100 mol %)	−78 °C → 40 °C	60 h	2%
15	**5**	hydroquinone (200 mol %)	DCM/MeCN (1:1)	TMSOTf (50 mol %)	−78 °C → 40 °C	21 h	6%
15	**5**	hydroquinone (150 mol %)	DCM/MeCN (1:1)	TMSOTf (50 mol %)	−78 °C → r.t.	40 h	2%
15	**5**	hydroquinone (150 mol %)	DCM/MeCN (5:1)	TMSOTf (50 mol %)	−78 °C → 40 °C	40 h	6%
15	**5**	hydroquinone (150 mol %)	DCM/MeCN (2:1)	TMSOTf (50 mol %)	−78 °C → 40 °C	24 h	6%
15	**5**	hydroquinone (200 mol %)	MeCN	TMSOTf (100 mol %)	−78 °C → 82 °C	72 h	1%
15	**4**	hydroquinone (150 mol %)	DCM/MeCN (5:1)	$BF_3{\cdot}Et_2O$ 100 mol%	−78 °C → 40 °C	96 h	7%
15	**6**	hydroquinone (150 mol %)	DCM/MeCN (5:1)	$BF_3{\cdot}Et_2O$ (100 mol %)	−78 °C → 40 °C	40 h	8%

[a]DCM, dichloromethane.

The observed regioselectivity of these *O*-acylation reactions may be related with stereochemical hindrance and eventual hydrogen bonding between the free hydroxy group and sugar, thus enhancing the relative reactivity of the remaining phenol hydroxy group toward esterification. Accordingly, regioselective esterification was not observed with glucosylcatechol derivatives **7** and **12** (structure type b, Figure 1 and Table 2). Instead, by applying the same experimental procedure, an inseparable mixture of mono-benzoylated compounds was obtained, which supports this hypothesis. For comparison of bioactivity, the dibenzoate catechol analogues of compounds **18** and **22** were

https://dx.doi.org/10.1021/acs.jmedchem.0c00841
J. Med. Chem. 2020, 63, 11663−11690

Scheme 2. Preparation of Glucosylhydroquinone Benzoates[a]

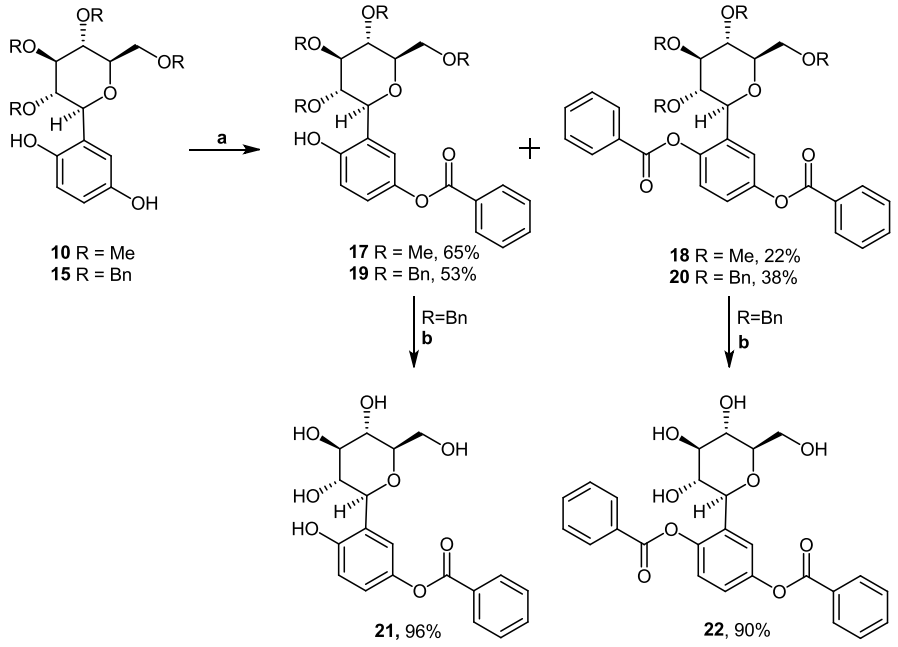

[a]Reagents and conditions: (a) dichloromethane, imidazole, DMAP, BzCl, 0 °C → r.t., 60−120 h; (b) EtOAc, Pd/C, H_2, r.t., 16−22 h (R = Bn).

Scheme 3. Preparation of *O*-Glucosyl Hydroquinone and *O*-Glucosyl Catechol Benzoates[a]

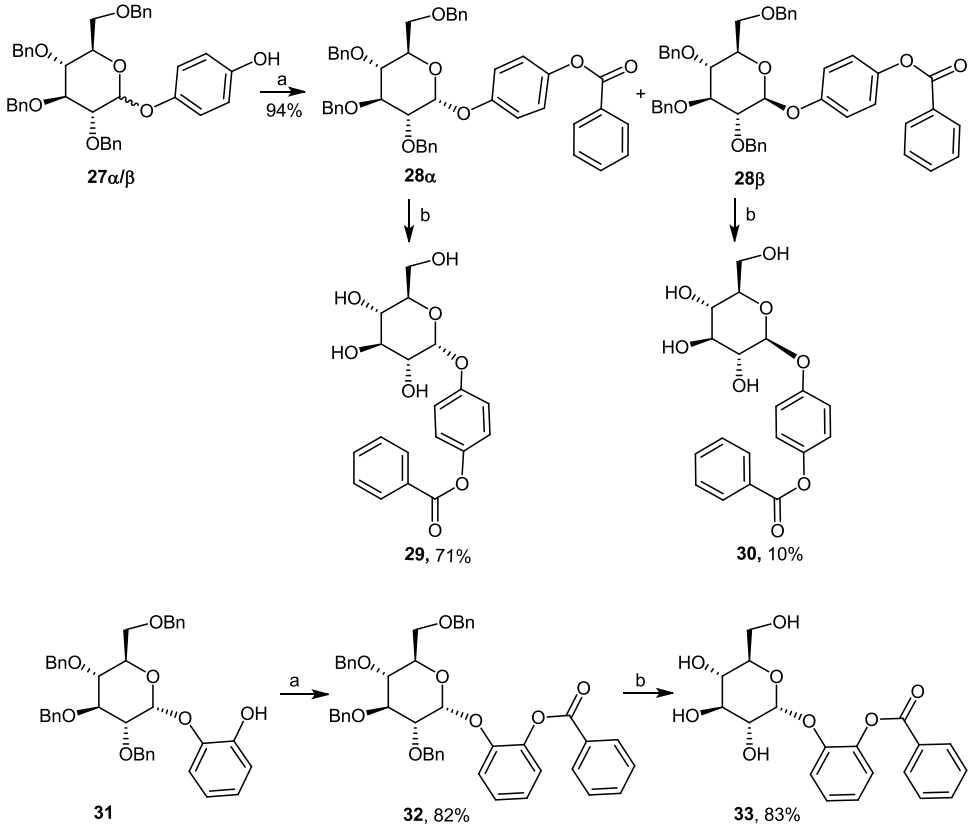

[a]Reagents and conditions: (a) dichloromethane, imidazole, DMAP, BzCl, 0 °C → r.t., 60−120 h; (b) EtOAc, Pd/C, H_2, r.t., 16−22 h.

also synthesized (*vd.* Experimental Section, compounds **25** and **26**, respectively).

Moreover, the hydroquinone and catechol per-*O*-benzyl glucosides **27*α*,*β*** and **31** (Scheme 3), obtained as major products under the *C*-glucosylation reaction conditions (Table 2), were also benzoylated and deprotected to afford the corresponding *α*-glucosides **29** and **33** as major products in excellent overall yield.

C-Acylation. The glucosylphloroglucinol **13** was originally chosen as the precursor of the planned analogue of compound **1**

https://dx.doi.org/10.1021/acs.jmedchem.0c00841
J. Med. Chem. 2020, 63, 11663−11690

Scheme 4. Preparation of Compound 37[a]

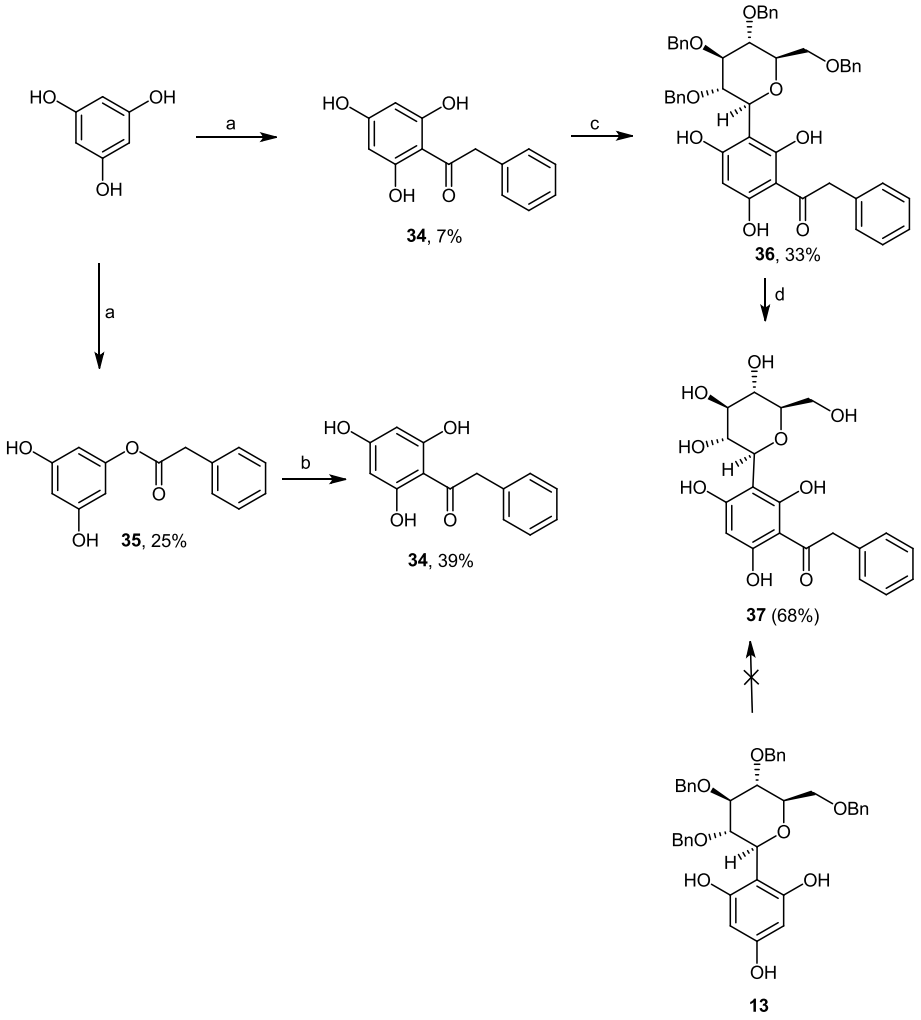

[a]Reagents and conditions: (a) phenylacetyl chloride, 2% TfOH/MeCN, 0 °C → r.t., overnight; **34**, 7%; **35**, 25%; (b) TfOH, 100 °C, 2 h, 39%; (c) TMSOTf, dichloromethane/MeCN, compound **4**, drierite, −40 °C → r.t., overnight, 33%; (d) MeOH/EtOAc, Pd/C, H_2, r.t., 3 h, 68%.

with the *meta* hydroxylation pattern (c, Figure 1). Provided that this trihydroxybenzene is an extremely electron-rich aromatic system, we were expecting a very straightforward Friedel–Crafts-type acylation to occur with phenylacetyl chloride in the presence of a Lewis acid. After much experimentation employing a number of Lewis acids (*e.g.*, $BF_3{\cdot}Et_2O$, TMSOTf, $FeCl_3$, TfOH) and several different conditions without any success, we hypothesized that the sugar moiety could be reducing the reactivity of the aromatic ring or even being degraded in the course of these reactions. The initial *C*-acylation of the phenol residue followed by *C*-glucosylation turned out to be the best option to address this issue. Due to the dual reactivity of unprotected polyphenols toward electrophiles, hydroxy groups, and as in this case, highly activated nucleophilic carbons, the control of *O*-/*C*-acylation was not an easy task. While an equimolecular amount or an excess of TfOH in the absence of solvent generated the di-*C*-acylated product, the use of 2% TfOH in MeCN rendered a mixture of the *O*-/*C*-acylated products in a ratio of ca. 1/0.3 (Scheme 4). Then, using an excess of TfOH, which acted as both the solvent and catalyst, compound **35**, obtained in 25% yield from trihydroxybenzene, was rearranged into the *C*-acylated analogue **34** in 39% yield, which was subsequently *C*-glucosylated to afford compound **36** in 33% yield. After catalytic hydrogenation, the final analogue **37** was isolated in 68% isolated yield.

Computational Studies, Epitope Mapping, and Bioactivity Assays. *DFT Calculations and Molecular Interactions of Rationally Designed Analogues with hIAPP by STD-NMR.* IAPP is co-secreted with insulin by pancreatic β-cells. In prediabetes, insulin resistance leads to a compensatory hypersecretion of insulin and IAPP, leading to its aggregation and deposition in the pancreas in the form of cytotoxic amyloid oligomers and fibrils. Along with disease progression, this accumulation will lead to the loss and dysfunction of β-cells, which justifies why patients with advanced T2D are no longer able to produce insulin despite being insulin-resistant.[2] Hence, IAPP is an important therapeutic target in T2D, particularly in the prevention of pancreatic dysfunction arising from aberrant insulin secretion. In this context, the interaction of **1** against hIAPP was previously unveiled by saturation-transfer difference (STD) NMR techniques, also being shown, by atomic force microscopy, the ability of this compound to inhibit hIAPP aggregation into amyloid oligomers and fibrils.[23] Based on these findings, we were interested in assessing if the rationally designed analogues **21** and **37** (aimed at mimicking the original scaffold) would exhibit the same level of interaction with hIAPP

https://dx.doi.org/10.1021/acs.jmedchem.0c00841
J. Med. Chem. 2020, 63, 11663−11690

and if the binding epitope would be maintained in the absence of the central fused ring system. Being more easily accessed in fewer synthetic steps, both **21** and **37** have increased molecular flexibility when compared to the lead compound **1**. DFT calculations [PBE0/6-311G** (H_2O)] show that low-energy conformations of compounds **21** and **37** are superimposable with compound **1** (Figure 2), namely, with its *anti*-conformer

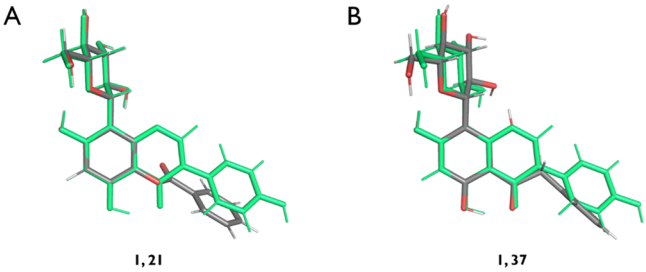

Figure 2. DFT-calculated structure of *anti*-**1** (in green), which is the preferentially adopted conformation in the presence of Aβ(1−42) oligomers,[25] superimposed to the lowest energy conformations identified at the PBE0/6-311G** (H_2O) level of theory for compounds (A) **21** and (B) **37** (in gray, red, and white), obtained by root-mean-square (RMS) fitting using all ring A carbon atoms of each compound.

(defined by an antigeometry for the H1″-C1″-C8-C7 torsion angle, see Figures 1 and 2), which is the preferentially adopted conformation of **1** in the presence of Aβ(1−42) oligomers,[25] suggesting that these molecules are able to mimic the original spatial orientation of the sugar moiety relative to rings A and B (see Figures S1 and S2 and further details in the Supporting Information).

The STD-derived binding epitope obtained for compounds **1**, **21**, and **37** against hIAPP by STD-NMR (Figure 3 and Figures

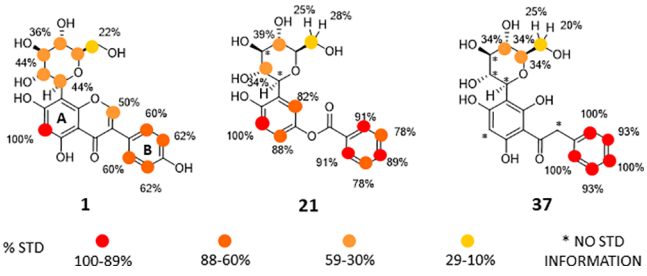

Figure 3. STD-derived epitope mapping obtained for compounds **1**,[25] **21**, and **37** with hIAPP oligomers.

S3 and S4) suggests that molecular planarity is not a structural requirement for binding and the absence of the central fused ring system in compounds **21** and **37** does not disrupt the interaction of these compounds with hIAPP. As in the case of compound **1**, the highest STD intensities correspond to the protons of the aromatic core of compounds **21** and **37** (% STD > 80%) when compared to those detected for the glucosyl group (% STD < 40%).

These experiments show that the binding affinity of the antidiabetic lead **1** is not related to the molecular planarity of the isoflavone core. Being accessed in only five synthetic steps (instead of the nine needed for the synthesis of the lead molecule **1**), compounds **21** and **37** exhibit a clear binding against hIAPP. Given the reported anti-amyloidogenic properties of **1** against hIAPP,[25] these results encourage further studies of these two simpler analogues to evaluate their potential for the prevention of IAPP-induced pancreatic failure.

Inhibition of PrP^C−Aβ Oligomer Interaction. In the past few years, the failure of several clinical trials targeting soluble and fibrillar Aβ by monoclonal antibodies have motivated the scientific community to work in the diversification of therapeutic targets for AD. One possible strategy is to focus on the downstream effects of Aβ rather than on its accumulation and aggregation.[44] Soluble Aβos were shown to bind to PrP^C on the neuronal cell surface, initiating a cascade through activation of Fyn kinase. Indeed, it is possible to monitor the activation of Src family kinases (SFKs) such as Fyn kinase by measuring the expression of phosphospecific epitopes, as previously reported.[3]

Furthermore, it is commonly assumed that formation of Aβ fibrils and plaque deposits is a crucial event in the pathogenesis of AD.[45] However, there is accumulating evidence that soluble oligomers are the most cytotoxic form of Aβ, although it is still unclear which size and morphology of the aggregates exert neurotoxicity. As with most of the identified Aβ receptors, PrP^C was found to bind Aβos with much higher affinity than monomeric Aβ (mAβ). In this work, natural Aβos, a kind gift from Sheffield Institute for Translational Neuroscience (SITraN, U.K.), were used. These were derived from Chinese hamster ovary cells (7PA2 cells) stably transfected with cDNA encoding APP751, an amyloid precursor protein that contains the Val717Phe familial Alzheimer's disease mutation, as previously described.[46] The Aβos solution contains between 12,000 and 14,000 pg/mL total Aβos as measured by ELISA. This concentration is comparable to that of Aβ peptides detected in human cerebrospinal fluid. The Aβos prepared represent a heterogeneous population of monomers, dimers, trimers, tetramers, higher state soluble oligomers, and other cellular proteins as previously reported by western blotting[44] without further purification. The Aβos preparation using the same protocol has been applied in the same way by other groups.[46] The same batch of the recombinant soluble Aβos was used for all experiments described in the paper to minimize the impact of experimental variations caused by the heterogeneous preparation of the Aβos. Natural Aβos (1000 pg/mL) were used to treat HEK 293 cells, immunocytochemistry (ICC) was performed to detect cellular prion protein, and then the slides were imaged with a Confocal Microscope Leica TCS SP5 II objective 63× oil Leica Microsystems (Figure 4A). To validate the observed binding between PrP^C and Aβos, we performed a PRNP knockdown by using the commercially available kit ON-TARGETplus Human PRNP (5621) siRNA−SMARTpool. Because only the PrP^C on the cell surface fraction is involved in the interaction with Aβos, the knockdown was combined with acute cleavage promoted by phospholipase C (PLC). Live cell staining and imaging were performed, and cells were analyzed by flow cytometry. Untreated cells as controls and cells treated with ON-TARGETplus Non-targeting siRNA Pool (scrambled siRNA) were used. A reduction of PrP^C expression by more than 80% was observed (Figure 4B). It is also interesting to note that phospholipase C (PLC) can cleave PrP^C on the cell surface and improve the effects of knockdown further, *i.e.*, further reducing the amount of PrP^C on the cell surface.

We were able to test the Aβos binding to the prion protein in both HEK 293 cell lines with endogenous or "high" PrP^C expression (Figure 4C2) and "low" PrP^C expression through siRNA knockdown (Figure 4C3). The two populations were treated with the same concentration (1×10^3 pg/mL) of Aβos for 2 h. Cells were then washed and stained with anti-Aβos

https://dx.doi.org/10.1021/acs.jmedchem.0c00841
J. Med. Chem. 2020, 63, 11663−11690

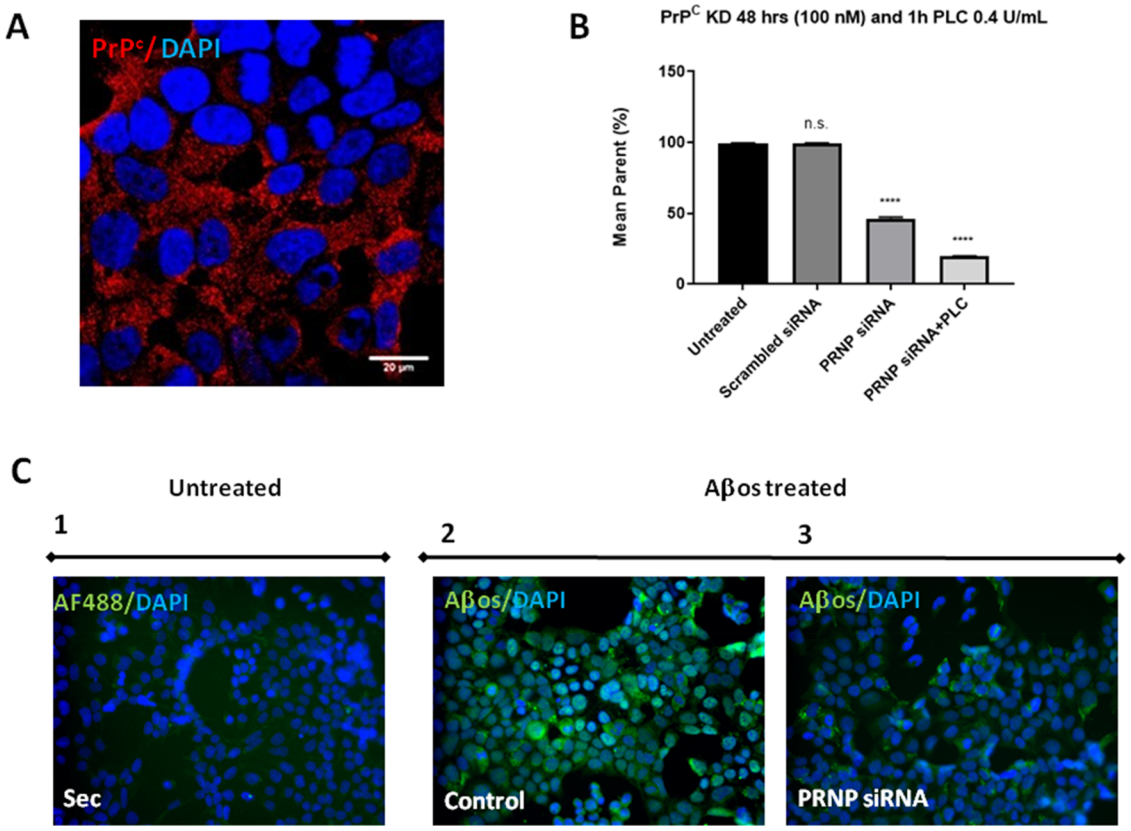

Figure 4. (A) Immunocytochemistry (ICC) images of HEK 293 cells treated with natural Aβos (1×10^3 pg/mL). Pictures captured with a Leica TCS SP5 II. (B) Flow cytometry analysis of transfected HEK 293 cells with PRNP siRNA against cellular prion protein (PrP^C). Results are expressed as the mean ± standard error mean (SEM); $n = 3$. Significant differences between control are indicated with ****($p \leq 0.0001$). (C) Immunocytochemistry (ICC) analysis by the ImageXpress. (1) Negative control represented by HEK cells not transfected, treated with Aβos and stained with only the secondary antibody AF488. (2) Aβos binding to the prion protein in HEK 293 cell line with "high" PrP^C expression. (3) Aβos binding to the prion protein in HEK 293 cell line with "low" PrP^C expression following knockdown performed by PRNP siRNA.

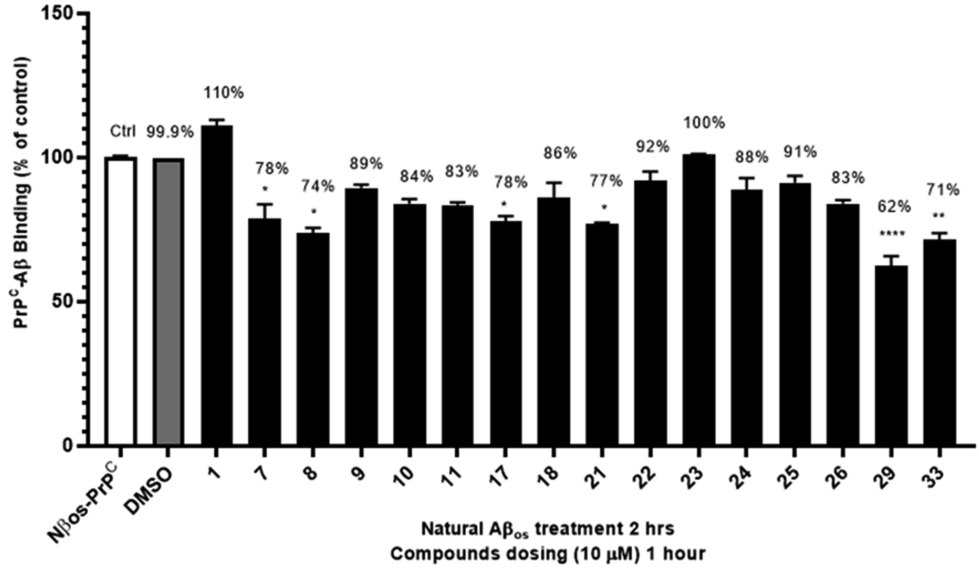

Figure 5. Screening for compounds that are able to induce a PrP^C–NAβos binding inhibition. All compounds were tested at 10 μM as the final concentration. Results are expressed as the mean ± standard error mean (SEM); $n = 3$. Significant differences between control are indicated with *($p < 0.05$), **($p < 0.01$) and ****($p \leq 0.0001$). The PrP^C–NAβ(1–42) binding (%) after treatment with the compounds is also indicated.

antibodies and imaged by the ImageXpress Micro Widefield High Content Screening System (Figure 4C). It is clearly seen that the binding of Aβos to the cell surface is PrP^C-dependent; *i.e.*, Aβos binds to PrP^C on the cell surface.

Compound screening in HEK 293 cell lines, previously treated with fresh natural Aβos, showed compounds interfering with the PrP^C–Aβos binding (Figure 5).

https://dx.doi.org/10.1021/acs.jmedchem.0c00841
J. Med. Chem. 2020, 63, 11663–11690

Inhibition of Aβ-Induced Fyn Activation. The Opera High Content Screening System was used in this section as it has been widely applied to test drugs capable of reversing the altered phenotype observed in AD such as Fyn activation.

Figure 6 shows that the level of Fyn activation of hiPSC-derived neural progenitor cells from healthy donors increased upon treatment with Aβ; *i.e.*, pFyn production is increased.

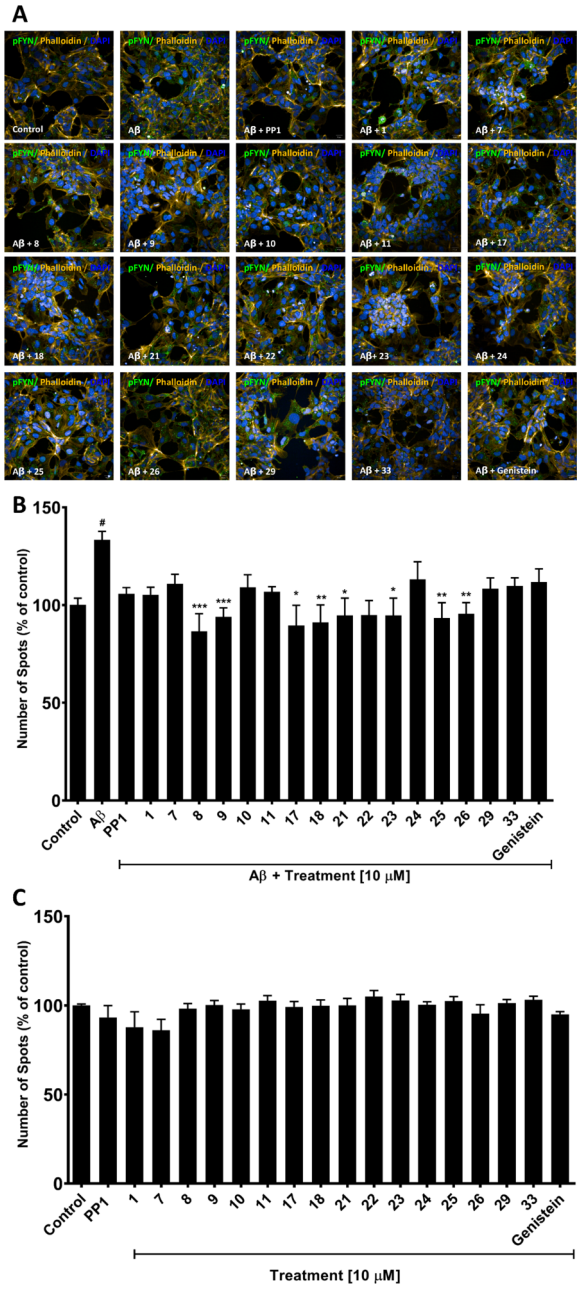

Figure 6. (A, B) Effect of glucosylphenols in Aβ-induced Fyn activation and (C) effect of glucosylphenols on the basal levels of pFyn in the absence of Aβ. The indirect activation of Fyn kinase was measured by immunofluorescence using Opera High Content Screening System (A). Cells were exposed to 10 μM of compounds in association with Aβ. The results were normalized against the control group, which was considered as 100%. (B, C) Percentage of number of pFyn + spots in each treatment group. Results are expressed as the mean ± standard error mean (SEM); $n = 3$. Significant differences between control are indicated with $^{\#}(p \leq 0.05)$ and $*(p < 0.05)$ when compared to Aβ treatment $*(p < 0.05)$ or $**(p < 0.01)$ or $***(p < 0.001)$.

However, we observed that the level of Aβ-induced Fyn activation was reduced back to normal control values in the presence of the commercial Fyn kinase inhibitor PP1, an inhibitor of Src family tyrosine kinases Lck, Fyn, Hck, and Src. Moreover, it shows that compounds **8** and **9** (simple per-*O*-methylglucosylphenols), **18** (per-*O*-methylglucosylhydroquinone dibenzoate), **21** (rationally designed glucosylhydroquinone monobenzoate), **25** and **26** (both glucosylcathecol dibenzoate derivatives), and **23** and **24** (fully unprotected glucosylacetophloroglucinol and glucosylnaphthalen-2-ol) were able to significantly reduce Aβ-induced Fyn activation at 10 μM. Moreover, these *C*-glucosyl polyphenols are indeed more active than aglycone genistein (Figure 6A,B).

Fyn kinase plays an important role in the physiology of neuronal cells by regulating cell proliferation and differentiation during the development of the CNS. This enzyme is also involved in signaling transduction pathways that regulate survival, metabolism, and neuronal migration.[47] Considering that Fyn inhibition below the physiological levels (basal levels) could be deleterious for the homeostasis of the cells, we decided to investigate the effects of the compounds on the basal levels of pFyn. Thus, neuronal progenitor cells were treated with the compounds without the addition of Aβ to determine whether the effects observed are independent of Aβ treatment, and it was confirmed that tested compounds and PP1 alone do not reduce the basal levels of pFyn (Figure 6C).

A rather diverse selection of compounds was able to produce the desired effects, ranging from per-*O*-methyl and polyhydroxy forms. Curiously, the natural compound that served as the inspiration for this study (**1**) was only able to cause a nonsignificant reduction in Aβ-induced Fyn activation. Yet, the rationally designed and more flexible hydroquinone monobenzoate (**21**) exhibited significant differences when compared to Aβ alone. In fact, chemical modifications made in the original scaffold toward simpler versions of compound **1** without ring B (*e.g.*, in compounds **8**, **9**, and **23**) were generally more beneficial for the desired activity. On the other hand, no conclusions could be drawn regarding the advantages or disadvantages of sugars decorated with per-*O*-methyl groups as no correlation between structure and activity could be found regarding this matter. A good example is the presence and absence of these groups in the two most complex hits found in this assay, compounds **25** and **26**, respectively.

We also evaluated the activity of Fyn kinase in the presence of some compounds by ADP-Glo kinase assay, a luminescent ADP detection assay (Figure 7). This assay provides a homogeneous and high-throughput screening method to measure kinase activity by quantifying the amount of ADP produced during a kinase reaction.

As presented in Figure 7, PP1 was able to reduce the Fyn kinase activity at different concentrations from 1 to 50 μM, as expected. Furthermore, from the evaluated compounds, only **8** and **10** were able to act as Fyn kinase inhibitors, denoting that they may have an added therapeutic value against DID given the recognized role of Fyn kinase activity in insulin sensitivity and lipid utilization.[8−10] The fact that compounds **8** and **10**, but not **9**, were able to inhibit Fyn activity indicates that in per-*O*-methyl sugar-containing structures, the acetyl moiety is detrimental for activity, and the *para*- and *ortho*-hydroxylation pattern of the polyphenol is not relevant.

It is also important to note that, as tested by a thioflavin-T (ThT) fluorescence assay with Aβ(1−42) (see Figure S5 in the Supporting Information), compounds of this series do not

https://dx.doi.org/10.1021/acs.jmedchem.0c00841
J. Med. Chem. 2020, 63, 11663−11690

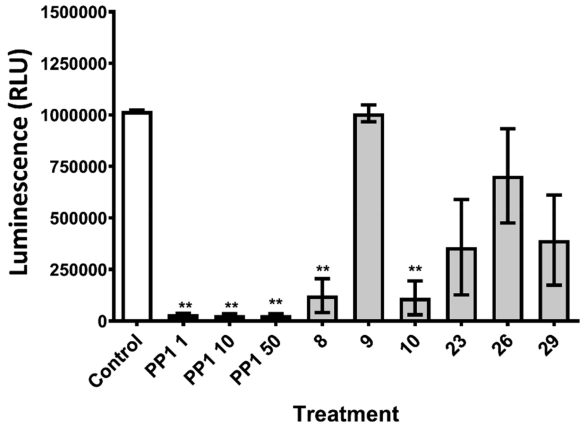

Figure 7. Effect of glucosylpolyphenols and the polyphenol glucoside **29** in the inhibition of Fyn kinase activity measured by the ADP-Glo kinase assay. Results are expressed as the mean ± SEM; $n = 3$. Significant differences between control are indicated with $**(p < 0.01)$ when compared with Aβ treatment.

significantly inhibit Aβ(1−42) aggregation *per se*, which suggests that the inhibition of Aβ-induced Fyn kinase activation is unlikely to occur exclusively *via* direct interaction with Aβ. Most importantly, these results indicate that these compounds are not pan-assay interference compounds (PAINS) acting *via* autoxidation of catechol/hydroquinone and subsequent covalent binding to proteins, contrary to quercetin, a well-known PAIN compound[48] used as positive control in this assay.

To estimate eventual behavior of compounds **9**, **23**, and **26** as PAINS, in particular as membrane PAINS, we have evaluated their potential using a computational protocol. The potential of mean force (PMF) for translocating a hydrophobic probe across a POPC bilayer loaded with compounds **9**, **23**, and **26** (10% mol/mol) and their calculated membrane permeabilities are shown in Figure S6 and Table S1 in the Supporting Information. Membrane PAINS, even mild ones such as resveratrol,[49] make the membrane significantly more permeable to hydrophobic compounds. In contrast, none of our compounds led to a significant increase in membrane permeability, thus indicating that they do not act as membrane PAINS. In addition, we

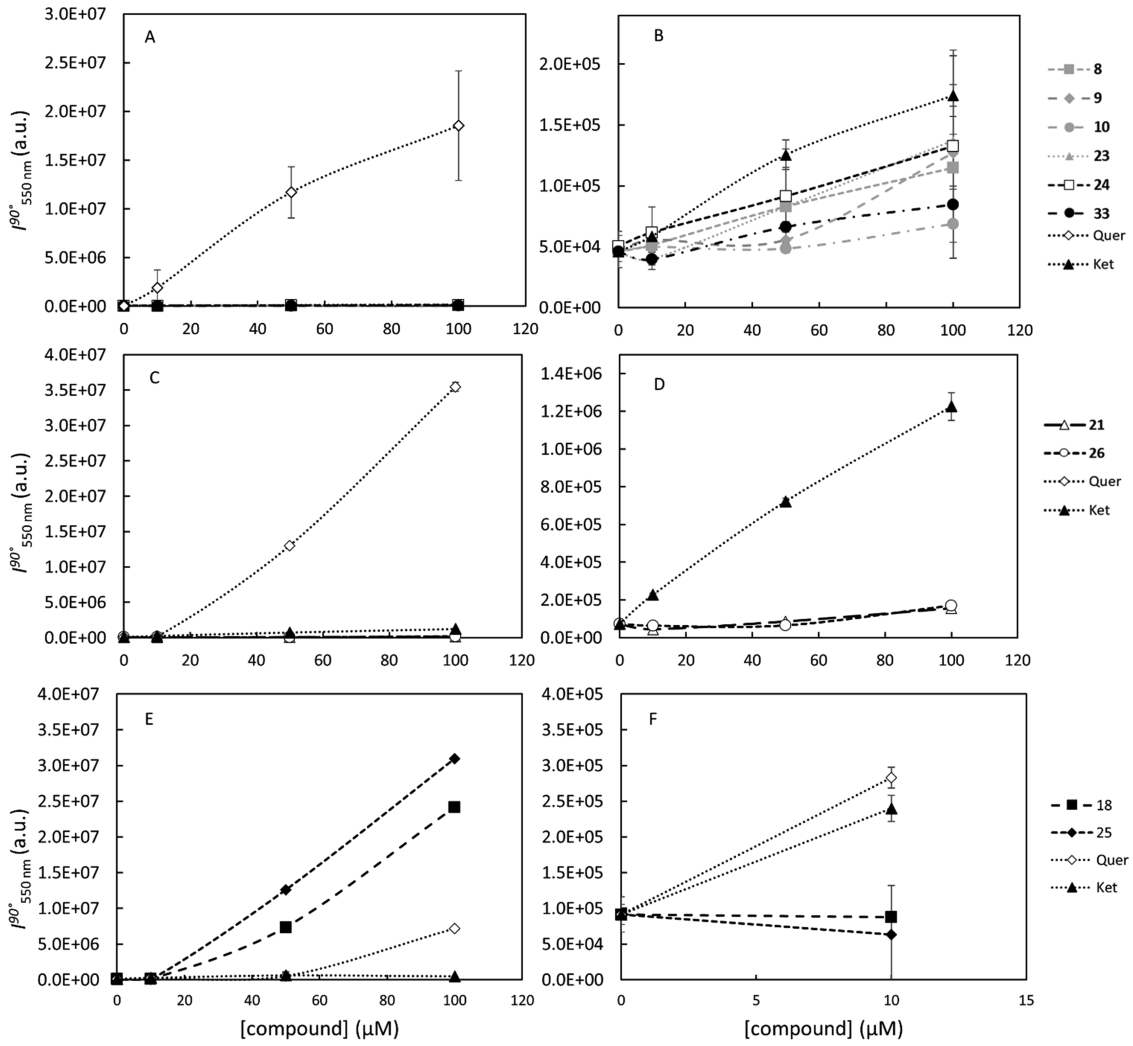

Figure 8. Static light scattering intensity at 550 nm and 90° for compounds (A, B) **8**, **9**, **10**, **23**, **24**, and **33**, (C, D) **21** and **26**, and (E, F) **18** and **25** and the respective controls: ketoconazole (Ket) and quercetin (Quer) at 10, 50, and 100 μM. Samples were dissolved in 10 mM PBS (with 100 mM NaCl, pH 7.4) and 1.25% (A, B), 2.5% (C, D), or 5% (E, F) DMSO. The values are the mean ± SD of at least two independent experiments. The graphics without Quer (B, D) are for a better depiction of the behavior of low scattering compounds. Graphic (F) is a zoom-in of (E) for a better observation of what is happening for the lowest concentration of the compounds. The lines are merely to guide the eye.

https://dx.doi.org/10.1021/acs.jmedchem.0c00841
J. Med. Chem. 2020, 63, 11663−11690

submitted their structure to the Badapple online service,[50] and the resulting promiscuity indicators also confirm that these compounds will unlikely act as PAINS.

Aggregation Studies. With the formation of aggregates, which can inhibit protein targets,[51] the concentration of free monomers in solution decreases, while the number and/or size of particles in suspension increase, and consequently, so does light scattering. On the other hand, aggregate formation might also induce changes in vibrational progression and the appearance of exciton bands, which are readily detected in the electronic absorption spectra through changes in the spectral envelope, such as emergence of new bands, band broadening, and variation of the absorbance at λ_{max}, which if there is no aggregation and other interferences, should have a linear relation with the concentration of the molecule.[52]

Aggregating and nonaggregating compounds have been successfully identified using static light scattering and/or electronic absorption spectroscopy. For instance, quercetin[53] and miconazole[54,55] were found to aggregate, while fluconazole and ketoconazole are nonaggregating molecules.[54]

Taking these findings into consideration, static light scattering and electronic absorption spectroscopy were used to assess compound aggregation behavior. Only compounds with interesting bioactivity were selected for these experiments, namely, compounds **8**, **9**, **10**, **18**, **21**, **23**, **24**, **25**, **26**, and **33**. The compounds under study were compared with ketoconazole, a known nonaggregating molecule acting as the negative control, and with quercetin, a promiscuous aggregator, used as the positive control.

Light scattering intensity for compounds **8**, **9**, **10**, **23**, **24**, and **33** (Figure 8A,B) and **21** and **26** (Figure 8C,D) was similar or weaker than that for ketoconazole, for concentrations ranging from 10 to 100 μM. Moreover, the values for those compounds were significantly lower than the light scattering intensity measured for quercetin. These results indicate that those eight compounds do not aggregate in this concentration range. Moreover, by comparing the normalized absorption spectra for each compound at different concentrations (Figures S7 and S8, Supporting Information), no alterations were observed in the absorption spectra of those eight compounds, neither in terms of energy nor vibrational progression n or number of bands, also pointing to the absence of aggregation for these compounds. On the other hand, at high concentrations, the absorption spectra of the positive control, quercetin, suffers drastic changes (Figure S7, quercetin). First, the typical band of the monomeric species, with a maximum at ca. 385 nm,[56] suffers a blue shift to 330 nm and becomes broader. This is caused by the loss of the double bond character due to rotation of the 2−1′ bond out of plane and, consequently, the loss of the planar conformation.[56] Also, new bands are visible at ca. 375 nm that indicate the presence of extended conjugation through catechol−catechol interactions. A new band is also visible for the highest concentration of 100 μM between 245 and 270 nm, which when compared with the absorption spectra of the different ionization states of the molecule,[57,58] may indicate an increase of the nonprotonated quercetin species.[59] All these changes are related to the aggregation of the compound. In fact, the pK_a of a compound in an aggregate (*e.g.*, micellar) environment is different from the one of the monomeric species in solution, shifting the ionization equilibrium.[60] If any of the compounds tested were aggregating, then changes in the absorption spectra would be readily detected, which was not the case.

For compounds **18** and **25,** solutions with only 1.25 and 2.5% DMSO were visibly turbid, especially for 100 μM, which is an indication of the low aqueous solubility of these compounds that might be due to their high lipophilicity. With a value as high as 5% of DMSO, the solutions with higher compound concentrations (50 and 100 μM) were still turbid. However, this was not the case at 10 μM and, as can be observed in Figure 8 for this concentration (at which the cellular studies were conducted), the light scattering intensity is lower than for the nonaggregator ketoconazole. This indicates that at this concentration, these two compounds are not aggregating.

Finally, a linear relationship was confirmed between the concentration and peak absorbance for the lower energy band of each compound and for the nonaggregating ketoconazole (Figures S9 and S10), while for the promiscuous quercetin, such relation does not follow a linear behavior (Figure S9, quercetin).

In summary, compounds **8**, **9**, **10**, **21**, **23**, **24**, **26**, and **33** are not promiscuous aggregators in the concentration range tested, which encompasses all the concentrations used for the other assays. Our results for compounds **18** and **25** show that at the concentration of 10 μM, no aggregation was detected but, at high concentrations,, the herein presented inhibition constants should be considered only as estimates and interpreted with caution.

The aggregation studies confirm that bioactivities herein reported are not due to nonspecific effects resulting from the formation of compound aggregates and are thus the result of bona fide specific compound activity.

Inhibition of Aβ-Induced Tau Phosphorylation. Intraneuronal neurofibrillary tangles (NFTs) of paired helical filaments (PHFs) are a histopathological hallmark of Alzheimer's disease (AD). This NFTs are formed of hyperphosphorylated Tau. Tau is hyperphosphorylated in the AD brain at multiple sites including at residues Thr181.[61−64] To assess if the compounds are indeed able to accomplish the desired downstream effects by reducing Aβ-induced Tau pathology, we performed a high-content image screening (HCS) for phosphorylated Tau (pTau), at Thr181 as recognized by the antibody AT270, using compounds that were previously revealed to inhibit Aβ-induced Fyn activation. Our data (Figure 9) revealed that cortical neurons exposed to Aβ have increased pTau levels when compared to DMSO controls. On the other hand, neurons treated with Aβ in addition to 10 μM of compounds **9**, **10**, **18**, **23**, **25**, **26**, and **29** and genistein significantly reduced the levels of pTau when compared to the Aβ controls. Even though there was a reduction of pTau in cells treated with compounds **8** and **33**, this reduction was found not to be statistically significant. From all tested compounds, **9**, **18**, **23**, **25**, and **26** were able to reduce Aβ-induced Fyn activation, with concomitant decrease in Aβ-induced pTau.

Cytotoxicity in Neuronal Cells Derived from hiPSCs. To confirm that the synthesized compounds are not cytotoxic at relevant concentrations, we have differentiated hiPSC cells derived from health control MIFF1[65] into neural cells. We observed that after 20 days of differentiation, these cells express specific neural progenitor markers such as Nestin. NPCs were treated with each compound for 24 h, and none presented any signs of cytotoxicity at 10 μM (Figure 10). Furthermore, compounds **23**, **26**, and **29** were not cytotoxic in concentrations up to 100 μM, while **9** is safe to administer up to a 50 μM concentration (data not shown).

https://dx.doi.org/10.1021/acs.jmedchem.0c00841
J. Med. Chem. 2020, 63, 11663−11690

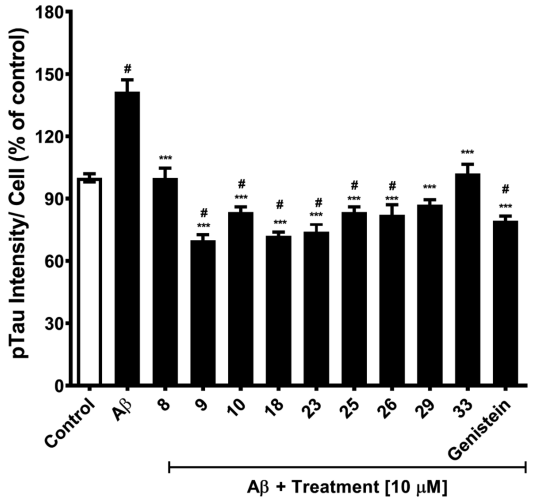

Figure 9. Effect of compounds against hyperphosphorylation of Tau induced by Aβ. Neurons treated with Aβ oligomers were evaluated against pTau (AT270). Tau hyperphosphorylation was measured by immunofluorescence using the Opera High Content Screening System. Cells were exposed to 10 μM of each compound in association with Aβ for 4 days. Results were normalized against the control group considered as 100%. The values are expressed as the mean ± SEM; n = 3. Significant differences between control are indicated with $^{\#}(p \leq 0.05)$ and ***($p < 0.001$) when compared with Aβ treatment.

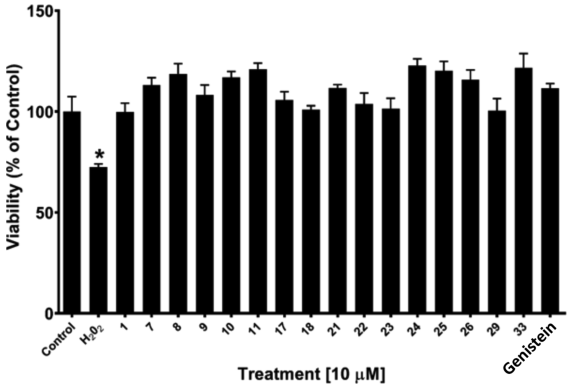

Figure 10. Cytotoxicity of *C*-glucosyl phenols and glucosides **29** and **33** in neuronal cells derived from hiPSCs. Cell viability was measured in an MTT assay. Cells were exposed to 10 μM of each compound for 24 h. Results were normalized relative to a control group considered as 100%. The values are expressed as the mean ± SEM; n = 3. Significant differences between control are indicated with * ($p < 0.05$).

Glycosidase and Cholinesterase Inhibitory Activity Screening. Postprandial glycemia control is key in managing T2D clinical manifestations. This control can be achieved through the inhibition of intestinal glucosidases, in particular α-glucosidase.[66] These enzymes catalyze the hydrolysis of complex carbohydrates present in the gut into simple sugars that are able to be absorbed into the bloodstream and thus contribute to the increase in glycemia levels.[67] Since we had previously elucidated the powerful α-glucosidase inhibitory activity of the ethyl acetate extract of *Genista tenera* where compound **1** is the major component (97.6% for the extract *vs* 82.2% for the commercial drug acarbose), we were interested in finding out if it was due to the presence of the lead *C*-glucosyl isoflavone.[68] However, **1** was found to have only modest activity, with 14% inhibition at 100 μM (Table 3). This compound was a slightly better β-glucosidase inhibitor, being able to decrease its activity in 23% at the same concentration. Notably, these activities are cumulative with the antihyperglycemic effects of **1** observed in Wistar rats since treatment was administered intraperitoneally.

Genistein, on the other hand, is a powerful α-glucosidase uncompetitive inhibitor (84% inhibition at 100 μM; $K_{ib} = 12 \pm 2$ μM) and moderate β-glucosidase competitive inhibitor (44% inhibition at 100 μM; $K_{ia} = 66 \pm 13$ μM), indicating that the presence of the C−C linked sugar moiety at C-8 is, in this case, detrimental to activity. Remarkably, the catechol glucoside **33** was found to be the best glucosidase inhibitor among the synthesized analogues, with a good α-glucosidase competitive inhibitor activity (74% inhibition at 100 μM; $K_{ia} = 39 \pm 4$ μM) and modest β-glucosidase inhibitor activity (13% inhibition at 100 μM). Apart from this compound, only three others were able to concomitantly inhibit both glucosidases: the hydroquinone derivatives **17** and **29** and the 2-naphthol derivative **24**.

Acetylcholinesterase (AChE) and butyrylcholinesterase (BuChE) are two well-characterized therapeutic targets in AD owing to their ability to catalyze the hydrolysis of the neurotransmitter acetylcholine, which is responsible for the cognitive functionality and whose level is particularly low in AD patients. Three of the so far four FDA-approved drugs for AD consist of selective or dual cholinesterase inhibitors, including donepezil, galantamine, and rivastigmine.[2] The inhibition of AChE and BuChE correlates with lower Aβ levels, decreased Aβ aggregation, improved learning and memory.[69−72] BuChE is considered to play a minor role in the regulation in acetylcholine levels in healthy brains; however, the levels of this enzyme progressively increase in AD, whereas those of AChE decline or remain unchanged.[73]

Not so well studied and divulged is the role of butyrylcholinesterase in the etiology of T2D. However, elevated AChE, but especially serum BuChE activity, has been correlated with insulin resistance, increased adiposity, and abnormal serum lipid profile, being regarded as a risk factor for T2D.[74−77] Thus, these two enzymes may be regarded as additional therapeutic targets for DID.

Similar to what was described for α-glucosidase, the ethyl acetate extract of *G. tenera* was capable of inhibiting this enzyme (77.0% at 130 μg/mL).[68] Hence, we were interested in assessing whether the anticholinergic activity of the extract was due to the presence of **1** as a major component. This compound was however able to inhibit AChE only by 26% at 100 μM (43 μg/mL) and, in this assay, genistein presented merely half of the inhibitory capacity of **1** (Table 3). On the contrary, genistein was a much stronger BuChE inhibitor than **1**, displaying 41% inhibition at 100 μM. From the synthesized analogues of **1**, only compounds **7**, **17**, **18**, and **33** were active against AChE, while roughly all presented a BuChE inhibition capacity of at least 10%. Compounds **10**, **11**, **22**, and **26** were able to inhibit BuChE in over 20% at 100 μM, from which compound **26** stands out with 39% inhibition.

Membrane Permeability Assays. Compounds were tested in a parallel artificial membrane permeability assay (PAMPA) to measure and rationalize their potential to cross membrane barriers. Testosterone was used as the positive control in this assay. It is important to note that this assay merely looks into the ability of compounds to passively diffuse through cell membranes. Being glycosides, it is possible that the sugar moiety acts as a shuttle for their passage into the brain through GLUT-1 transporters highly expressed in the blood−brain barrier (BBB), as previously reported for similar molecules.[78]

https://dx.doi.org/10.1021/acs.jmedchem.0c00841
J. Med. Chem. 2020, 63, 11663−11690

Table 3. Glycosidase and Cholinesterase (AChE and BuChE) Inhibitory Efficacy of Compound 1 and Analogues at 100 μM[a]

Compound	α-Glucosidase Inhibition	β-Glucosidase Inhibition	AChE Inhibition	BuChE Inhibition
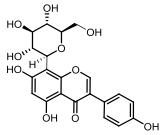 1	**14%**	**23%**	**26%**	n.i.
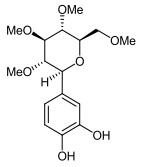 7	n.i.	**14%**	**15%**	**16%**
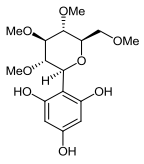 8	n.i.	**15%**	n.i.	**10%**
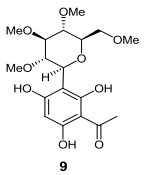 9	n.i.	n.i.	n.i.	**16%**
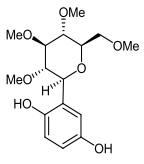 10	n.i.	n.i.	n.i.	**21%**
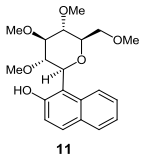 11	n.i.	**16%**	n.i.	**23%**
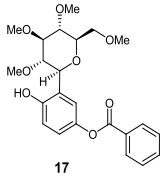 17	**11%**	**24%**	**14%**	**12%**
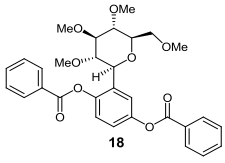 18	n.i.	**18%**	**19%**	**16%**

https://dx.doi.org/10.1021/acs.jmedchem.0c00841
J. Med. Chem. 2020, 63, 11663−11690

Table 3. continued

Compound	α-Glucosidase Inhibition	β-Glucosidase Inhibition	AChE Inhibition	BuChE Inhibition
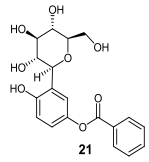 21	n.i.	**17%**	n.i.	n.i.
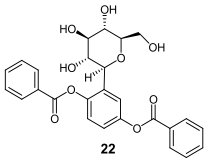 22	n.i.	**18%**	n.i.	**21%**
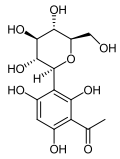 23	n.i.	**24%**	n.i.	**15%**
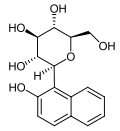 24	**12%**	**23%**	n.i.	**10%**
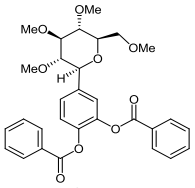 25	n.i.	**27%**	n.i.	**12%**
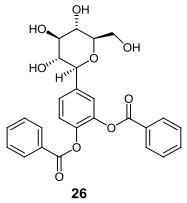 26	n.i.	**17%**	n.i.	**39%**
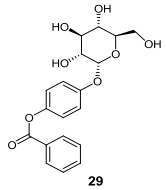 29	**18%**	**19%**	n.i.	**10%**

https://dx.doi.org/10.1021/acs.jmedchem.0c00841
J. Med. Chem. 2020, 63, 11663−11690

Table 3. continued

Compound	α-Glucosidase Inhibition	β-Glucosidase Inhibition	AChE Inhibition	BuChE Inhibition
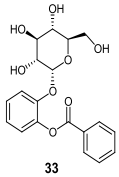 33	**74%** Competitive inhibition K_{ia} = 39 ± 4 μM	**13%**	**10%**	**17%**
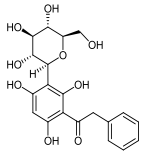 37	n.i.	n.i.	n.i.	**17%**
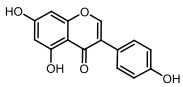 Genistein	**84%** Uncompetitive inhibition K_{ib} = 12 ± 2 μM	**44%** Competitive inhibition K_{ia} = 66 ± 13 μM	**12%**	**41%**

[a] K_{ia}, inhibition constant of the inhibitor binding the free enzyme; K_{ib}, inhibition constant of the inhibitor binding the enzyme−substrate complex; n.i., no inhibition; n.d., not determined.

To complete our analysis, the partition coefficient at physiological pH (log $D_{7.4}$) was also determined for most compounds. Ideally, log D values should be located between 1 and 4 for a good compromise between solubility and membrane permeability, allowing oral availability, good cell permeation, and low metabolic susceptibility.[79] Results are presented in Table 4.

The optimal effective permeability of compound **1** (log P_e > −5.7) indicates that it can cross membrane barriers, which is consistent with the therapeutic use of the plant *G. tenera* in traditional medicine in the form of an antidiabetic tea infusion. Moreover, our results for compounds **7**−**11** suggest that the transformation of the sugar hydroxy groups into methyl ether moieties succeeded at enhancing membrane permeability (see fully unprotected compounds **23** and **24**). Among these compounds is **9**, the per-methylglucosyl derivative of aceto-phloroglucinol, which was found to decrease A*β*-induced Fyn activation with consequent downstream effects in the reduction of Tau hyperphosphorylation. This compound presented an effective permeability (log P_e = −4.74 ± 0.02) and determined log D values (2.3 ± 0.3) that are compatible with the desired pharmacokinetic profile and thus contrasting with its bioactive polyhydroxy analogue **23**.

When applied to compounds with more than one aromatic ring, this sugar per-methylation approach resulted in extremely lipophilic compounds with a tendency to equilibrate or to get retained in biological membranes (compounds **17**, **18**, and **25**). In contrast, with three aromatic rings but without the sugar *O*-methyl groups, compound **26**, another promising hit in our bioactivity experiments, presents an acceptable effective permeability (log P_e = − 5.06 ± 0.08).

Table 4. Calculated Partition Coefficient (*c* Log *P*), Effective Permeability (Log P_e ±SD), and Partition Coefficient at pH 7.4 (Log $D_{7.4}$ ±SD) of the Synthesized Compounds and Genistein[c]

compound no.	*c* log *P*[a,b]	log P_e	log $D_{7.4}$
1	−0.17	−4.63 ± 0.15	−0.1 ± 0.1
7	0.74	−5.33 ± 0.08	1.1 ± 0.1
8	0.58	−5.24 ± 0.17	1.6 ± 0.2
9	1.06	−4.74 ± 0.02	2.3 ± 0.3
10	0.75	−5.52 ± 0.07	n.d.
11	1.96	−4.39 ± 0.04	2.7 ± 0.2
17	2.70	membrane retention over 80%	3.2 ± 0.1
18	3.95	equilibrated	>2.5
21	0.60	−6.35 ± 0.12	<0.5
22	1.93	−5.18 ± 0.61	2.0 ± 0.2
23	−1.23	below detection limit	n.d.
24	−0.44	−6.41 ± 0.24	n.d.
25	3.81	partial membrane retention	>2.5
26	1.95	−5.06 ± 0.08	n.d.
29	0.59	below detection limit	1.0 ± 0.1
33	0.58	−5.85 ± 0.54	0.1 ± 0.3
37	0.13	n.d.	n.d.
genistein	2.45	−4.49 ± 0.04	3.3 ± 0.2
testosterone	2.99	−4.42 ± 0.09	

[a]Calculated using ALOGPS 2.1. [b]Based on *c* log *P* values, **1**, **23**, and **24** are classified as hydrophilic compounds (*c* log *P* < 0); **7**, **8**, **10**, **21**, **29**, **33**, and **37** are classified as moderately lipophilic (*c* log *P* = 0−1); **9**, **11**, **17**, **18**, **22**, **25**, and **26** and genistein are classified as lipophilic compounds (*c* log *P* > 1) (Table 5 and Experimental Section). [c]n.d., not determined.

https://dx.doi.org/10.1021/acs.jmedchem.0c00841
J. Med. Chem. 2020, 63, 11663−11690

DISCUSSION AND CONCLUSIONS

In the present work, we have developed a library of glucosylpolyphenols inspired in the natural product with therapeutic potential **1** and explored their activity against multiple AD and T2D targets, namely, Fyn kinase, Tau hyperphosphorylation, hIAPP, glucosidase, and cholinesterase enzymes. On the path toward their synthesis, we disclosed the feasibility and effectiveness of *C*-glucosylation of polyphenols with different hydroxylation patterns and rationalized the importance of sugar protecting groups in these reactions. Moreover, we present an exception to the Fries-type rearrangement, leading to the *C*-glucosylation of unprotected polyphenols, which afforded compounds **7** and **12**, two important precursors in the synthesis of novel bioactive molecular entities against our targets of interest.

Being structurally less complex and synthesized in only five steps (*vs* nine steps required for the generation of the natural isoflavone **1**), the rationally designed analogue **21** is here presented as a new alterative for tackling hIAPP detrimental effects in T2D and DID. STD-NMR experiments show that compound **21** clearly binds to hIAPP and, in general, with a similar binding epitope to that of compound **1**, which highlights that the absence of the central fused ring system of isoflavone core does not disrupt the binding toward hIAPP. This result opens the door to further exploit this compound as a molecular probe against IAPP-induced pancreatic failure and IAPP-promoted cross-seeding events with Aβ. Even though it is not the right option when it comes to glucosidase or cholinesterase inhibition, our investigation revealed that compound **21** is effective in the prevention of Aβ-induced Fyn activation. Yet, we herein disclose that much simpler *C*-glucosyl polyphenols embody the right scaffold to tackle the chain of processes culminating in Tau hyperphosphorylation. One of these compounds is **9**, embodying a per-*O*-methylglucosyl C−C linked to 2,4,6-trihydroxyacetophenone. It was found to inhibit Aβ-induced Fyn kinase activation and to consequently reduce the levels of hyperphosphorylated Tau. Moreover, it has the right balance between effective permeability and lipophilicity to be orally available and brain penetrant, as revealed in PAMPA and log $D_{7.4}$ determination assays. With the additional advantage of being efficiently synthesized in only two steps, our results indicate that **9** should indeed be regarded as a new promising scaffold for further development against Aβ-induced Tau pathology in AD.

Another promising compound discovered in this study was **26**, with the free glucosyl group C−C linked to catechol dibenzoate. Indeed, it stood out in the PAMPA assay for being one of the polyhydroxy sugar derivatives with potential to cross biological membranes with the desired activity when it comes to Aβ-induced Fyn kinase activation and consequent Tau hyperphosphorylation levels. Furthermore, it was found to be a BuChE inhibitor (39% inhibition at 100 μM). Curiously, when it comes to therapeutic potential through glucosidase inhibition, its *O*-glucosyl catechol monobenzoate analogue **33** was the best within this series. It was able to inhibit α-glucosidase in 74% at 100 μM, as well as β-glucosidase, AChE and BuChE, but only to a lower extent (10−17% at 100 μM). These results illustrate the impact of *C*-glucosylation *vs* *O*-glucosylation in the fine tuning of bioactivity of analogue structures and present both the *C*-glucosyl catechol **26** and O-glucosyl catechol **33** as new lead compounds against DID.

Ultimately, this study strongly evidences the potential of glucosylpolyphenols as therapeutic agents against AD and T2D and offers several lead structures with different hydroxylation patterns and adequate physicochemical profiles for further development against relevant therapeutic targets for both diseases. Very importantly, it shows, for the first time, that *C*-glucosyl polyphenols are promising scaffolds that are able to tackle Aβ-induced Fyn kinase activation with enough efficacy to reduce Tau phosphorylation, thus having the potential to change the paradigm of drug discovery against AD and DID.

EXPERIMENTAL SECTION

Chemistry. HPLC-grade solvents and reagents were obtained from commercial suppliers and were used without further purification. Genistein was purchased from Sigma-Aldrich, while compound **1** was synthesized according to the previously described methodology.[25] Thin-layer chromatography (TLC) was carried out on aluminum sheets (20 × 20 cm) coated with silica gel 60F-254 (0.2 mm thick, Merck) with detection by charring with 10% H_2SO_4 in ethanol. Column chromatography (CC) was performed using silica gel 230−400 mesh (Merck). Melting points were obtained with a SMP3 Melting Point Apparatus, Stuart Scientific, Bibby. Optical rotations were measured with a PerkinElmer 343. Nuclear magnetic resonance (NMR) experiments were recorded on a Bruker Avance 400 spectrometer at 298 K, operating at 100.62 MHz for ^{13}C and at 400.13 MHz for ^{1}H for solutions in $CDCl_3$, $CO(CH_3)_2$, or CD_3OD (Sigma-Aldrich). Chemical shifts are expressed in δ (ppm) and the proton coupling constants J in Hertz (Hz), and spectra were assigned using appropriate COSY, DEPT, HMQC, and HMBC spectra (representative examples are provided in the Supporting Information appendix). The high-resolution mass spectra of new compounds were acquired on a Bruker Daltonics HR QqTOF Impact II mass spectrometer (Billerica, MA, USA). The nebulizer gas (N_2) pressure was set to 1.4 bar, and the drying gas (N_2) flow rate was set to 4.0 L/min at a temperature of 200 °C. The capillary voltage was set to 4500 V and the charging voltage was set to 2000 V. The purity of the final compounds tested was above 95% as confirmed by HPLC-DAD and/or HPLC-DAD-MS.

*General Methodology for the Synthesis of 2,3,4,6-Tetra-O-methyl-β-D-glucopyranosyl)polyphenols (**7**−**10**) and 1-(2,3,4,6-Tetra-O-methyl-β-D-glucopyranosyl)naphthalen-2-ol (**11**).* Methyl 2,3,4,6-tetra-*O*-methyl-α-D-glucopyranoside[39] (1.0 g, 4.0 mmol) and the polyphenol/2-hydroxyhaphthalene (8.0 mmol, 2 equiv) were dissolved in dry MeCN (18 mL). The mixture was stirred in the presence of 0.2 g of drierite, under a N_2 atmosphere, for 10 min at room temperature. Then, TMSOTf (0.73 mL, 4.0 mmol, 1 equiv) was added dropwise at −78 °C. The temperature was kept at −78 °C in the first 30 min and then allowed to increase to room temperature. The mixture was stirred for 18−48 h, after which the reaction was quenched by adding a few drops of triethylamine. The mixture was washed with brine and extracted with EtOAc (3 × 20 mL), and the organic layers were combined, dried over $MgSO_4$, and concentrated under reduced pressure.

*4-(2,3,4,6-Tetra-O-methyl-β-D-glucopyranosyl)benzene-1,2-diol (**7**).* The reaction crude was purified by column chromatography (dichloromethane/MeOH 1:0 → 50:1) to give **7** as a yellowish solid in 63% yield. R_f (dichloromethane/MeOH, 20:1) = 0.31; m.p. = 117.5−118.4 °C; $[\alpha]_D^{20} = -2°$ (c 0.7, $CHCl_3$); ^1H NMR [$(CD_3)_2CO$] δ 6.96 (s, 1H, H-3), 6.84 (d, 1H, J_{ortho} = 8.07 Hz, H-6), 6.78 (br d, 1H, J_{ortho} = 8.07 Hz, H-5), 3.98 (d, 1H, $J_{1'-2'}$ = 9.47 Hz, H-1′), 3.65 (s, 3H, OCH_3), 3.61−3.51 (m, 5H, H-6′a and H-6′b, OCH_3), 3.43−3.39 (m, 1H, H-5′), 3.37 (s, 3H, OCH_3), 3.29−3.24 (m, 2H, H-3′, H-4′), 3.06−3.02 (m, 4H, H-2′, OCH_3). ^{13}C NMR [$(CD_3)_2CO$] δ 144.8 (C-1)*, 144.6 (C-2)*, 131.5 (C-4), 119.31 (C-5), 114.7 (C-6), 114.6 (C-3), 88.34 (C-3′), 85.9 (C-2′), 81.0 (C-1′), 79.8 (C-4′), 78.8 (C-5′), 71.7 (C-6′), 60.0, 59.6, 59.4, 58.5 (OCH_3). *Permutable signals. HRMS-ESI (m/z): $[M + H]^+$ calcd for $C_{16}H_{25}O_7$, 329.1595; found, 329.1597; $[M + Na]^+$ calcd for $C_{16}H_{24}NaO_7$, 351.1414; found, 351.1411.

*2-(2,3,4,6-Tetra-O-methyl-β-D-glucopyranosyl)benzene-1,3,5-triol (**8**).* The reaction crude was purified by column chromatography

https://dx.doi.org/10.1021/acs.jmedchem.0c00841
J. Med. Chem. 2020, 63, 11663−11690

(dichloromethane/MeOH, 1:0 → 40:1) followed by recrystallization in diethyl ether, affording **8** as a white solid in 53% yield. R_f (dichloromethane/MeOH, 20:1) = 0.35; m.p. = 181.5−182.1 °C; $[\alpha]_D^{20}$ = +25° (*c* 0.4, $CHCl_3$); ^{1}H NMR [$(CD_3)_2CO$] δ 8.17 (br s, 1H, OH-5), 7.94 (br s, 2H, OH-1, OH-3), 5.93 (s, 2H, H-4, H-6), 4.77 (d, 1H, $J_{1'-2'}$ = 9.53 Hz, H-1′), 3.62−3.54 (m, 5H, H-6′a and H-6′b, OCH_3), 3.52 (s, 3H, OCH_3), 3.41 (br d, $J_{4'-5'}$ = 9.14 Hz, 1H, H-5′), 3.34 (s, 3H, OCH_3), 3.31−3.19 (m, 3H, H-2′, H-3′, H-4′), 3.10 (s, 3H, OCH_3). ^{13}C NMR [$(CD_3)_2CO$] δ 159.6 (C-5), 158.3 (C-1, C-3), 104.0 (C-2), 96.5 (C-4, C-6), 88.7 (C-3′), 84.7 (C-2′), 80.0 (C-4′), 79.5 (C-5′), 75.3 (C-1′), 71.7 (C-6′), 60.9, 60.6, 60.2, 59.3 (OCH_3). $[M + H]^+$ calcd for $C_{16}H_{25}O_8$, 344.1544; found, 344.1545; $[M + Na]^+$ calcd for $C_{16}H_{24}NaO_8$, 367.1363; found, 367.1369.

1-[2,4,6-Trihydroxy-3-(2,3,4,6-tetra-O-methyl-β-D-glucopyranosyl)phenyl]ethan-1-one (***9***). The reaction crude was purified by column chromatography (dichloromethane/MeOH, 1:0 → 50:1) to give **9** as a colorless oil in 46% yield. R_f (dichloromethane/MeOH, 20:1) = 0.38 $[\alpha]_D^{20}$ = +91° (*c* 0.4, $CHCl_3$); ^{1}H NMR ($CDCl_3$) δ 8.11 (br s, 1H, OH), 5.91 (br s, 1H, H-5), 4.73 (d, 1H, $J_{1'-2'}$ = 9.80 Hz, H-1′), 3.68−3.64 (m, 5H, H-6′a and H-6′b, OCH_3), 3.58 (s, 3H, OCH_3), 3.48−3.44 (m, 4H, H-5′, OCH_3), 3.35−3.26 (m, 6H, H-2′, H-3′, H-4′, OCH_3), 2.66 (CH_3-Ac); ^{13}C NMR ($CDCl_3$) δ 203.9 (C═O), 164.4 (C-2), 161.8 (C-4)*, 160.1 (C-6)*, 106.0 (C-1), 102.3 (C-5), 97.2 (C-3), 87.7 (C-3′), 84.9 (C-2′), 79.0 (C-5′), 78.8 (C-4′), 75.1 (C-1′), 71.0 (C-6′), 61.1, 61.0, 60.7, 59.2 (OCH_3). *Permutable signals. HRMS-ESI (*m*/*z*): $[M + H]^+$ calcd for $C_{18}H_{27}O_9$, 387.1660; found, 387.1600; $[M + Na]^+$ calcd for $C_{18}H_{26}NaO_9$, 409.1469; found, 409.1473.

2-(2,3,4,6-Tetra-O-methyl-β-D-glucopyranosyl)benzene-1,4-diol (***10***). The reaction crude was purified by column chromatography (dichloromethane/MeOH, 1:0 → 40:1), followed by recrystallization in diethyl ether to afford **10** as a white solid in 37% yield. R_f (dichloromethane/MeOH 20:1) = 0.34; m.p. = 124.5−125.0 °C; $[\alpha]_D^{20}$ = +18° (*c* 0.5, $CHCl_3$); ^{1}H NMR [$(CD_3)_2CO$] δ 7.77 (s, 1H, OH-1), 7.36 (s, 1H, OH-4), 6.74 (s, 1H, H-3), 6.69−6.64 (m, 2H, H-5, H-6), 4.38 (d, 1H, $J_{1'-2'}$ = 9.59 Hz, H-1′), 3.66−3.56 (m, 5H, OCH_3, H-6′a and H-6′b), 3.52 (s, 3H, OCH_3), 3.41 (br d, 1H, $J_{5'-4'}$ = 8.11 Hz, H-5′), 3.34 (s, 3H, OCH_3), 3.29−3.21 (m, 2H, H-3′, H-4′), 3.14 (t, 1H, $J_{2'-1'\sim2'-3'}$ = 9.72 Hz, H-2′), 3.09 (s, 3H, OCH_3). ^{13}C NMR [$(CD_3)_2CO$] δ 150.9 (C-4), 148.7 (C-1), 126.4 (C-2), 117.5 (C-6)*, 116.0 (C-5)*, 115.3 (C-3), 88.7 (C-3′), 85.4 (C-2′), 80.0 (C-4′), 79.2 (C-5′), 78.0 (C-1′), 71.0 (C-6′), 60.5, 60.2, 60.1, 58.9 (OCH_3). *Permutable signals. HRMS-ESI (*m*/*z*): $[M + H]^+$ calcd for $C_{16}H_{25}O_7$, 329.1595; found, 329.1582; $[M + Na]^+$ calcd for $C_{16}H_{24}NaO_7$, 351.1414; found, 351.1395.

1-(2,3,4,6-Tetra-O-methyl-β-D-glucopyranosyl)naphthalen-2-ol (***11***). The reaction crude was purified by column chromatography (Hex/dichloromethane, 1:1 → dichloromethane/MeOH, 100:1) to give **11** as a yellow oil in 66% yield. R_f (Hex/EtOAc) = 0.58; $[\alpha]_D^{20}$ = +89° (*c* 1.0, $CHCl_3$); ^{1}H NMR ($CDCl_3$) δ (ppm) 8.54 (s, 1H, OH-2), 7.97 (d, 1H, J_{ortho} = 7.46 Hz, H-8), 7.72−7.68 (m, 2H, H-4, H-5), 7.43 (t, 1H, J_{ortho} = 7.64 Hz, H-7), 7.28 (t, 1H, J_{ortho} = 7.39 Hz, H-6), 7.14 (d, 1H, J_{ortho} = 8.83 Hz, H-3), 5.24 (d, 1H, $J_{1'-2'}$ = 9.65 Hz, H-1′), 3.67−3.58 (m, 8H, 2 × OCH_3, H-6′a and H-6′b), 3.51−3.45 (m, 3H, H-2′, H-4′, H-5′), 3.43−3.27 (m, 4H, H-3′, OCH_3), 2.70 (s, 3H, OCH_3). ^{13}C NMR ($CDCl_3$) δ (ppm) 154.5 (C-2), 132.6 (C-8a), 130.3 (C-4), 128.7 (C-4a), 128.3 (C-5), 126.4 (C-7), 123.0 (C-6), 122.6 (C-8), 119.7 (C-3), 114.7 (C-1), 87.8 (C-3′), 84.2 (C-2′), 78.7 (C-4′), 78.6 (C-5′), 76.7 (C-1′), 70.5 (C-6′), 61.0, 60.7, 60.2, 59.3 (OCH_3). $[M + H]^+$ calcd for $C_{20}H_{27}O_6$, 363.1802; found, 363.1796; $[M + Na]^+$ calcd for $C_{20}H_{26}NaO_6$, 385.1622; found, 385.1624.

4-(2,3,4,6-Tetra-O-benzyl-β-D-glucopyranosyl)benzene-1,2-diol (***12***) *and 2-(2,3,4,6-Tetra-O-benzyl-α-D-glucopyranosyloxy)phenol* (***31***). To a solution of 2,3,4,6-tetra-*O*-benzyl-α-/β-D-glucopyranose (**4**, 2 g, 3.70 mmol) in dry dichloromethane (50 mL), catechol (0.81 g, 7.40 mmol, 2 equiv) in dry MeCN (10 mL) was added, together with drierite (0.25 g), under a N_2 atmosphere. The mixture was stirred for 5 min at room temperature, which was then lowered to −78 °C. TMSOTf (0.68 mL, 3.70 mmol, 1 equiv) was added in a dropwise manner. After stirring for 30 min, the mixture was stirred for 64 h at 40 °C. The reaction was stopped by adding a few drops of triethylamine; then, the mixture was filtered through a pad of Celite, washed with dichloromethane, and concentrated under vacuum. The residue was purified by column chromatography (1:0 → 15:1 cyclohexane/AcOEt), affording compound **12** in 6% yield as a colorless oil and compound **18** as a white solid in 35% yield.

4-(2,3,4,6-Tetra-O-benzyl-β-D-glucopyranosyl)benzene-1,2-diol (***12***). R_f (hexane/AcOEt, 4:1) = 0.14; $[\alpha]_D^{20}$ = −2° (*c* 0.1, $CHCl_3$); ^{1}H NMR ($CDCl_3$) δ (ppm) 7.37−7.16 (m, 18H, benzyl aromatics), 6.99−6.97 (m, 2H, benzyl aromatics), 6.85−6.82 (m, 2H, H-3, H-6), 6.79−6.76 (m, 1H, H-5), 5.00, 4.96 (part A_1 of A_1B_1 system, 1H, J_{A1-B1} = 11.23 Hz, Ph-CH_2), 4.90 (m, 2H, part B_1 of A_1B_1 system, part A_2 of A_2B_2 system, Ph-CH_2), 4.64−4.55 (m, 3H, part B_2 of A_2B_2 system, Ph-CH_2 and Ph-CH_2), 4.40, 4.36 (part A_3 of A_3B_3 system, 1H, J_{A3-B3} = 10.28 Hz, Ph-CH_2), 4.12 (d, 1H, $J_{1'-2'}$ = 9.63 Hz, H-1′), 3.92, 3.88 (part B_3 of A_3B_3 system, 1H, J_{A3-B3} = 10.27 Hz, Ph-CH_2), 3.81−3.72 (m, 4H, H-3′, H-4′, H-6′a and H-6′b), 3.65−3.61 (m, 1H, H-5′), 3.51 (t, 1H, $J_{2'-3'\sim2'-1'}$ = 9.15 Hz, H-2′). ^{13}C NMR ($CDCl_3$) δ (ppm) 144.7 (C-2), 143.2 (C-1), 138.6, 138.1, 137.8, 137.7 (benzyl C_q-aromatics), 131.3 (C-4), 128.4−127.6 (benzyl *C*H-aromatics), 120.7 (C-5), 115.2 (C-6), 114.9 (C-3), 86.7 (C-3′), 83.9 (C-2′), 81.7 (C-1′), 79.0 (C-5′), 78.4 (C-4′), 75.7, 75.1, 74.8, 73.5 (CH_2-Ph), 69.2 (C-6′). HRMS-ESI (*m*/*z*): $[M + H]^+$ calcd for $C_{40}H_{41}O_7$, 633.2847; found, 633.2853; $[M + Na]^+$ calcd for $C_{40}H_{40}NaO_7$, 655.2666; found, 655.2667.

2-(2,3,4,6-Tetra-O-benzyl-α-D-glucopyranosyloxy)phenol (***31***). R_f (Hex/AcOEt, 4:1) = 0.58; m.p. = 104.2−106.0 °C; $[\alpha]_D^{20}$ = +68° (*c* 1.0, $CHCl_3$); ^{1}H NMR ($CDCl_3$) δ (ppm) 7.37−7.22 (m, 17H, benzyl aromatics), 7.18−7.15 (m, 3H, benzyl aromatics), 7.09 (d, 1H, J_{ortho} = 8.06 Hz, H-3), 7.02−6.95 (m, 2H, H-4, H-6), 6.75 (dt, 1H, J_{ortho} = 7.68 Hz, J_{meta} = 1.58 Hz, H-5), 4.99−4.90 (m, 3H, H-1′, Ph-CH_2), 4.87−4.81 (m, 2H, part A_1 of A_1B_1 system, part A_2 of A_2B_2 system, Ph-CH_2), 4.72, 4.68 (part A_2 of A_2B_2 system, 1H, J_{A2-B2} = 11.96 Hz, Ph-CH_2), 4.64, 4.60 (part A_3 of A_3B_3 system, 1H, J_{A3-B3} = 12.08 Hz, Ph-CH_2), 4.55, 4.51 (part B_1 of A_1B_1 system, 1H, J_{A1-B1} = 11.04 Hz, Ph-CH_2), 4.50, 4.46 (part B_3 of A_3B_3 system, 1H, J_{A3-B3} = 11.93 Hz, Ph-CH_2), 4.21−4.14 (m, 2H, H-3′, H-4′), 3.81−3.69 (m, 3H, H-6′a and H-6′b, H-5′), 3.67 (dd, 1H, $J_{1'-2'}$ = 3.53 Hz, $J_{2'-3'}$ = 9.65 Hz, H-2′). ^{13}C NMR ($CDCl_3$) δ (ppm) 148.6 (C-2), 145.2 (C-1), 138.4, 138.1, 137.8, 137.0 (benzyl C_q-aromatics), 128.5−127.7 (benzyl *C*H-aromatics), 125.2 (C-4), 120.3 (C-5)*, 119.9 (C-3)*, 115.8 (C-6), 101.1 (C-1′), 81.9 (C-3′), 79.0 (C-2′), 77.5 (C-5′), 75.6, 75.0, 74.2, 73.5 (CH_2-Ph), 71.5 (C-4′), 68.3 (C-6′). *Permutable signals. HRMS-ESI (*m*/*z*): $[M + H]^+$ calcd for $C_{40}H_{41}O_7$, 633.2847; found, 633.2853; $[M + Na]^+$ calcd for $C_{40}H_{40}NaO_7$, 655.2666; found, 655.2667.

2-(2,3,4,6-Tetra-O-benzyl-β-D-glucopyranosyl)benzene-1,3,5-triol (***13***). To a solution of 2,3,4,6-tetra-*O*-benzyl-α-/β-D-glucopyranose (2 g, 3.70 mmol) in dry dichloromethane (50 mL), 2,4,6-trihydroxyacetophenone (0.93 g, 7.40 mmol, 2 equiv) in dry MeCN (50 mL) was added, together with drierite (0.25 g), under a N_2 atmosphere. The mixture was stirred for 5 min at room temperature, which was then lowered to −78 °C. TMSOTf (0.68 mL, 3.70 mmol, 1 equiv) was added in a dropwise manner. After stirring for 30 min, the mixture was left at room temperature under stirring overnight. The reaction was stopped by adding a few drops of triethylamine; then, dichloromethane was evaporated and the mixture was washed with brine and extracted with ethyl acetate (3 × 50 mL). The organic layers were combined, dried over $MgSO_4$, filtered, and concentrated under vacuum. The residue was purified by column chromatography (10:1 → 5:1 cyclohexane/acetone), affording compound **13** in 42% yield as a colorless oil. R_f (cyclohexane/acetone, 3:2) = 0.41; $[\alpha]_D^{20}$ = +12° (*c* 0.2, $CHCl_3$); ^{1}H NMR ($CDCl_3$) δ (ppm) 7.35−7.19 (m, 16H, benzyl aromatics), 7.16−7.12 (m, 2H, benzyl aromatics), 7.08−7.04 (m, 2H, benzyl aromatics), 6.02 (s, 2H, H-4, H-6), 4.93 (A_1B_1 system, 2H, Ph-CH_2), 4.83−4.79 (m, 2H, H-1′, part A_2 of A_2B_2 system, Ph-CH_2), 4.65, 4.63 (part A_3 of A_3B_3 system, 1H, J_{A3-B3} = 10.21 Hz, Ph-CH_2), 4.59, 4.55 (part A_4 of A_4B_4 system, 1H, J_{A4-B4} = 12.05 Hz, 1H, Ph-CH_2), 4.54, 4.50 (part B_3 of A_3B_3 system, 1H, J_{A3-B3} = 10.91 Hz, Ph-CH_2), 4.45, 4.41 (part B_4 of A_4B_4 system, 1H, J_{A4-B4} = 12.05 Hz, Ph-CH_2), 3.88 (t, 1H, $J_{4'-3'\sim4'-5'}$ = 8.80 Hz, H-4′), 3.79−3.65 (m, 4H, H-2′, H-3′, H-6′a and H-6′b), 3.56 (br d, 1H, $J_{5'-4'}$ = 9.71 Hz, H-5′). ^{13}C NMR ($CDCl_3$) δ (ppm) 157.3

https://dx.doi.org/10.1021/acs.jmedchem.0c00841
J. Med. Chem. 2020, 63, 11663−11690

(C-1, C-3), 156.3 (C-5), 138.4, 138.9, 137.6, 136.4 (benzyl C_q-aromatics), 128.8−127.5 (benzyl *C*H-aromatics), 104.1 (C-2), 97.8 (C-4, C-6), 86.2 (C-3′), 82.7 (C-2′), 78.7 (C-5′), 77.2 (C-4′), 76.2 (C-1′), 75.6, 75.5, 75.2, 73.4 (*C*H_2-Ph), 67.6 (C-6′). HRMS-ESI (*m*/*z*): $[M + H]^+$ calcd for $C_{40}H_{41}O_8$, 649.2796; found, 649.2806; $[M + Na]^+$ calcd for $C_{40}H_{40}NaO_8$, 671.2615; found, 671.2621.

*1-[2,4,6-Trihydroxy-3-(2,3,4,6-tetra-O-benzyl-β-D-glucopyranosyl)phenyl]ethan-1-one (**14**).* Synthesis and characterization as described in the literature.[25]

*2-(2,3,4,6-Tetra-O-benzyl-β-D-glucopyranosyl)benzene-1,4-diol (**15**) and 4-(2,3,4,6-Tetra-O-benzyl-α-/β-D-glucopyranosyloxy)-phenol (**27α,β**).* To a solution of 1-*O*-acetyl-2,3,4,6-tetra-*O*-benzyl-α-/-β-D-glucopyranose (**6**, 2.16 g, 3.70 mmol) in dry dichloromethane (50 mL), hydroquinone (0.61 g, 5.55 mmol, 1.5 equiv) in dry MeCN (10 mL) was added, together with drierite (0.25 g), under a N_2 atmosphere. The mixture was stirred for 5 min at room temperature, which was then lowered to 0 °C. $BF_3{\cdot}Et_2O$ (1.1 mL, 3.70 mmol, 1 equiv) was added in a dropwise manner. After stirring for 30 min, the temperature was raised to 40 °C and the mixture was stirred for 44 h. The reaction was stopped by adding a few drops of triethylamine; then, the mixture was filtered through a pad of Celite, washed with dichloromethane, and concentrated under vacuum. The residue was purified by column chromatography (50:1 → 30:1 toluene/acetone) followed by recrystallization in diethyl ether to afford compound **15** in 8% yield as a white solid and **27α,β** isolated as a white solid with α/β ratio = 4:1 in 36% yield.

*2-(2,3,4,6-Tetra-O-benzyl-β-D-glucopyranosyl)benzene-1,4-diol (**15**).* R_f (toluene/acetone, 10:1) = 0.43; m.p. = 107.2−109.1 °C; $[\alpha]_D^{20}$ = +16° (*c* 0.3, $CHCl_3$); ^1H NMR [$CO(CD_3)_2$] δ (ppm) 7.40−7.19 (m, 18H, benzyl aromatics), 7.10−7.07 (m, 2H, benzyl aromatics), 6.86 (d, 1H, J_{meta} = 2.15 Hz, H-3), 6.75−6.69 (m, 2H, H-5, H-6), 4.97, 4.93 (part A_1 of A_1B_1 system, 1H, J_{A1-B1} = 11.24 Hz, Ph-CH_2), 4.89−4.87 (m, part B_1 of A_1B_1 system, part A_2 of A_2B_2 system, 2H, Ph-CH_2), 4.67−4.53 (m, 4H, part B_2 of A_2B_2 system, Ph-CH_2, H-1′), 4.46, 4.42 (A_3 of A_3B_3 system, 1H, J_{A3-B3} = 10.41 Hz, Ph-CH_2), 4.01, 3.97 (B_3 of A_3B_3 system, 1H, J_{A3-B3} = 10.45 Hz, Ph-CH_2), 3.84−3.75 (m, 4H, H-3′, H-4′, H-6′a and H-6′b), 3.68−3.64 (m, 2H, H-2′, H-5′). ^{13}C NMR [$CO(CD_3)_2$] δ (ppm) 151.2 (C-1), 149.2 (C-4), 140.0, 139.5, 139.4, 139.0 (benzyl C_q-aromatics), 129.0−128.0 (benzyl *C*H-aromatics), 126.3 (C-2), 117.8 (C-6), 116.4 (C-5), 116.1 (C-3), 87.0 (C-3′), 83.5 (C-2′), 79.6 (C-5′), 78.8 (C-1′), 78.7 (C-4′), 75.8, 75.3, 75.2, 73.7 (*C*H_2-Ph), 69.5 (C-6′). HRMS-ESI (*m*/*z*): $[M + H]^+$ calcd for $C_{40}H_{41}O_7$, 633.2851; found, 633.2853; $[M + Na]^+$ calcd for $C_{40}H_{40}NaO_7$, 655.2666; found, 655.2671.

*4-(2,3,4,6-Tetra-O-benzyl-α-/β-D-glucopyranosyloxy)phenol (**27α,β**).* R_f (toluene/acetone, 10:1) = 0.50; m.p. = 138.4−141.2 °C; $[\alpha]_D^{20}$ = +53° (*c* 0.4, $CHCl_3$); ^1H NMR ($CDCl_3$) δ 7.38−7.24 (m, 95H, C*H*-Ph), 3.18−3.12 (m, 5H, C*H*-Ph), 6.92−6.88 (m, 10H, H-3$_\alpha$, H-3$_\beta$, H-5$_\alpha$, H-5$_\beta$), 6.62 (d, 10H, J_{ortho} = 8.73 Hz, H-2$_\alpha$, H-2$_\beta$, H-6$_\alpha$, H-6$_\beta$), 5.32 (d, 4H, $J_{1'-2'}$ = 3.33 Hz, H-1′$_\alpha$), 5.06, 5.02 (part A_1 of A_1B_1 system, 5H, J_{A1-B1} = 10.81 Hz, CH_2-Ph), 4.97, 4.93 (part A_2 of A_2B_2 system, 1H, J_{A2-B2} = 10.90 Hz, CH_2-Ph), 4.89−4.76 (m, 16H, H-1′$_\beta$, part B_1 of A_1B_1 system, part B_2 of A_2B_2 system, CH_2-Ph), 4.69, 4.65 (part A_3 of A_3B_3 system, 4H, J_{A3-B3} = 11.98 Hz, CH_2-Ph), 4.59−4.47 (m, 11H, CH_2-Ph), 4.40, 4.36 (part B_3 of A_3B_3 system, 4H, J_{A3-B3} = 11.99 Hz, CH_2-Ph), 4.20 (t, 4H, $J_{3'-2'}$ = $J_{3'-4'}$ = 9.28 Hz, H-3′$_\alpha$), 3.93 (br d, 4H, $J_{5'-4'}$ = 9.59 Hz, H-5′$_\alpha$), 3.78−3.63 (m, 17H, H-2′$_\alpha$, H-4′$_\alpha$, H-2′$_\beta$, H-3′$_\beta$, H-4′$_\beta$, H-5′$_\beta$, H-6′a$_\alpha$, H-6′a$_\beta$), 3.57 (br d, 5H, $J_{6'a-6'b}$ = 9.94 Hz, H-6′b$_\alpha$, H-6′b$_\beta$). ^{13}C NMR ($CDCl_3$) δ 151.6 (C-4$_\beta$), 151.3 (C-1$_\beta$), 151.2 (C-4$_\alpha$), 150.5 (C-1$_\alpha$), 138.7, 138.5, 138.2, 137.9, 137.9, 137.7 (C_q-Ph), 128.6−127.8 (C*H*-Ph), 118.5 (C-3$_\beta$, C-5$_\beta$), 118.3 (C-3$_\alpha$, C-5$_\alpha$), 116.1 (C-2$_\beta$, C-6$_\beta$), 116.1 (C-2$_\alpha$, C-6$_\alpha$), 102.8 (C-1′$_\beta$), 96.4 (C-1′$_\alpha$), 84.6 (C-2′$_\beta$), 82.1 (C-3′$_\beta$), 82.0 (C-3′$_\alpha$), 79.8 (C-2′$_\alpha$), 77.8 (C-4′$_\beta$), 77.5 (C-4′$_\alpha$), 75.9 75.2, 75.2 (*C*H_2-Ph), 73.5, 73.5, 73.4 (*C*H_2-Ph), 70.7 (C-5′$_\alpha$), 70.2 (C-5′$_\beta$), 68.9 (C-6′$_\beta$), 68.3 (C-6′$_\alpha$). HRMS-ESI (*m*/*z*): $[M + H]^+$ calcd for $C_{40}H_{41}O_7$, 633.2847; found, 633.2847; $[M + Na]^+$ calcd for $C_{40}H_{40}NaO_7$, 655.2666; found, 655.2669.

*1-(2,3,4,6-Tetra-O-benzyl-β-D-glucopyranosyl)naphthalen-2-ol (**16**).* To a solution of 2,3,4,6-tetra-*O*-benzyl-α-D-glucopyranosyl trichloroacetimidate (**5**, 1.27 g, 1.85 mmol) in dry dichloromethane (10 mL), 2-naphthol (0.222 g, 0.83 equiv) was added in the presence of activated molecular sieves (3 Å), at 0 °C, under a N_2 atmosphere. TMSOTf (0.33 mL, 1.85 mmol, 1 equiv) was then added in a dropwise manner and the mixture stirred for 20 h at room temperature. The reaction was stopped by adding a few drops of triethylamine; then, the mixture was filtered through a pad of Celite, washed with dichloromethane, and concentrated under vacuum. The residue was purified by column chromatography (p. ether/EtOAc, 1:0 → 15:1), affording compound **16** as a colorless oil in 43% yield. R_f (hexane/EtOAc, 5:1) = 0.47; $[\alpha]_D^{20}$ = +3° (*c* 0.3, $CHCl_3$); ^1H NMR ($CDCl_3$) δ (ppm) 8.73 (br s, 1H, OH-2), 8.07 (d, 1H, J_{ortho} = 7.75 Hz, H-8), 7.87−7.79 (m, 2H, H-4, H-5), 7.48−6.95 (m, 22H, benzyl aromatics, H-6, H-7), 6.33 (d, 1H, J_{ortho} = 7.13 Hz, H-3), 5.47 (d, 1H, $J_{1'-2'}$ = 9.68 Hz, H-1′), 5.06−5.46 (m, 6H, Ph-CH_2), 4.25−3.41 (m, 8H, H-2′, H-3′, H-4′, H-5′, H-6′a and H-6′b, Ph-CH_2). ^{13}C NMR ($CDCl_3$) δ (ppm) 154.8 (C-2), 138.7, 138.1, 137.8, 136.8, (benzyl C_q-aromatics), 132.7 (C-8a), 130.5 (C-4), 128.7−127.5 (benzyl *C*H-aromatics, C-4a, C-5), 126.7 (C-7), 123.2 (C-6), 122.9 (C-8), 119.8 (C-3), 114.6 (C-1), 86.2 (C-3′), 81.9 (C-2′), 78.7 (C-4′), 77.8 (C-5′), 77.1 (*C*H_2-Ph), 76.9 (C-1′), 75.7, 75.4, 73.4 (*C*H_2-Ph), 67.8 (C-6′). HRMS-ESI (*m*/*z*): $[M + H]^+$ calcd for $C_{44}H_{43}O_6$, 667.3054; found, 667.3047; $[M + Na]^+$ calcd for $C_{44}H_{42}NaO_6$, 689.2874; found, 689.2874.

*4-Hydroxy-3-(2,3,4,6-tetra-O-methyl-β-D-glucopyranosyl)-benzen-1-yl Benzoate (**17**) and 3-(2,3,4,6-Tetra-O-methyl-β-D-glucopyranosyl)benzen-1,4-diyl Dibenzoate (**18**).* Compound **10** (0.50 g, 1.55 mmol, 1 equiv) was dissolved in dry dichloromethane (21 mL) together with imidazole (0.12 g, 1.71 mmol, 1.1 equiv) and DMAP (cat.). After stirring for 10 min at 0 °C, benzoyl chloride (0.2 mL, 1.71 mmol, 1.1 equiv) was added dropwise. The reaction mixture was stirred at room temperature for 66 h, after which it was washed with brine and extracted with dichloromethane (2 × 20 mL). The organic layers were combined, dried over $MgSO_4$, and concentrated under reduced pressure. The residue was purified by column chromatography (p. ether/EtOAc, 1:0 → 2:1), affording compound **17** as a colorless oil in 65% yield and compound **18** as a white solid in 22% yield.

*4-Hydroxy-3-(2,3,4,6-tetra-O-methyl-β-D-glucopyranosyl)-benzen-1-yl Benzoate (**17**).* R_f (p. ether/EtOAc, 2:1) = 0.31; $[\alpha]_D^{20}$ = +16° (*c* 0.7, MeOH); ^1H NMR ($CDCl_3$) δ 8.18 (d, 2H, J_{ortho} = 7.38 Hz, H-2′, H-6′), 7.75 (s, 1H, OH-4), 7.62 (t, 1H, J_{ortho} = 7.38 Hz, H-4′), 7.50 (t, 2H, J_{ortho} = 7.61 Hz, H-3′, H-5′), 7.08−7.04 (m, 2H, H-2, H-6), 6.95 (d, 1H, J_{ortho} = 6.95 Hz, H-5), 4.32 (d, 1H, $J_{1''-2''}$ = 9.60 Hz, H-1″), 3.67 (s, 3H, OCH_3), 3.64−3.62 (m, 2H, H-6″a and b), 3.58 (s, 3H, OCH_3), 3.43−3.40 (m, 4H, H-5″, OCH_3), 3.36−3.28 (m, 2H, H-3″, H-4″), 3.24 (s, 3H, OCH_3), 3.21−3.19 (m, 1H, H-2″). ^{13}C NMR ($CDCl_3$) δ 165.6 (C═O), 152.7 (C-4), 144.0 (C-1), 133.6 (C-4′), 130.2 (C-2′, C-6′), 129.8 (C-1′), 128.6 (C-3′, C-5′), 125.0 (C-3), 122.4 (C-6), 121.3 (C-2), 118.1 (C-5), 88.2 (C-3″), 84.8 (C-2″), 79.2 (C-4″), 79.1 (C-1″), 78.8 (C-5″), 70.9 (C-6″), 61.0, 60.7, 59.4 (OCH_3). HRMS-ESI (*m*/*z*): $[M + H]^+$ calcd for $C_{23}H_{29}O_8$, 433.1857; found, 433.1861; $[M + Na]^+$ calcd for $C_{23}H_{28}NaO_8$, 455.1676; found, 455.1678.

*3-(2,3,4,6-Tetra-O-methyl-β-D-glucopyranosyl)benzene-1,4-diyl Dibenzoate (**18**).* R_f (p. ether/EtOAc, 2:1) = 0.47; m.p. = 102.6−103.8 °C; $[\alpha]_D^{20}$ = +5° (*c* 0.7, $CHCl_3$); ^1H NMR ($CDCl_3$) δ 8.24−8.20 (m, 4H, H-2′, H-6′), 7.65 (t, 2H, J_{ortho} = 6.99 Hz, H-4′), 7.56−7.51 (m, 4H, H-3′, H-5′), 7.40 (d, 1H, J_{meta} = 2.22 Hz, H-3), 7.32−7.24 (m, 2H, H-5, H-6), 4.43 (d, 1H, $J_{1''-2''}$ = 8.77 Hz, H-1″), 3.58 (s, 3H, OCH_3), 3.56 (br s, 1H, H-6″a), 3.51 (s, 3H, OCH_3), 3.48−3.44 (m, 1H, H-6″b), 3.39−3.33 (m, 4H, OCH_3, H-5″), 3.23−3.12 (m, 6H, OCH_3, H-2″, H-3″, H-4″). ^{13}C NMR ($CDCl_3$) δ 165.1 (C═O), 164.7 (C═O), 148.5 (C-1), 146.3 (C-4), 133.8, 133.6 (C-4′), 132.8 (C-3), 130.4, 130.3 (C-2′, C-6′), 129.8, 129.5 (C-1′), 128.7 (C-3′, C-5′), 124.0 (C-5), 122.1 (C-6), 121.9 (C-2), 88.5 (C-3″), 85.5 (C-2″), 80.0 (C-4″), 79.4 (C-5″), 76.2 (C-1″), 71.8 (C-6″), 60.9, 60.7, 60.6, 59.5 (OCH_3). HRMS-ESI (*m*/*z*): $[M + H]^+$ calcd for $C_{30}H_{33}O_9$, 537.2119; found, 537.2108; $[M + Na]^+$ calcd for $C_{30}H_{32}NaO_9$, 559.1939; found, 559.1900.

*4-Hydroxy-3-(2,3,4,6-tetra-O-benzyl-β-D-glucopyranosyl)-benzen-1-yl Benzoate (**19**) and 3-(2,3,4,6-Tetra-O-benzyl-β-D-glucopyranosyl)benzen-1,4-diyl Dibenzoate (**20**).* Compound **15** (0.48 g, 0.77 mmol) was dissolved in dry dichloromethane (50 mL) together with imidazole (0.081 g, 1.18 mmol, 1.5 equiv) and DMAP

https://dx.doi.org/10.1021/acs.jmedchem.0c00841
J. Med. Chem. 2020, 63, 11663−11690

(cat.). After stirring for 10 min at 0 °C, benzoyl chloride (1.4 mL, 1.18 mmol, 1.5 equiv) was added dropwise. The reaction mixture was stirred at room temperature for 72 h, after which it was washed with brine and extracted with dichloromethane (2 × 20 mL). The organic layers were combined, dried over $MgSO_4$, and concentrated under reduced pressure. The residue was purified by column chromatography (hexane/acetone, 1:0 → 10:1), affording compound **19** as a colorless oil in 53% yield and compound **20** as a white solid in 38% yield.

*4-Hydroxy-3-(2,3,4,6-tetra-O-benzyl-β-D-glucopyranosyl)-benzen-1-yl Benzoate (**19**).* R_f (hexane/acetone, 3:1) = 0.22; $[\alpha]_D^{20}$ = +25° (*c* 0.1, $CHCl_3$); ^1H NMR ($CDCl_3$) δ (ppm) 8.18 (d, 2H, J_{ortho} = 7.46 Hz, H-2′, H-6′), 7.64 (t, 1H, J_{ortho} = 7.20 Hz, H-4′), 7.51 (t, 2H, J_{ortho} = 7.83 Hz, H-3′, H-5′), 7.35−7.07 (m, 22H, benzyl aromatics, H-2, H-6), 6.98 (d, 1H, J_{ortho} = 7.73 Hz, H-5), 4.98−4.89 (m, A_1B_1 system, 2H, Ph-CH_2), 4.87, 4.83 (part A_2 of A_2B_2 system, 1H, J_{A2-B2} = 10.85 Hz, Ph-CH_2), 4.63−4.47 (m, 4H, part B_2 of A_2B_2 system, part A_3 of A_3B_3 system, Ph-CH_2), 4.44 (d, 1H, $J_{1''-2''}$ = 9.18 Hz, H-1″), 4.03, 3.99 (part A_3 of A_3B_3 system, 1H, J_{A3-B3} = 10.15 Hz, Ph-CH_2), 3.89 (t, 1H, $J_{4''-3''\sim4''-5''}$ = 9.04 Hz, H-4″), 3.80−6.69 (m, 4H, H-2″, H-3″, H-6″a and H-6″b), 3.59 (br d, 1H, $J_{5''-4''}$ = 9.72 Hz, H-5″). ^{13}C NMR ($CDCl_3$) δ (ppm) 165.3 (C═O), 153.0 (C-4), 143.7 (C-1), 138.5, 137.9, 137.8, 137.0 (benzyl C_q-aromatics), 133.5 (C-4′), 130.1 (C-2′, C-6′), 129.6 (C-1′), 128.8−127.6 (C-3′, C-5′, benzyl CH-aromatics), 124.1 (C-3), 122.6 (C-6), 121.9 (C-2), 118.3 (C-5), 86.1 (C-3″), 81.7 (C-2″), 80.5 (C-5″), 78.6 (C-1″), 77.3 (C-4″), 75.6, 75.6, 75.2, 73.4 (Ph-CH_2), 67.8 (C-6″). HRMS-ESI (*m*/*z*): $[M + H]^+$ calcd for $C_{47}H_{45}O_8$, 737.3109; found, 737.3116; $[M + Na]^+$ calcd for $C_{47}H_{44}NaO_8$, 759.2928; found, 759.2936.

*3-(2,3,4,6-Tetra-O-benzyl-β-D-glucopyranosyl)benzen-1,4-diyl Dibenzoate (**20**).* R_f (hexane/acetone, 3:1) = 0.34; $[\alpha]_D^{20}$ = +11° (*c* 0.2, $CHCl_3$); ^1H NMR ($CDCl_3$) δ (ppm) 8.21, 8.16 (d, 4H, J_{ortho} = 7.48 Hz, H-2′, H-6′), 7.64, 7.59 (t, 2H, J_{ortho} = 7.31 Hz, H-4′), 7.52, 7.45 (t, 4H, J_{ortho} = 7.69 Hz, H-3′, H-5′), 7.35−7.05 (m, 23H, benzyl aromatics, H-2, H-5, H-6), 4.91−4.82 (A_1B_1 system, 2H, J_{A1-B1} = 10.82 Hz, Ph-CH_2), 4.81, 4.87 (part A_2 of A_2B_2 system, 1H, J_{A2-B2} = 10.73 Hz, Ph-CH_2), 4.55−4.46 (m, 5H, H-1″, part B_2 of A_2B_2 system, part A_3 of A_3B_3 system, Ph-CH_2), 4.22, 4.18 (part B_3 of A_3B_3 system, 1H, J_{A3-B3} = 10.75 Hz, Ph-CH_2), 3.77−3.52 (m, 6H, H-2″, H-3″, H-4″, H-5″, H-6″a and H-6″b). ^{13}C NMR ($CDCl_3$) δ (ppm) 164.9, 164.7 (C═O), 148.5 (C-1), 146.4 (C-4), 138.6, 138.2, 138.1, 137.8 (benzyl C_q-aromatics), 133.7, 133.6 (C-4′), 132.6 (C-3), 130.4 (C-2′, C-6′), 129.5, 129.4 (C-1′), 128.7−127.6 (C-3′, C-5′, benzyl CH-aromatics), 124.0 (C-5), 122.4 (C-2)*, 122.3 (C-6)*, 86.8 (C-3″), 82.8 (C-2″), 79.5 (C-5″), 78.2 (C-4″), 77.3 (C-1″), 75.6, 75.1, 74.9, 74.3 (Ph-CH_2), 69.0 (C-6″). *Permutable signals. HRMS-ESI (*m*/*z*): $[M + H]^+$ calcd for $C_{54}H_{49}O_9$, 841.3371; found, 841.3381.

*3-(β-D-Glucopyranosyl)-4-hydroxybenzen-1-yl Benzoate (**21**).* To a solution of compound **19** (0.215 mg, 0.29 mmol) in ethyl acetate (15 mL), Pd/C (10%, 50 mg) was added. The mixture was stirred under a H_2 atmosphere for 26 h at room temperature. After reaching completion, the reaction was stopped by filtering Pd/C through a pad of Celite and the solvent was evaporated under reduced pressure. The residue was purified by column chromatography (30:1 → 10:1 dichloromethane/MeOH) to afford compound **21** as a yellowish oil in 96% yield. R_f (dichloromethane/MeOH, 7:1) = 0.44; $[\alpha]_D^{20}$ = +50° (*c* 0.2, MeOH); ^1H NMR [$CO(CD_3)_2$] δ (ppm) 8.17 (d, 2H, J_{ortho} = 7.38 Hz, H-2′, H-6′), 7.72 (t, 2H, J_{ortho} = 7.45 Hz, H-3′, H-5′), 7.59 (t, 1H, J_{ortho} = 7.67 Hz, H-4′), 7.26 (d, 1H, J_{meta} = 2.35 Hz, H-2), 7.06 (dd, 1H, J_{ortho} = 8.74 Hz, J_{meta} = 2.58 Hz, H-6), 6.89 (d, 1H, J_{ortho} = 8.69 Hz, H-5), 4.60 (d, 1H, $J_{1''-2''}$ = 9.34 Hz, H-1″), 3.87 (d, 1H, $J_{6''a-6''b}$ = 10.59 Hz, H-6″a), 3.76 (dd, 1H, $J_{6''b-6''a}$ = 10.99 Hz, $J_{6''b-5''}$ = 4.28 Hz, H-6″b), 3.63−3.47 (m, 4H, H-2″, H-3″, H-4″, H-5″). ^{13}C NMR [$CO(CD_3)_2$] δ (ppm) 165.9 (C═O), 153.7 (C-4), 144.8 (C-1), 134.5 (C-4′), 130.8 (C-1′), 130.7 (C-2′, C-6′), 129.6 (C-3′, C-5′), 128.5 (C-3), 122.6 (C-2), 121.7 (C-6), 117.9 (C-5), 81.9 (C-5″), 79.7 (C-3″), 77.7 (C-1″), 76.6 (C-2″), 71.3 (C-4″), 62.6 (C-6″). HRMS-ESI (*m*/*z*): $[M + H]^+$ calcd for $C_{19}H_{21}O_8$, 377.1231; found, 377.1226; $[M + Na]^+$ calcd for $C_{19}H_{20}NaO_8$, 399.1050; found, 399.1045.

*3-(β-D-Glucopyranosyl)benzene-1,4-diyl Dibenzoate (**22**).* To a solution of compound **20** (0.273 g, 0.32 mmol) dissolved in ethyl acetate (15 mL), Pd/C (10%, 64 mg) was added. The mixture was stirred under a H_2 atmosphere for 22 h at room temperature. After reaching completion, the reaction was stopped by filtering Pd/C through a pad of Celite and the solvent was evaporated under reduced pressure. The residue was purified by column chromatography (EtOAc) to afford compound **22** as a white solid in 90% yield. R_f (EtOAc) = 0.48; m.p. = 99.7−102.5 °C; $[\alpha]_D^{20}$ = +11° (*c* 0.8, MeOH); ^1H NMR [$CO(CD_3)_2$] δ (ppm) 8.25, 8.21 (d, 2H, J_{ortho} = 7.46 Hz, H-2′, H-6′), 7.77−7.72 (m, 2H, H-4′), 7.64−7.60 (m, 4H, H-3′, H-5′), 7.50 (d, 1H, J_{meta} = 2.11 Hz, H-2), 7.40 (d, 1H, J_{ortho} = 8.76 Hz, H-5), 7.35 (dd, 1H, J_{ortho} = 8.78 Hz, J_{meta} = 2.55 Hz, H-6), 4.59 (d, 1H, $J_{1''-2''}$ = 9.41 Hz, H-1″), 3.73 (d, 1H, $J_{6''a-6''b}$ = Hz, H-6″a), 3.59−3.37 (m, 5H, H-2″, H-3″, H-4″, H-5″, H-6″b). ^{13}C NMR [$CO(CD_3)_2$] δ (ppm) 165.5 (C═O), 165.2 (C═O), 149.3 (C-1), 147.6 (C-4), 134.6 (C-3), 134.4 (C-4′), 130.8, 130.7 (C-2′, C-6′), 130.6, 130.3 (C-1′), 129.6, 129.6 (C-3′, C-5′), 124.6 (C-5), 122.7 (C-6), 122.6 (C-2), 81.8 (C-3″), 79.6 (C-2″), 77.3 (C-1″), 75.4 (C-4″), 71.6 (C-5″), 63.0 (C-6″). HRMS-ESI (*m*/*z*): $[M + H]^+$ calcd for $C_{26}H_{25}O_9$, 481.1493; found, 481.1499; $[M + Na]^+$ calcd for $C_{26}H_{24}NaO_9$, 503.1313; found, 503.1308.

*4-(2,3,4,6-Tetra-O-methyl-β-D-glucopyranosyl)benzene-1,2-diyl Dibenzoate (**25**).* Compound **7** (0.650 g, 1.98 mmol) was dissolved in dichloromethane (43 mL) and imidazole (0.447 g, 6.57 mmol, 3.3 equiv) was added at 0 °C. After stirring for 10 min at 0 °C, benzoyl chloride (0.78 mL, 6.67 mmol, 3.3 equiv) was added dropwise. The reaction mixture was stirred at room temperature for 24 h, after which it was washed with brine and extracted with dichloromethane (2 × 20 mL). The organic layers were combined, dried over $MgSO_4$, and concentrated under reduced pressure. The residue was purified by column chromatography (hexane/acetone, 10:0 → 5:1), affording compound **25** as a colorless oil in 88% yield. R_f (hexane/EtOAc, 2:1) = 0.38; $[\alpha]_D^{20}$ = −18° (*c* 0.1, $CHCl_3$); ^1H NMR ($CDCl_3$) δ 8.05 (br d, 4H, J_{ortho} = 7.49 Hz, H-2′, H-6′), 7.53 (t, 2H, J_{ortho} = 6.71 Hz, H-4′), 7.46 (br s, 1H, H-3), 7.42−7.34 (m, 6H, H-3′, H-5′, H-5, H-6), 4.16 (d, 1H, $J_{1''-2''}$ = 9.45 Hz, H-1″), 3.69 (s, 3H, OCH_3), 3.66−3.65 (m, 2H, H-6″a and H-6″b), 3.59 (s, 3H, OCH_3), 3.47−3.42 (m, 4H, H-5″, OCH_3), 3.37−3.25 (m, 2H, H-3″, H-4″), 3.16 (s, 3H, OCH_3), 3.07 (t, 1H, $J_{2''-1''\sim2''-3''}$ = 9.13 Hz, H-2″). ^{13}C NMR ($CDCl_3$) δ 164.3 (C−O), 142.4 (C-2), 142.3 (C-1), 138.2 (C-4), 133.7 (C-4′), 130.2 (C-2′, C-6′), 128.9, 128.9 (C-1′), 128.6 (C-3′, C-5′), 125.6 (C-5), 123.2 (C-6), 122.6 (C-3), 88.5 (C-3″), 86.2 (C-2″), 80.5 (C-1″), 79.8 (C-4″), 79.2 (C-5″), 71.8 (C-6″), 61.0, 60.7, 60.6, 59.6 (OCH_3). HRMS-ESI (*m*/*z*): $[M + H]^+$ calcd for $C_{30}H_{33}O_9$, 537.2119; found, 537.2102; $[M + Na]^+$ calcd for $C_{30}H_{32}NaO_9$, 559.1939; found, 559.1914.

*4-(β-D-Glucopyranosyl)benzene-1,2-diyl Dibenzoate (**26**).* To a solution of compound **25** (0.810 g, 1.51 mmol) in dry dichloroethane (90 mL), $BBr_3{\cdot}SMe_2$ (11.5 g, 37.12 mmol, 25 equiv) was slowly added and the reaction was stirred under reflux for 17 h. The mixture was allowed to reach room temperature, washed with sodium bicarbonate, and extracted with dichloromethane (3 × 100 mL). The organic layers were combined, dried over $MgSO_4$, filtered, and concentrated under vacuum. The residue was purified by column chromatography (40:1 → 30:1 EtOAc/MeOH), affording compound **26** in 8% yield as a brownish solid. R_f (dichloromethane/MeOH, 6:1) = 0.60; m.p. = 77.3−78.1 °C; $[\alpha]_D^{20}$ = −11° (*c* 0.3, $CHCl_3$); ^1H NMR [$CO(CD_3)_2$] δ (ppm) 8.05 (t, 4H, J_{ortho} = 7.23 Hz, H-2′, H-6′), 7.67−7.62 (m, 2H, H-4′), 7.55 (br s, 1H, H-3), 7.51−7.44 (m, 6H, H-3′, H-5′, H-5, H-6), 4.38 (br s, 1H, OH), 4.31 (d, 1H, $J_{1''-2''}$ = 9.41 Hz, H-1″), 3.90 (br d, 1H, $J_{6''a-6''b}$ = 10.75 Hz, H-6″a), 3.80 (br s, 1H, OH), 3.74 (dd, 1H, $J_{6''b-6''a}$ = 10.89 Hz, $J_{6''b-5''}$ = 4.37 Hz, H-6″b), 3.61−3.47 (m, 3H, H-3″, H-4″, H-5″), 3.42 (t, 1H, $J_{2''-1''\sim2''-3''}$ = 8.83 Hz, H-2″). ^{13}C NMR [$CO(CD_3)_2$] δ (ppm) 164.7 (C═O), 143.1 (C-2), 142.8 (C-1), 140.4 (C-4), 134.7 (C-4′), 130.7 (C-2′, C-6′), 129.8 (C-1′), 129.6 (C-3′, C-5′), 126.9 (C-5), 123.6 (C-6), 123.4 (C-3), 81.8 (C-1″), 81.7 (C-5″), 79.8 (C-3″), 76.3 (C-2″), 71.7 (C-4″), 63.1 (C-6″). HRMS-ESI (*m*/*z*): $[M + Na]^+$ calcd for $C_{26}H_{24}NaO_9$, 503.1313; found, 503.1326.

*4-(2,3,4,6-Tetra-O-benzyl-α-/β-D-glucopyranosyloxy)benzen-1-yl Benzoate (**28α,β**).* Compound **27α,β** (α/β ratio = 4:1, 0.570 g, 0.90 mmol) was dissolved in dry dichloromethane (20 mL) together with imidazole (0.135 g, 1.98 mmol, 2.2 equiv) and DMAP (cat). After

https://dx.doi.org/10.1021/acs.jmedchem.0c00841
J. Med. Chem. 2020, 63, 11663−11690

stirring for 10 min at 0 °C, benzoyl chloride (0.230 mL, 1.98 mmol, 2.2 equiv) was added dropwise. The reaction mixture was stirred at room temperature for 24 h, after which it was washed with brine and extracted with dichloromethane (2 × 20 mL). The organic layers were combined, dried over $MgSO_4$, and concentrated under reduced pressure. The residue was purified by column chromatography (hexane/EtOAc, 10:1 → 5:1), affording **28*α,β*** as a mixture in α/β ratio = 10:1 as a colorless oil isolated in 94% yield; R_f (hexane/EtOAc, 10:1) = 0.23; $[\alpha]_D^{20} = -4°$ (*c* 0.2, $CHCl_3$); ^{1}H NMR ($CDCl_3$) δ (ppm) 8.20 (d, 20H, J_{ortho} = 7.65 Hz, H-2′$_\alpha$, H-6′$_\alpha$), 8.10 (d, 2H, J_{ortho} = 7.65 Hz, H-2′$_\beta$, H-6′$_\beta$), 7.66–7.58 (m, 11H, H-4′$_\alpha$, H-4′$_\beta$), 7.54–7.45 (m, 22H, H-3′$_\alpha$, H-5′$_\alpha$, H-3′$_\beta$, H-5′$_\beta$), 7.40–7.10 (m, 264H, benzyl aromatics, H-2$_\alpha$, H-3$_\alpha$, H-5$_\alpha$, H-6$_\alpha$, H-2$_\beta$, H-3$_\beta$, H-5$_\beta$, H-6$_\beta$), 5.44 (d, 10H, $J_{1''-2''}$ = 2.84 Hz, H-1″$_\alpha$), 5.08–4.80 (m, 38H, H-1″$_\beta$, Ph-CH_2), 4.71–4.40 (m, 51H, Ph-CH_2), 4.20 (t, 10H, $J_{3''\alpha-2''\alpha\sim3''\alpha-4''\alpha}$ = 9.17 Hz, H-3″$_\alpha$), 3.90–3.57 (m, 57H, H-2″$_\alpha$, H-4″$_\alpha$, H-5″$_\alpha$, H-6″a$_\alpha$, H-6″b$_\alpha$, H-2″$_\beta$, H-3″$_\beta$, H-4″$_\beta$, H-5″$_\beta$, H-6″a$_\beta$, H-6″b$_\beta$). ^{13}C NMR ($CDCl_3$) δ (ppm) 165.4 (C═O$_\alpha$), 165.4 (C═O$_\beta$), 155.1 (C-4$_\beta$), 154.4 (C-4$_\alpha$), 146.0 (C-1$_\beta$), 145.6 (C-1$_\alpha$), 138.7, 138.5, 138.1, 138.0, 139.0, 137.7 (benzyl C_q-aromatics), 133.6 (C-4′$_{\alpha/\beta}$), 130.2 (C-2′$_\alpha$, C-6′$_\alpha$), 129.9 (C-2′$_\beta$, C-6′$_\beta$), 128.6–127.6 (benzyl CH-aromatics, C-3′$_\alpha$, C-5′$_\alpha$, C-3′$_\beta$, C-5′$_\beta$), 122.6 (C-2$_\beta$, C-6$_\beta$), 122.5 (C-2$_\alpha$, C-6$_\alpha$), 117.9 (C-3$_\beta$, C-5$_\beta$), 117.5 (C-3$_\alpha$, C-5$_\alpha$), 102.1 (C-1″$_\beta$), 95.9 (C-1″$_\alpha$), 82.0 (C-3″$_\beta$), 81.9 (C-3″$_\alpha$), 79.6 (C-5″$_{\alpha/\beta}$), 77.6 (C-4″$_\beta$), 77.2 (C-4″$_\alpha$), 75.8, 75.2, 75.1, 73.5, 73.4 (Ph-CH_2), 70.9 (C-2″$_\beta$), 70.8 (C-2″$_\beta$), 68.1 (C-6″$_{\alpha/\beta}$). HRMS-ESI (*m*/*z*): $[M + H]^+$ calcd for $C_{47}H_{45}O_8$, 737.3109; found, 737.3117; $[M + Na]^+$ calcd for $C_{47}H_{44}NaO_8$, 759.2928; found, 759.2938.

*4-(α-D-Glucopyranosyloxy)benzen-1-yl Benzoate (**29**).* To a solution of the mixture **28*α,β*** (α/β ratio = 10:1) (0.350 g, 0.47 mmol) in ethyl acetate (20 mL), Pd/C (10%, 50 mg) was added. The mixture stirred under a H_2 atmosphere for 18 h at room temperature. After reaching completion, the reaction was stopped by filtering Pd/C through a pad of Celite and the solvent was evaporated under reduced pressure. The residue was purified by column chromatography (100:1 → 5:1 AcOEt/MeOH) to afford compound **29** as a white powder in 71% yield. R_f (dichloromethane/MeOH 9:1) = 0.35; m.p. = 161.7–162.6 °C; $[\alpha]_D^{20}$ = +74° (*c* 0.1, $CHCl_3$); ^{1}H NMR (MeOD) δ (ppm) 8.16 (d, 2H, J_{ortho} = 7.72 Hz, H-2′, H-6′), 7.68 (t, 1H, J_{ortho} = 7.56 Hz, H-4′), 7.55 (t, 2H, J_{ortho} = 7.66 Hz, H-3′, H-5′), 7.26 (d, 2H, J_{ortho} = 8.91 Hz, H-2, H-6), 7.15 (d, 2H, J_{ortho} = 8.95 Hz, H-3, H-5), 5.49 (d, 1H, $J_{1''-2''}$ = 3.36 Hz, H-1″), 3.99 (t, 1H, $J_{3''-2''\sim3''-4''}$ = 9.11 Hz, H-3″), 3.81–3.68 (m, 3H, H-5″, H-6″a and H-6″b), 3.50 (dd, 1H, $J_{2''-1''}$ = 3.35 Hz, $J_{2''-3''}$ = 9.40 Hz, H-2″), 3.45 (t, 1H, $J_{4''-3''\sim4''-5''}$ = 9.16 Hz, H-4″). ^{13}C NMR (MeOD) δ (ppm) 166.9 (C═O), 156.4 (C-4), 147.2 (C-1), 134.9 (C-4′), 131.0 (C-2′, C-6′), 130.8 (C-1′), 129.8 (C-3′, H-5′), 123.6 (C-2, C-6), 119.0 (C-3, C-5), 99.8 (C-1″), 74.9 (C-3″), 74.5 (C-5″), 73.3 (C-2″), 71.5 (C-4″), 62.4 (C-6″). HRMS-ESI (*m*/*z*): $[M + H]^+$ calcd for $C_{19}H_{21}O_8$, 377.1231; found, 377.1220; $[M + Na]^+$ calcd for $C_{19}H_{20}NaO_8$, 399.1050; found, 399.1040.

*4-(β-D-Glucopyranosyloxy)benzen-1-yl Benzoate (**30**).* Minor product of the reaction that gave compound **29**. Colorless crystals obtained in 10% yield; R_f (dichloromethane/MeOH, 9:1) = 0.35; m.p. = 192.0–193.3 °C; ^{1}H NMR (MeOD) δ (ppm) 8.16 (d, 2H, J_{ortho} = 8.06 Hz, H-2′, H-6′), 7.69 (t, 1H, J_{ortho} = 7.45 Hz, H-4′), 7.56 (t, 1H, J_{ortho} = 7.65 Hz, H-3′, H-5′), 7.20–7.14 (m, 4H, H-2, H-3, H-5, H-6), 4.91 (H-1″, superimposed with H_2O solvent peak), 3.91 (d, 1H, $J_{6''a-6''b}$ = 12.06 Hz, H-6″a), 3.72 (dd, 1H, $J_{6''b-6''a}$ = 12.00 Hz, $J_{6''b-5''}$ = 5.36 Hz, H-6″b), 3.50–3.38 (m, 4H, H-2″, H-3″, H-4″, H-5″). ^{13}C NMR (MeOD) δ (ppm) 166.9 (C═O), 156.9 (C-4), 147.2 (C-2), 134.9 (C-4′), 131.0 (C-2′, C-6′), 130.7 (C-1′), 129.8 (C-3′, C-5′), 123.6 (C-2, C-6), 118.7 (C-3, C-5), 102.7 (C-1″), 78.2 (C-3″), 77.9 (C-5″), 74.9 (C-2″), 71.3 (C-4″), 62.5 (C-6″). HRMS-ESI (*m*/*z*): $[M + Na]^+$ calcd for $C_{19}H_{20}NaO_8$, 399.1050; found, 399.1052.

*2-(2,3,4,6-Tetra-O-benzyl-α-D-glucopyranosyloxy)benzen-1-yl Benzoate (**32**).* Compound **31** (0.360 g, 0.57 mmol) was dissolved in dry dichloromethane (15 mL) together with imidazole (0.086 g, 1.26 mmol, 2.2 equiv) and DMAP (cat.). After stirring for 10 min at 0 °C, benzoyl chloride (0.143 mL, 1.18 mmol, 2.2 equiv) was added dropwise. The reaction mixture was stirred at room temperature for 72 h, after which it was washed with brine and extracted with dichloromethane (2 × 20 mL). The organic layers were combined, dried over $MgSO_4$, and concentrated under reduced pressure. The residue was purified by column chromatography (p. ether/EtOAc, 15:1 → 3:1), affording compound **32** as a colorless oil in 82% yield. R_f (p. ether/EtOAc, 4:1) = 0.52; $[\alpha]_D^{20}$ = +50° (*c* 0.1, $CHCl_3$); ^{1}H NMR ($CDCl_3$) δ (ppm) 8.17 (d, 2H, J_{ortho} = 7.90 Hz, H-2′, H-6′), 7.33 (t, 1H, J_{ortho} = 7.34 Hz, H-4′), 7.35–7.06 (m, 24H, benzyl aromatics, H-3, H-4, H-5, H-6, H-3′, H-5′), 5.49 (d, 1H, $J_{1''-2''}$ = 2.81 Hz, H-1″), 4.77, 4.73 (part A_1 of A_1B_1 system, 1H, J_{A1-B1} = 10.95 Hz, Ph-CH_2), 4.58–4.56 (m, 3H, part A_2 of A_2B_2 system, Ph-CH_2), 4.43–4.37 (m, 2H, part B_1 of A_1B_1 system, part B_2 of A_2B_2 system), 4.34, 4.30 (part A_3 of A_3B_3 system, 1H, J_{A3-B3} = 10.77 Hz, Ph-CH_2), 4.25, 4.21 (part B_3 of A_3B_3 system, 1H, J_{A3-B3} = 10.95 Hz, Ph-CH_2), 3.88 (br d, 1H, $J_{2''-3''}$ = 9.46 Hz, H-2″), 3.79–3.46 (m, 3H, H-3″, H-4″, H-6″a), 3.60–3.54 (m, 2H, H-5″, H-6″b). ^{13}C NMR ($CDCl_3$) δ (ppm) 164.9 (C═O), 148.4 (C-2), 141.1 (C-1), 138.7, 138.5, 138.3, 137.9 (benzyl C_q-aromatics), 133.2 (C-4′), 130.5 (C-2′, C-6′), 129.6 (C-1′), 128.3–127.5 (benzyl CH-aromatics, C-3′, C-5′), 126.8 (C-4), 123.0 (C-5)*, 122.5 (C-6)*, 116.0 (C-3), 96.2 (C-1″), 81.7 (C-3″), 77.2 (C-5″), 76.9 (C-4″), 75.3, 74.7, 73.4, 72.6 (Ph-CH_2), 71.2 (C-2″), 68.2 (C-6″). HRMS-ESI (*m*/*z*): $[M + H]^+$ calcd for $C_{47}H_{45}O_8$, 737.3109; found, 737.3109; $[M + Na]^+$ calcd for $C_{47}H_{44}NaO_8$, 759.2928; found, 759.2934.

*2-(α-D-Glucopyranosyloxy)benzen-1-yl Benzoate (**33**).* To a solution of compound **32** (0.275 mg, 0.37 mmol) in ethyl acetate (6 mL), Pd/C (10%, 32 mg) was added. The mixture stirred under a H_2 atmosphere for 20 h at room temperature. After reaching completion, the reaction was stopped by filtering Pd/C through a pad of Celite and the solvent was evaporated under reduced pressure. The residue was purified by column chromatography (1:0 → 30:1 AcOEt/MeOH) to afford compound **33** as colorless crystals in 83% yield. R_f (dichloromethane/MeOH, 7:1) = 0.35; m.p. = 54.5–55.0 °C; $[\alpha]_D^{20}$ = +123° (*c* 0.1, MeOH); ^{1}H NMR [$CO(CD_3)_2$] δ (ppm) 8.20 (d, 2H, J_{ortho} = 7.88 Hz, H-2′, H-6′), 7.70 (t, 1H, J_{ortho} = 7.56 Hz, H-4′), 7.58 (t, 2H, J_{ortho} = 7.59 Hz, H-3′, H-5′), 7.42 (d, 1H, J_{ortho} = 8.56 Hz, H-3), 7.28–7.24 (m, 2H, H-4, H-6), 7.10 (t, 1H, J_{ortho} = 7.73 Hz, H-5), 5.56 (d, 1H, $J_{1''-2''}$ = 3.19 Hz, H-1″), 3.74–3.59 (m, 4H, H-3″, H-4″, H-6″a and H-6″b), 3.53–3.43 (m, 2H, H-2″, H-5″). ^{13}C NMR [$CO(CD_3)_2$] δ (ppm) 165.0 (C═O), 149.6 (C-2), 141.3 (C-1), 134.1 (C-4′), 130.6 (C-2′, C-6′), 130.1 (C-1′), 129.3 (C-3′, C-5′), 127.4 (C-4), 123.7 (C-6), 122.9 (C-5), 117.9 (C-3), 99.1 (C-1″), 74.4 (C-4″), 74.0 (C-3″), 72.7 (C-2″), 70.8 (C-5″), 62.0 (C-6″). HRMS-ESI (*m*/*z*): $[M + Na]^+$ calcd for $C_{19}H_{21}O_8$, 399.1050; found, 399.1064.

*General Procedure for Debenzylation Leading to C-Glucosyl Polyphenols **23** and **24**.* To a solution of 0.016 mmol of benzylated *C*-glucosyl polyphenol (**14** or **16**) in ethyl acetate (6 mL), Pd/C (10%, 32 mg) was added. The mixture stirred under a H_2 atmosphere for 15–26 h at room temperature. After reaching completion, the reaction was stopped by filtering Pd/C through a pad of Celite and the solvent was evaporated under reduced pressure. The residue was purified by column chromatography.

*1-[5-(β-D-Glucopyranosyl)-2,4,6-trihydroxyphenyl]ethan-1-one (**23**).* Compound synthesized by debenzylation of compound **14.** The reaction crude was purified by column chromatography (10:1 → 5:1 dichloromethane/MeOH) to give **23** as a yellowish powder in 93% yield. R_f (dichloromethane/MeOH, 5:1) = 0.23; m.p. = 150.8–153.0 °C; $[\alpha]_D^{20}$ = +57° (*c* 0.6, MeOH); ^{1}H NMR (MeOD) δ (ppm) 5.88 (s, 1H, H-5), 4.79 (s, 1H, $J_{1'-2'}$ = 9.94 Hz, H-1′), 3.93 (t, 1H, $J_{2'-1'\sim2'-3'}$ = 9.26 Hz, H-2′), 3.82 (d, 1H, $J_{6'a-6'b}$ = 11.91 Hz, H-6′a), 3.71 (dd, 1H, $J_{6'b-6'a}$ = 12.11 Hz, $J_{6'b-5'}$ = 4.87 Hz, H-6′b), 3.46–3.31 (m, 3H, H-3′, H-4′, H-5′). ^{13}C NMR (MeOD) δ (ppm) 204.9 (C═O), 165.7 (C-2), 165.1 (C-4), 164.2 (C-6), 105.6 (C-1), 104.1 (C-3), 96.7 (C-5), 82.5 (C-5′), 79.9 (C-3′), 75.6 (C-1′), 73.1 (C-2′), 71.5 (C-4′), 62.5 (C-6′), 33.0 (CH_3-Ac). HRMS-ESI (*m*/*z*): $[M + H]^+$ calcd for $C_{14}H_{19}O_9$, 331.1024; found, 331.1020; $[M + Na]^+$ calcd for $C_{14}H_{18}NaO_9$, 353.0843; found, 353.0843.

*1-(β-D-Glucopyranosyl)pyranosyl)naphthalen-2-ol (**24**).* Compound synthesized by debenzylation of compound **16.** The reaction crude was purified by column chromatography (20:1 → 10:1 dichloromethane/MeOH) to give **24** as a yellowish oil in 91% yield. R_f (dichloromethane/MeOH, 10:1) = 0.26; $[\alpha]_D^{20}$ = +45° (*c* 0.5,

https://dx.doi.org/10.1021/acs.jmedchem.0c00841
J. Med. Chem. 2020, 63, 11663–11690

MeOH); ^{1}H NMR [$CO(CD_3)_2$] δ (ppm) 8.16 (br s, 1H, H-8), 7.75 (m, 2H, H-4, H-5), 7.39 (t, 1H, J_{ortho} = 7.58 Hz, H-6), 7.27 (t, 1H, J_{ortho} = 7.36 Hz, H-7), 7.07 (t, 1H, J_{ortho} = 8.31 Hz, H-3), 5.43 (d, 1H, $J_{1'-2'}$ = 9.64 Hz, H-1′), 3.93−3.83 (m, 3H, H-2′, H-6′a and H-6′b), 3.78−3.68 (m, 2H, H-3′, H-4′), 3.64−3.60 (m, 1H, H-5′). ^{13}C NMR [$CO(CD_3)_2$] δ (ppm) 155.2 (C-2), 134.3 (C-8a), 130.5 (C-4), 129.7 (C-5), 129.0 (C-4a), 126.6 (C-7), 124.8 (C-8), 123.4 (C-6), 120.2 (C-3), 116.7 (C-1), 82.0 (C-5′), 79.4 (C-3′), 78.2 (C-1′), 74.4 (C-2′), 70.7 (C-4′), 61.8 (C-6′). HRMS-ESI (m/z): [M + Na]$^+$ calcd for $C_{16}H_{19}NaO_6$, 329.0996; found, 329.1001.

*2-Phenyl-1-(2,4,6-trihydroxyphenyl)ethan-1-one (**34**) and 3,5-Dihydroxyphenyl 2-Phenylacetate (**35**).* 1,3,5-Trihydroxybenzene (1.0 g, 7.93 mmol) was dissolved in 2% TfOH/CH_3CN (10 mL) and cooled down to 0 °C. Phenylacetyl chloride (1.0 mL, 7.93 mmol) was added at 0 °C and the reaction was stirred overnight at room temperature. Then, the crude was poured into ice and extracted with EtOAc. The organic phase was washed with 2 M HCl, $NaHCO_3$, and brine and dried over $MgSO_4$ and the solvent was eliminated under reduced pressure. After column chromatography (5:1 → 3:1 hexane/acetone), compounds **34** and **35** were obtained in 7 and 25% yields, respectively.

*3,5-Dihydroxyphenyl 2-Phenylacetate (**35**).* R_f = 0.36 (hexane/acetone, 3:1); m.p. = 77.9−79.6 °C; ^{1}H NMR ($CDCl_3$) δ (ppm) 11.70 (s, 2H, OH), 9.30 (s, 1H, OH), 7.30−7.20 (m, 5H, ArC*H*), 5.94 (s, 2H, Ar*H*), 4.41 (s, 2H, CH_2). ^{13}C NMR ($CDCl_3$) δ (ppm) 200.5 (C═O), 165.6 (Ar*C*, C-4), 165.4 (ArCx2, C-2, C-6), 137.1 (Ar*C*, C-1′), 130.6 (ArCHx2, C-2′, C-6′), 128.5 (ArCHx2, C-3′, C-5′), 127.0 (Ar*C*H, C-4′), 104.8 (ArC, C-1), 96.2 (ArCHx2, C-3, C-5), 50.0 (CH_2). HRMS-ESI (m/z): [M + H]$^+$ calcd for $C_{14}H_{13}O_4$, 245.0808; found, 245.0806; [M + Na]$^+$ calcd for $C_{14}H_{12}NaO_4$, 267.0628; found, 267.0627.

*2-Phenyl-1-(2,4,6-trihydroxyphenyl)ethan-1-one (**34**).* Compound **35** (0.56, 2.49 mmol) was treated with trifluoromethanesulfonic acid (2.2 mL, 25 mmol) at 0 °C. The reaction mixture was warmed up at room temperature for 1 h and then heated for 1 h at 40 °C and then at 100 °C. After an additional 1 h, the crude was poured into ice and extracted with EtOAc. The organic phase was washed with 2 M HCl, $NaHCO_3$, and brine and dried over $MgSO_4$ and the solvent was eliminated under reduced pressure. After column chromatography (5:1 → 3:1 hexane/acetone), compound **34** was isolated in 39% yield. R_f = 0.4 (hexane/acetone, 3:1); ^{1}H NMR ($CDCl_3$) δ (ppm) 7.30−7.27 (m, 5H, ArC*H*), 6.03−6.00 (m, 3H, Ar*H*, C-2, C-4, C-6), 3.82 (s, 2H, CH_2). ^{13}C NMR ($CDCl_3$) δ (ppm) 171.9 (C═O), 157.2 (*C*-2, C-3, C-5), 157.1 (C-1), 129.3 (C-2′, C-6′), 128.8 (C-3′, C-5′), 127.5 (C-4′), 101.7 (C-2, C-6), 101.2 (C-4), 41.3 (CH_2). HRMS-ESI (m/z): [M + H]$^+$ calcd for $C_{14}H_{13}O_4$, 245.0808; found, 245.0805; [M + Na]$^+$ calcd for $C_{14}H_{12}NaO_4$, 267.0628; found, 267.0729.

*2,4,6-Trihydroxy-3-(2,3,4,6-tetra-O-benzyl-β-D-glucopyranosyl)-phenyl]-2-phenylethan-1-one (**36**).* A solution of compound **34** (0.22 g, 0.89 mmol), 2,3,4,6-tetra-*O*-benzyl-D-glucopyranose (0.34, 0.64 mmol), and drierite (0.3 g) in a mixture of dichloromethane/CH_3CN (1:1) was stirred for 10 min at room temperature. To this solution lowered at −40 °C, TMSOTf (0.16 mL, 0.89 mmol) was added dropwise. The mixture was left at room temperature under stirring overnight. Then, the reaction was stopped by adding trimethylamine and the reaction mixture was filtered through a Celite pad. The solvent was evaporated under reduced pressure and the residue was purified by column chromatography (hexane/acetone, 7:1) to render compound **36** in 33% yield. R_f = 0.24 (hexane/acetone, 3:1); m.p. = 113.0−114.9 °C; $[\alpha]_D^{20}$ = +25° (c 1, $CHCl_3$); ^{1}H NMR ($CDCl_3$) δ (ppm) 7.38−7.19 (m, 23H, benzyl aromatics), 7.03−7.01 (m, benzyl aromatics), 6.02 (br s, 1H, Ph-H5), 4.98 (br s, 2H, Ph-CH_2), 4.89−4.85 (m, 2H, H-1‴; part A_1 of A_1B_1 system, Ph-CH_2), 4.74 (d, J = 10.5 Hz, 1H, part A_2 of A_2B_2 system, Ph-CH_2), 4.60−4.56 (m, 2H, part A_3 of A_3B_3 system; part B_1 of system A_1B_1, Ph-CH_2), 4.48 (d, J = 11.9 Hz, 1H, part B_3 of A_3B_3 system, Ph-CH_2), 4.35−4.31 (m, 2H, part A_4 of A_4B_4 system, part B_2 of A_2B_2 system, Ph-CH_2), 4.22 (d, J = 16.8 Hz, part B_4 of A_4B_4 system, Ph-CH_2), 3.94 (t, J = 9.2 Hz, 1H, H-3‴), 3.85−3.70 (m, H-5‴, H-2‴, H-6‴a, H-6‴b), 3.63−3.60 (m, 1H, H-4‴). ^{13}C NMR ($CDCl_3$) δ (ppm) 203.4 (C-1), 164.4 (C-6), 161.3 (C-4), 160.5 (C-2), 138.3, 137.6, 137.4, 135.9, 135.4 (benzyl C_q-aromatics), 129.8−126.6 (benzyl CH-aromatics), 105.9 (C-1), 102.8 (C-3), 98.2 (C-5), 86.2 (C-5′), 82.1 (C-2′), 78.6 (C-4′), 76.8 (C-3′), 76.3, 75.7, 75.3 (CH_2-Ph), 74.8 (C-1′), 73.3 (CH_2-Ph), 67.4 (C-6′), 50.3 (CH_2-Ph). HRMS-ESI (m/z): [M + H]$^+$ calcd for $C_{48}H_{47}O_9$, 767.3215; found, 767.3223; [M + Na]$^+$ calcd for $C_{48}H_{46}NaO_9$, 789.3034; found, 789.3049.

*3-[(β-D-Glucopyranosyl)-2,4,6-trihydroxyphenyl]-2-phenylethan-1-one (**37**).* Compound **36** (0.13 g, 0.17 mmol) was dissolved in ethyl acetate (4.0 mL) and methanol (4.0 mL). Then, a suspension of Pd/C (10%) (130 mg) in ethyl acetate−methanol was added and the mixture was stirred under a H_2 atmosphere for 3 h at room temperature. Pd/C was filtered through a pad of Celite and the solvent was evaporated under reduced pressure. The residue was purified by column chromatography (dichloromethane/MeOH, 7:1) to afford compound **37** in 68% yield. m.p. = 128.5−129.3 °C; $[\alpha]_D^{20}$ = +47° (c 0.4, MeOH); ^{1}H NMR [$CO(CD_3)_2$] δ (ppm) 7.28−7.15 (m, 5H, ArCH), 5.93 (s, 1H, H-5), 4.86 (d, J = 9.8 Hz, 1H, H-1″), 4.38 (s, 2H, CH_2), 3.80−3.70 (m, 3H, H6″a, H6″b, H-2), 3.59−3.47 (m, 2H, H-4″, H-3″), 3.42 (dt, J = 9.5, 3.2 Hz, 1H, H-5″). ^{13}C NMR [$CO(CD_3)_2$] δ (ppm) 203.0 (C-1), 163.5 (C-4), 163.4 (C-2), 162.6 (C-6), 135.9 (C-1′), 129.7 (C-4′), 127.9 (C-3′, C-5′), 126.1 (C-2′, C-6′), 104.1 (C-1), 103.3 (C-3), 95.1 (C-5), 80.9 (C-5″), 78.3 (C-3″), 74.9 (C-1″), 72.6 (C-2″), 69.6 (C-4″), 60.7 (C-6″), 49.4 (CH_2). HRMS-ESI (m/z): [M + H]$^+$ calcd for $C_{20}H_{23}O_9$, 407.1337; found, 407.1341.

Biological Activity Assays. *STD-NMR Binding Studies with IAPP.* NMR experiments were recorded on a Bruker Avance 600 MHz spectrometer equipped with a triple channel cryoprobe head. Immediately before use, lyophilized IAPP was dissolved in 10 mM NaOD in D_2O at a concentration of 160 μM and then diluted 1:1 with 10 mM phosphate-buffered saline (pH 7.4) containing 100 mM NaCl. To these samples were added the compounds in study, **21** and **37**, to a final concentration of 2 mM. The pH of each sample was verified with a Microelectrode (Mettler Toledo) for 5 mm NMR tubes and adjusted with NaOD and/or DCl. Selective saturation of the protein resonances (on resonance spectrum) was performed by irradiating at −0.5 ppm using a series of Eburp2.1000-shaped pulses (50 ms) for a total saturation time of 2.0 s. For the reference spectrum (off-resonance), the samples were irradiated at 100 ppm. STD experiments were recorded at two temperatures, 298 and 310 K, with a ligand/amyloid oligomer molar ratio of 12:1. Control STD experiments with IAPP without any ligand and only with ligands **21** and **37** without IAPP were also recorded and taken into account in the STD epitope determination. To determine the epitope mapping of each ligand shown in Figure 3, the STD intensities of each proton were normalized with respect to that with the highest response. Proton resonances from which it was not possible to have an accurate STD information are identified with an asterisk symbol in Figure 3.

Glucosidase and Cholinesterase Inhibition Assays. Measurement of the glycosidase inhibition was carried out using the methodology previously reported by Bols and co-workers.[80] Inhibition assays were conducted in a double-beam Hitachi U-2900 spectrophotometer, with PS cuvettes at 400 nm. α-Glucosidase (*Saccharomyces cerevisiae*) and β-glucosidase (almonds) were used as model enzymes and the corresponding *p*-nitrophenyl glycosides as substrates. Initial screening for determining the percentage of inhibition was conducted at a 100 μM inhibitor concentration. Inhibitor mother solutions were prepared in DMSO and the ratio of DMSO in the cuvette was maintained at 5%. Two 1.2 mL samples in PS cuvettes containing 0.1 M phosphate buffer (pH 6.8) were prepared using the corresponding nitrophenyl glucopyranoside as a substrate at a concentration equal to the expected value of K_M. Water (control) or inhibitor solution plus water (100 μM final concentration) was added to a constant value of 1.14 mL. Finally, reaction was initiated by the addition of a solution of properly diluted enzyme (60 μL) at 25 °C and monitored by registering the increase in absorbance at 400 nm for 125 s.

Initial rates were obtained from the slopes of the plots (Abs. *vs t*) and used for calculating the percentage of inhibition using the following equation

$$\%\text{Inhibition} = \frac{v_o - v}{v_o} \times 100$$

https://dx.doi.org/10.1021/acs.jmedchem.0c00841
J. Med. Chem. 2020, 63, 11663−11690

where v_o refers to the rate in the control experiment (enzyme), and v refers to the rate in the experiment containing the inhibitor solution. For determining the percentage of inhibition, the substrate concentration was fixed at the K_M value for each enzyme ([S] = 0.25 mM for α-glucosidase, and [S] = 4.0 mM for β-glucosidase). For compounds showing a significant percentage of inhibition, the mode of inhibition was obtained using the Lineweaver−Burk plot and Cornish−Bowden ($1/v$ *vs* [I], [S]/v *vs* [I]) plots.[81] The procedure followed was the same as above, but using five different substrate concentrations, ranging from 0.25 to 4.0-fold the expected K_M, while keeping the inhibitor concentration constant (three different inhibitor concentrations). The reaction rate for the cuvette containing the highest substrate concentration was allowed to be within 0.12−0.15 Abs/min. Kinetic parameters (K_M, V_{max}) were obtained using nonlinear regression analysis (least squares fit) using the Michaelis−Menten equation tool implemented in GraphPad Prism 8.01 software, which in turn were used to calculate the inhibition constants, according to the equations indicated below.

For cholinesterase inhibition tests (acetylcholinesterase, AChE; *Electrophorus electricus*) and butyrylcholinesterase (BuChE, equine serum), Ellman's cholorimetric assay[82] was followed, with minor modifications. DMSO was kept within 1.25% cuvette concentration. The chromogenic agent DTNB [5,5′-dithiobis(2-nitrobenzoic acid)] was fixed at 0.975 mM concentration; 0.1 M phosphate buffer (pH 8.0) was employed, T = 25 °C, and the reaction was monitored for 125 s at 405 nm. For determining the percentage of inhibition, the substrate concentration (acetylthiocholine iodide for AChE; *S*-butyrylthiocholine iodide for BuChE) was fixed at 29 μM for AChE and at 18.2 μM for BuChE.

The mode of inhibition and inhibition constants were obtained as described above for glycosidases.

Competitive inhibition (inhibitor only binds the free enzyme)

$$K_{ia} = \frac{[I]}{\frac{K_{M\,app}}{K_M} - 1}$$

Mixed inhibition (inhibitor binds both the free and complexed enzymes)

$$K_{M\,app} = K_M \frac{1 + \frac{[I]}{K_{ia}}}{1 + \frac{[I]}{K_{ib}}}$$

$$V_{max\,app} = \frac{V_{max}}{1 + \frac{[I]}{K_{ib}}}$$

Uncompetitive (the inhibitors only bind the complexed enzyme)

$$K_{M\,app} = \frac{K_M}{1 + \frac{[I]}{K_{ib}}}$$

$$V_{max\,app} = \frac{V_{max}}{1 + \frac{[I]}{K_{ib}}}$$

Noncompetitive (inhibitor binds both the free enzyme and complexed enzyme with equal affinity)

$$K_{M\,app} = K_M$$

$$V_{max\,app} = \frac{V_{max}}{1 + \frac{[I]}{K_{ib}}}$$

The following inhibitor concentrations were used for the calculation of the inhibition constants:

Genistein

- α-Glucosidase: 0, 10, 20, 30 μM.
- β-Glucosidase: 0, 50, 83.3 μM.

Compound **33**

- α-Glucosidase: 0, 33.3, 50 μM.

Experiments were carried out in duplicate, and the data are expressed as the mean ± SD.

Cell Culture. The human induced pluripotent stem cell (hiPSC) line derived from a health control individual was used in this study. The hiPS (control MIFF1)[72] was kindly provided by Professor Peter Andrews and Dr. Ivana Barbaric (Centre for Stem Cell Biology, The University of Sheffield). hiPSCs were maintained in Vitronectin-coated plates (0.5 μg/cm^2; Thermo Fisher Scientific) according to the manufacturer's recommendations in complete TeSR-E8 Medium (StemCell Technologies). The culture medium was changed every day. Cells were passaged every 5−7 days as clumps using ReLeSR, an enzyme-free reagent for cell dissociation (StemCell Technologies), according to the manufacturer's recommendations. For all the experiments in this study, hiPSCs were used between passages 18 and 26, and all hiPSCs were cultured in 5% O_2 and 5% CO_2 at 37 °C.

Natural Aβ Oligomer and Control Solutions. A solution containing natural amyloid-beta (Aβ) oligomers (a kind gift of Dr. Claire Garwood) was derived from the conditioned medium of 7PA2 cells,[46] Chinese Hamster Ovary cells stably transfected with cDNA encoding APP751, and an amyloid precursor protein that contains the Val717Phe familial Alzheimer's disease mutation.[83,84] To obtain natural Aβ oligomers, 5×10^6 cells were seeded in a T175 flask and cultured in Dulbecco's modified Eagle's medium (DMEM, Sigma) supplemented with 10% fetal bovine serum (Thermo Fisher), 2 mM L-glutamine (Sigma-Aldrich), and 50 mg/mL penicillin/streptomycin. Cells were incubated for 24 h in 5% CO_2 at 37 °C. After 24 h of incubation, the cells were washed with serum-free medium and conditioned in 5 mL of plain DMEM without phenol red (Thermo Fisher) and lacking any additives overnight. The oligomer-containing conditioned medium (CM) was collected and cleared of cells and debris by centrifugation at 200*g* for 10 min at 4 °C. The CM was used as the natural Aβ oligomer solution in the fear conditioning experiments for HCS. The concentrated CM contained between 1000 and 2000 pg/mL Aβ(1−42) as measured by ELISA (Thermo Fisher).

Knockdown Experiment. The knockdown is an experimental technique by which the expression of a gene is transiently reduced; for this reason, it is necessary to find out the optimal condition in which we have the maximum effect preserving the cell viability. In HEK cells, we observed that the detection should not be carried out prior to 24 h post-transfection and, in terms of gene silencing, 24 h siRNA transfection at a nontoxic concentration of 200 nM and 0.2 μL of DharmaFECT reagent was found to yield good knockdown results. It was interesting to observe also how the gene expression started to recover after 24 h, even if still under treatment, and also when the transfection medium was replaced with complete medium and incubated for further 24 h.

Like other GPI-anchored proteins, PrP^C can be released from the cell surface *in vitro* by the action of exogenous bacterial phosphatidylinositol-specific phospholipase C (PI-PLC). PLC acute cleavage was therefore used to enhance the effect of the transient knockdown.

All reagents for the knockdown experiment, such as ON-TARGETplus Human PRNP (5621) siRNA−SMARTpool, ON-TARGETplus Non-targeting Pool, ON-TARGETplus GAPD Control Pool, 5× siRNA Buffer, DharmaFECT 1 Transfection Reagent, and Molecular Grade RNase-free water, were purchased from GE Healthcare Dharmacon. TrypLE Express Enzyme (1×) phenol red was from Gibco via Thermo Fisher. Opti-MEM Reduced Serum Medium and phospholipase C were obtained from Thermo Fisher.

HEK Cell Dosing. Cells from the routine cell culture were seeded in the 96-well plates (15,000 cells/well), previously coated with polyornithin hydrobromide. After 24 h, the cells were checked to ensure that they had attached and were ready for dosing. The complete medium was replaced with conditioning medium containing 1×10^3 pg/mL natural Aβ(1−42) for 2 h and washed with PBS Mg^{2+}/Ca^{2+} before being dosed with the compounds, dissolved in phenol red medium, for 1 h. After that, cells were dosed for 2 h with compounds at 10 μM final concentration. The screen of each compound was carried out in triplicate and repeated at least two times. Negative control cells

https://dx.doi.org/10.1021/acs.jmedchem.0c00841
J. Med. Chem. 2020, 63, 11663−11690

were treated with 0.5% DMSO, vehicle of dilution of the drug, and positive control cells with only Aβos. Once dosing was completed, cells were rinsed with PBS (Sigma) and fixed with 100 μL/well of 4% PFA and incubated for 15 min at room temperature. PFA was removed and cells were washed once or twice with 100 μL PBS if the plates have to be stored in the fridge in PBS. The cells were blocked in 100 μL of PBS-T 5% Donkey serum for 1 h at r.t. and incubated with anti-β amyloid 1−16 clone 6E10 anti-mouse (BioLegend) overnight at 4 °C. The antibody was made up in 50 μL of PBS-T 5% Donkey serum with a dilution factor of 1:250. The primary antibody was removed, and the cells washed three times with 50 μL of PBS-T for 5 min each at r.t. before adding the secondary antibody Alexa Fluor 594 to each well and incubating for 1 h at r.t. The antibody was made up in PBS-T with a dilution factor of 1:500. Cells were washed two times with PBS-T and one time with PBS (50 μL) and nuclei were stained with 100 ng/mL DAPI in PBS prepared from 5 mg/mL stock. After the last two washes, cells were left in 100 μL of PBS to be analyzed. Image acquisition was performed by the ImageXpress Micro Widefield High Content Screening System and analysis of data with MetaXpress Software Multi-Wavelength Translocation Application Module.

Neural Differentiation. Neural induction of hiPSCs (Figure 11) was performed using the modified version of dual SMAD inhibition

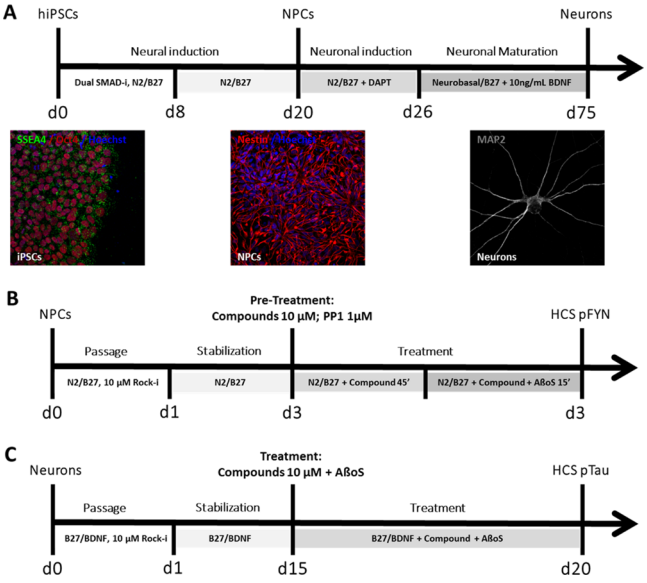

Figure 11. Differentiation of cortical neurons from iPSCs. (A) Outline of cortical differentiation protocol. (B) Outline of the treatment and high-content screening for pFyn kinase. (C) Outline of the treatment and high-content screening for pTau.

protocol.[85] hiPSCs were detached by 3 min of incubation with Versene solution (Gibco); after incubation, the solution was removed, 1 mL of complete TeSR-E8 Medium (StemCell Technologies) was added per well of a six-well plate and detached with a cell lifter (Corning), and then, the cell suspension was transferred to a Matrigel-coated plate (Corning Matrigel Growth Factor Reduced). On the day after plating (day 1), after the cells have reached ∼100% confluence, the cells were washed once with PBS and then the medium was replaced with neural medium (50% DMEM/F-12, 50% neurobasal, 0.5× N_2 supplement, 1× Gibco GlutaMAX Supplement, 0.5× B-27, 50 U mL^{-1} penicillin and 50 mg mL^{-1} streptomycin) supplemented with SMAD inhibitors (SMAD-i, 2 μM DMH-1, 2−10 μM SB43154, Tocris). The medium was changed every day for 7 days; on day 8, when it is possible to see a uniform neuroepithelial sheet, the cells were split into 1:1 with Accutase (StemPro Accutase Cell Dissociation Reagent, Gibco A1110501) onto a Matrigel substrate in the presence of 10 μM Rock inhibitor (Rock-i, Y-27632 dihydrochloride, Tocris), giving rise to a sheet of neural progenitor cells (NPCs). After 24 h of incubation, the medium was removed and replaced with neural medium without Rock-i. The culture medium was changed every second day and, once confluent, it was split.

Neuronal induction from neural progenitor cells was obtained from previously described methods with modifications.[84] NPCs were transferred to poly-L-ornithine/laminin-coated plates (10 μg/mL) and the medium was replaced with neuronal medium (neurobasal medium, 1× Gibco GlutaMAX Supplement, 1× B-27) supplemented with 10 μM DAPT. The medium was changed every day for 6 days, and immature neurons emerged around day 26. On day 40, the young neurons were split with Accutase onto to poly-L-ornithine/laminin-coated plates (10 μg/mL) and the medium was replaced with neuronal medium without DAPT and supplemented with 10 nM BDNF. The cells were then fed at alternate days with neuronal medium until day 75.

Flow Cytometry Analysis. After treatment with 100 nM siRNA (48 h), samples were washed with Ca^{++}/Mg^{++} PBS and treated for 1 h with 0.4 U/mL PLC before being harvested by TrypLE Express Enzyme (1×) phenol red. Cells were resuspended in fresh medium, counted with a hemocytometer, transferred into an Eppendorf tube (11.5×10^6 to 1.5×10^6 cells) and spun down at 1000 rpm for 5 min. The supernatant was decanted, and the pellets were resuspended with cold Ca^{++}/Mg^{++} PBS to wash the cells one time at 2000 rpm for 5 min at 4 °C. During the experiment, it was always useful to check the viability of the cells as in which should be around 95% and not less than 90%. The cells were then resuspended in 1 mL of ice-cold buffer (Ca^{++}/Mg^{++} PBS, 10% FBS, 1% sodium azide) for 5−10 min. Sodium azide prevents the modulation and internalization of surface antigens, which can produce a loss of fluorescence intensity. The primary anti-Aβos 8H4 (concentration, 0.01 M) was diluted 1:200 in 100 μL of PBS and 5% BSA and then the cells were resuspended in this solution, incubated for 1 h on ice, and protected from light. The same was done for the 0.8:200 isotype (concentration, 2.5 mg/mL). The cells were washed two times with cold Ca^{++}/Mg^{++} PBS by centrifugation at 2000 rpm for 5 min and incubated with the secondary antibody in the dark for 1 h under gentle agitation. The fluorochrome-labeled secondary antibody Alexa Fluor 488 was diluted 1:500 in 100 μL of PBS and 5% BSA. Before the analysis, the cells were washed and resuspended in 300 μL of cold Ca^{++}/Mg^{++} PBS and 2 μL of propidium iodide (PI) was added to each sample to exclude dead cells. For best results, all reagents/solutions used were cold and cells were kept on ice and analyzed immediately on the flow cytometer.

Immunocytochemistry (ICC) Analysis. After the transfection with 100 nM siRNA (48 h), the same samples were treated for 1 h with 0.4 U/mL PLC. The cells were rinsed with PBS and conditioning medium containing natural Aβ(1−42) (1×10^3 pg/mL) was added. After 2 h, cells were washed with Mg^{2+}/Ca^{2+} PBS, fixed with 100 μL/well 4% PFA, and incubated for 15 min at room temperature. PFA was removed and cells were washed once or twice with 100 μL of PBS if the plates had to be stored in the fridge in PBS. The cells were blocked in 100 μL of PBS-T 5% Donkey serum for 1 h at r.t. and incubated with anti-β amyloid 1−16 clone 6E10 anti-mouse overnight at 4 °C. The antibody was made up in 50 μL of PBS-T 5% Donkey serum with a dilution factor of 1:250. The primary antibody was removed, and the cells were washed three times with 50 μL of PBS-T for 5 min each at r.t. before adding the secondary antibody Alexa Fluor 488 to each well and incubating for 1 h at r.t. The antibody was made up in PBS-T with a dilution factor of 1:500. Cells were washed two times with PBS-T and one time with PBS (50 μL) and nuclei were stained with 100 ng/mL 4,6-diamidino-2-phenylindole (DAPI) in PBS prepared from 5 mg/mL stock. After the last two washes, cells were left in 100 μL of PBS to be analyzed. Image acquisition was performed by the ImageXpress Micro Widefield High Content Screening System and analysis of data with MetaXpress Software Multi-Wavelength Translocation Application Module.

Treatments. The cells were exposed to the solution containing natural Aβ oligomers obtained from 7PA2 cells [1000 pg/mL Aβ(1−42)]. The compounds were diluted at 10 mM in DMSO (Sigma Chemical Co) and kept out of light at −20 °C until use. PP1 (potent, selective Src family kinase inhibitor) was obtained from Tocris (1397), stored at 1 mM in DMSO (Sigma Chemical Co), and kept out of light at −20 °C until use. To determine the effects of the compounds on inhibiting the activation of Fyn Kinase, NPC cultures were pretreated

https://dx.doi.org/10.1021/acs.jmedchem.0c00841
J. Med. Chem. 2020, 63, 11663−11690

for 45 min with 10 μM of the compounds or 1 μM PP diluted in neurobasal medium without phenol red. After pretreatment, the cells were exposed to 1000 pg/mL of Aβ oligomers in association with the compounds for 15 min; control cultures were treated with DMSO, the vehicle of dilution of the drugs. PP1 was used as a control of inhibition of Fyn activation. To evaluate the potential of the compounds to inhibit the hyperphosphorylation of Tau, cortical neurons were exposed to 1000 pg/mL of Aβ oligomers in association with 10 μM of the compounds for 5 days.

Immunofluorescence. For immunostaining, hiPSCs, NPCs, and neurons were washed with phosphate-buffered saline (PBS) and fixed by immersion in 4% *p*-formaldehyde for 15 min at room temperature. Following fixation, samples were washed three times with PBS and permeabilized with 0.3% Triton X-100 in PBS (Sigma) for 5 min to detect intracellular antigens. After permeabilization, cells were blocked by incubation with PBS containing 5% Donkey serum (DS) (Millipore) for 1 h. After blocking, cell cultures were incubated overnight at 4 °C with primary antibodies diluted in PBS containing 1% DS. After three washes with PBS, cells were incubated with secondary antibodies diluted in PBS containing 1% DS for 1 h at room temperature in the dark. The samples were washed three more times with PBS and incubated with 1.0 mg/mL DAPI for nuclear staining. The following primary antibodies were used at the indicated dilutions: anti-SSEA4 (MC813−70) (mouse, 1:200; Thermo Fisher, 41-4000), anti-Oct4 [EPR17929] (rabbit, 1:250; Abcam, ab181557), anti-Nestin [EPR17929] (rabbit, 1:500; BioLegend, 841901), anti-Tubulin β3 (TUJ1) (mouse, 1:1000; BioLegend, 801201), anti-MAP2 (guinea pig, 1:1000; Synaptic Systems, 188004), anti-phospho-Tau PHF-Tau (Thr181) (mouse, 1:500; Thermo Fisher, MN1050), and Phospho-Fyn (Tyr530) (rabbit, 1:500; Thermo Fisher, PA5-36644). The following secondary antibodies were used at the indicated dilutions: Alexa Fluor 488-conjugated Donkey anti-mouse IgG (1:400; Thermo Fisher, A-21202), Alexa Fluor 594-conjugated Donkey anti-rabbit IgG (1:400; Thermo Fisher, A-31572), Alexa Fluor 594-conjugated Donkey anti-mouse IgG (1:400; Thermo Fisher, A-21203), Alexa Fluor 647-conjugated Goat anti-guinea pig IgG (1:400; Thermo Fisher, A-21450). All experiments included cultures where the primary antibodies were not added, and unspecific stain was not observed in such negative controls. Images were taken from the 63× objective on a Leica TCS SP5 confocal laser scanning microscope coupled with LAS AF lite software (Wetzlar, Germany). We used 386, 488, and 594 nm lasers, along with the appropriate excitation and emission filters. These settings were kept consistent while taking images from all cultures.

High-Content Image Screening (HCS). NPCs were plated at 1×10^4 cells per well on poly-L-ornithine/laminin-coated 96-well plates; after 3 days, the cells were treated. After the treatment, the cells were fixed and stained for pFyn kinase and Alexa Fluor 594 Phalloidin was used as a marker that defines the boundary of cells and DAPI for nuclear staining. A quantitative imaging analysis of the NPCs was conducted through the Opera Phenix High Content Screening System at 40× magnification using the Columbus Image analysis system. The morphological features such as the number of cells and number of spots per cell were assessed for both treated and control cells. At least 15 fields were randomly selected and scanned per well of a 96-well plate in triplicate. To identify and remove any false readings generated by the system, three random Aβ and control wells were selected and counted manually (blind to the group). For the pTau experiment, the treatment with compounds was done concomitantly, with Aβ medium being changed after 3 days of treatment, and cells were allowed to differentiate for 2 more days. On day 5, cells were fixed for immunocytochemistry. The morphological features assessed for both treated and control cells were the number of cells and intensity of Alexa 568 per cell.

MTT Assay. Cortical neural cells were plated on a 96-well plate at a density of 1×10^4 cells/well and kept in a controlled environment (37 °C and 5% CO_2). After 3 days, cells were exposed for 24 h to the medium containing the compounds at a concentration of 1−50 μM. The effect of treatment on cell viability was assessed by measuring mitochondrial enzymatic activity by the 3-(4,5-dimethylthiazol-2-yl)-2,5-diphenyltetrazolium bromide assay (MTT formazan; Sigma-Aldrich). Two hours before the end of the treatment, the MTT solution was added to each well (10 μL/well) at a final concentration of 1 μg/mL and diluted in neural medium. After 2 h, the cells were lysed with a volume of 60 μL/well acidified isopropanol solution at room temperature under agitation for 10 min to complete the dissolution of the formazan crystals. The optical absorbance of each sample was measured using the spectrophotometer at a wavelength of 490 nm (PHERAstar FS microplate reader). The cell cytotoxicity was quantified by measuring the conversion of MTT into MTT formazan by mitochondrial dehydrogenases of viable cells. Each experimental condition was performed in eight replicate wells in at least three independent experiments. The results show the percentage of viability of the cells, and control cells treated with DMSO were considered to be 100%.

Aggregation Assays. For light scattering and spectrophotometric measurements, each compound was dissolved in 10 mM phosphate-buffered saline (PBS) containing 100 mM NaCl (pH 7.4, filtered through paper with 5 μm pores) and 1.25% DMSO for compounds **8**, **9**, **10**, **23**, **24**, and **33**, 2.5% for compounds **21** and **26**, and 5% for compounds **18** and **25** to a final concentration of 10, 50, or 100 μM. After mixing with a vortex, samples were incubated for 2 h at room temperature and protected from light. The positive and negative controls were prepared under the same conditions, *i.e.*, in PBS and the same DMSO concentrations used for the compounds: 1.25, 2.5, or 5%.

Absorbance measurements were performed at room temperature (24 ± 1 °C) with a Jasco V-560 UV/Vis double beam spectrophotometer using quartz cuvettes with a 1 cm optical path.

Light scattering (Rayleigh) was determined by measuring the intensity of light scattered at 90° and 550 nm with a Fluorolog model 3.22 spectrofluorimeter in right-angle geometry (Horiba Jobin Yvon) at room temperature using 1 cm × 1 cm quartz Suprasil cuvettes and setting both excitation and emission wavelengths to 550 nm with a bandwidth of 1 nm. At least two independent replicates were performed for each compound at each concentration, with at least 10 measurements per replicate.

Log $D_{7.4}$ Determination. The *in silico* prediction tool ALOGPS[86] was used to estimate the octanol−water partition coefficients (log *P*) of the compounds. Depending on these values, the compounds were classified either as hydrophilic (log *P* below zero), moderately lipophilic (log *P* between zero and one), or lipophilic (log *P* above one) compounds. For each category, two different ratios (volume of octan-1-ol to volume of buffer) were defined as experimental parameters (Table 5).

Table 5. Compound Classification Based on Estimated Log *P* Values

compound category	log *P*	ratios (octan-1-ol:buffer)
hydrophilic	<0	30:140, 40:130
moderately lipophilic	0−1	70:110, 110:70
lipophilic	>1	3:180, 4:180

Equal amounts of phosphate buffer (0.1 M, pH 7.4) and octan-1-ol were mixed and shaken vigorously for 5 min to saturate the phases. The mixture was left until separation of the two phases, and the buffer was retrieved. Stock solutions of the test compounds were diluted with buffer to a concentration of 1 μM. For each compound, three determinations per octan-1-ol:buffer ratio were performed in different wells of a 96-well plate. The respective volumes of buffer containing an analyte (1 μM) were pipetted to the wells and covered by saturated octan-1-ol according to the chosen volume ratio. The plate was sealed with aluminum foil, shaken (1350 rpm, 25 °C, 2 h) on a Heidolph Titramax 1000 plate shaker (Heidolph Instruments GmbH & Co. KG, Schwabach, Germany), and centrifuged (2000 rpm, 25 °C, 5 min, 5804 R Eppendorf centrifuge, Hamburg, Germany). The aqueous phase was transferred to a 96-well plate for analysis by liquid chromatography−mass spectrometry (LC−MS, see below). Log *P* coefficients were calculated from the octan-1-ol:buffer ratio (o:b), the initial concentration of the analyte in buffer (1 μM), and the concentration of the analyte in buffer (c_B) according to the following equation

https://dx.doi.org/10.1021/acs.jmedchem.0c00841
J. Med. Chem. 2020, 63, 11663−11690

$$\log P = \log\left(\frac{1\ \mu M - c_B}{c_B} \times \frac{1}{o:\ b}\right)$$

Results are presented as the mean ± SD of three independent experiments. If the mean of two independent experiments obtained for a given compound did not differ by more than 0.1 units, then the results were accepted.

Parallel Artificial Membrane Permeability Assay (PAMPA). Effective permeability (log P_e) was determined in a 96-well format with PAMPA.[87] For each compound, measurements were performed at pH 7.4 in quadruplicates. Four wells of a deep-well plate were filled with 650 μL of PRISMA HT universal buffer, adjusted to pH 7.4 by adding the requested amount of NaOH (0.5 M). Samples (150 μL) were withdrawn from each well to determine the blank spectra by UV/Vis spectroscopy (190 to 500 nm, SpectraMax 190, Molecular Devices, Silicon Valley, CA, USA). Then, an analyte dissolved in DMSO (10 mM) was added to the remaining buffer to yield 50 μM solutions. To exclude precipitation, the optical density (OD) was measured at 650 nm, and solutions exceeding OD 0.01 were filtrated. Afterward, samples (150 μL) were withdrawn to determine the reference spectra. Further, 200 μL of samples was transferred to each well of the donor plate of the PAMPA sandwich (pIon, P/N 110163). The filter membranes at the bottom of the acceptor plate were infused with 5 μL of GIT-0 Lipid Solution and 200 μL of Acceptor Sink Buffer was filled into each acceptor well. The sandwich was assembled, placed in the GutBox, and left undisturbed for 16 h. Then, it was disassembled and samples (150 μL) were transferred from each donor and acceptor well to UV plates for determination of the UV/Vis spectra. Effective permeability (log P_e) was calculated from the compound flux deduced from the spectra, the filter area, and the initial sample concentration in the donor well with the aid of the PAMPA Explorer Software (pIon, version 3.5).

LC–MS Measurements. Analyses were performed using a 1100/1200 Series HPLC System coupled to a 6410 Triple Quadrupole mass detector (Agilent Technologies, Inc., Santa Clara, CA, USA) equipped with electrospray ionization. The system was controlled with the Agilent MassHunter Workstation Data Acquisition software (version B.01.04). The column used was an Atlantis T3 C18 column (2.1 × 50 mm) with a 3 μm particle size (Waters Corp., Milford, MA, USA). The mobile phase consisted of eluent A (10 mM ammonium acetate, pH 5.0, in 95:5 H_2O:MeCN) and eluent B (MeCN containing 0.1% formic acid). The flow rate was maintained at 0.6 mL/min. The gradient was ramped from 95% A/5% B to 5% A/95% B over 1 min and then held at 5% A/95% B for 0.1 min. The system was then brought back to 95% A/5% B, resulting in a total duration of 4 min. MS parameters such as fragmentor voltage, collision energy, and polarity were optimized individually for each drug, and the molecular ion was followed for each compound in the multiple reaction monitoring mode. The concentrations of the analytes were quantified by Agilent Mass Hunter Quantitative Analysis software (version B.01.04).

■ ASSOCIATED CONTENT

Supporting Information

The Supporting Information is available free of charge at https://pubs.acs.org/doi/10.1021/acs.jmedchem.0c00841.

DFT calculations, STD-NMR experiments, ThT fluorescence assays, membrane PAINS calculations, aggregation studies, ^{1}H NMR and ^{13}C NMR spectra of novel final compounds and key intermediates, analysis of the purity of tested compounds by HPLC-DAD-ESI(−)MS, and analysis of the purity of tested compounds by HPLC-DAD (PDF)

Molecular formula strings (CSV)

■ AUTHOR INFORMATION

Corresponding Authors

Amélia P. Rauter − *Centro de Química Estrutural, Faculdade de Ciências, Universidade de Lisboa, Lisboa 1749-016, Portugal;* orcid.org/0000-0003-3790-7952; Phone: +351968810971; Email: aprauter@fc.ul.pt

Beining Chen − *Department of Chemistry, The University of Sheffield, Sheffield S3 7HF, United Kingdom;* Phone: +447710075082; Email: b.chen@sheffield.ac.uk

Authors

Ana M. de Matos − *Centro de Química Estrutural, Faculdade de Ciências, Universidade de Lisboa, Lisboa 1749-016, Portugal*

M. Teresa Blázquez-Sánchez − *Centro de Química Estrutural, Faculdade de Ciências, Universidade de Lisboa, Lisboa 1749-016, Portugal*

Andreia Bento-Oliveira − *Centro de Química Estrutural, Faculdade de Ciências, Universidade de Lisboa, Lisboa 1749-016, Portugal*

Rodrigo F. M. de Almeida − *Centro de Química Estrutural, Faculdade de Ciências, Universidade de Lisboa, Lisboa 1749-016, Portugal*

Rafael Nunes − *Centro de Química Estrutural, Faculdade de Ciências and Biosystems & Integrative Sciences Institute, Faculdade de Ciências, Universidade de Lisboa, Lisboa 1749-016, Portugal;* orcid.org/0000-0002-9014-0570

Pedro E. M. Lopes − *Biosystems & Integrative Sciences Institute, Faculdade de Ciências, Universidade de Lisboa, Lisboa 1749-016, Portugal*

Miguel Machuqueiro − *Biosystems & Integrative Sciences Institute, Faculdade de Ciências, Universidade de Lisboa, Lisboa 1749-016, Portugal*

Joana S. Cristóvão − *Biosystems & Integrative Sciences Institute, Faculdade de Ciências, Universidade de Lisboa, Lisboa 1749-016, Portugal*

Cláudio M. Gomes − *Biosystems & Integrative Sciences Institute, Faculdade de Ciências, Universidade de Lisboa, Lisboa 1749-016, Portugal;* orcid.org/0000-0003-4662-6933

Cleide S. Souza − *Department of Chemistry, The University of Sheffield, Sheffield S3 7HF, United Kingdom*

Imane G. El Idrissi − *Dipartimento di Farmacia-Scienze del Farmaco, Università degli Studi di Bari "A. Moro", 70125 Bari, Italy*

Nicola A. Colabufo − *Dipartimento di Farmacia-Scienze del Farmaco, Università degli Studi di Bari "A. Moro", 70125 Bari, Italy;* orcid.org/0000-0001-5639-7746

Ana Diniz − *UCIBIO, REQUIMTE, Faculdade de Ciências e Tecnologia, Universidade Nova de Lisboa, Caparica 2829-516, Portugal*

Filipa Marcelo − *UCIBIO, REQUIMTE, Faculdade de Ciências e Tecnologia, Universidade Nova de Lisboa, Caparica 2829-516, Portugal*

M. Conceição Oliveira − *Mass Spectrometry Facility at CQE, Insituto Superior Técnico, Lisboa 1049-001, Portugal*

Óscar López − *Departamento de Química Orgánica, Facultad de Química, Universidad de Sevilla, Sevilla E-41071, Spain*

José G. Fernandez-Bolaños − *Departamento de Química Orgánica, Facultad de Química, Universidad de Sevilla, Sevilla E-41071, Spain;* orcid.org/0000-0003-1499-0650

Philipp Dätwyler − *Department of Pharmaceutical Sciences, University of Basel, Basel CH-4056, Switzerland*

Beat Ernst − *Department of Pharmaceutical Sciences, University of Basel, Basel CH-4056, Switzerland;* orcid.org/0000-0001-5787-2297

Ke Ning − *Department of Neuroscience, Sheffield Institute for Translational Neuroscience, The University of Sheffield, Sheffield S10 2HQ, United Kingdom*

Claire Garwood − *Department of Neuroscience, Sheffield Institute for Translational Neuroscience, The University of Sheffield, Sheffield S10 2HQ, United Kingdom*

Complete contact information is available at: https://pubs.acs.org/10.1021/acs.jmedchem.0c00841

Author Contributions

[¶]A.M.d.M. and M.T.B.-S. contributed equally to this work.

Notes

The authors declare no competing financial interest.

■ ACKNOWLEDGMENTS

The European Union is gratefully acknowledged for the support of the project entitled "Diagnostic and Drug Discovery Initiative for Alzheimer's Disease" (D3i4AD), FP7-PEOPLE-2013-IAPP, GA 612347. The authors also thank the Portuguese Foundation for Science and Technology (FCT) for the Ph.D. scholarships attributed to A.M.d.M. (SFRH/BD/93170/2013), R.N. (SFRH/BD/116614/2016), A.D. (PD/BD/142847/2018), and A.B.-O. (SFRH/BD/145600/2019), for the individual research grants CEECIND/03414/2018 given to R.F.M.d.A., and CEECIND/02300/2017 given to M.M. FCT is also acknowledged for the support of Centro de Química Estrutural (CQE project UIDB/00100/2020), Instituto de Biosistemas e Ciências Integrativas (BioISI project UIDB/04046/2020), and the Applied Molecular Biosciences Unit (UCIBIO project UIDB/04378/2020), and F.M. also thanks FCT for the IF investigator project (IF/00780/2015). The NMR spectrometers are part of the National NMR Network (PTNMR) and are partially supported by Infrastructure Project No. 22161 (cofinanced by FEDER through COMPETE 2020, POCI and PORL and FCT through PIDDAC). Diogo Vila-Viçosa is also acknowledged for fruitful discussion on performed DFT calculations. The Dirección General de Investigación of Spain (CTQ2016-78703-P), the Junta de Andalucía (FQM134), and FEDER (501100008530) are also acknowledged for the financial support.

■ ABBREVIATIONS USED

AChE, acetylcholinesterase; AD, Alzheimer's disease; Aβ, amyloid beta; Aβos, Aβ oligomers; AFM, atomic force microscopy; BBB, blood−brain barrier; BuChE, butyrylcholinesterase; cDNA, complementary DNA; CHO, Chinese hamster ovary cells; *c* log *P*, calculated partition coefficient; CM, conditioned medium; DAPI, 4,6-diamidino-2-phenylindole; DFT, density functional theory; DID, diabetes-induced dementia; DMAP, 4-dimethylaminopyridine; DMEM, Dulbecco's modified Eagle's medium; DMSO, dimethyl sulfoxide; DTNB, 5,5′-dithiobis(2-nitrobenzoic acid); ELISA, enzyme -linked immunosorbent assay; GLUT, glucose transporter; GPI, glycosylphosphatidylinositol; HCS, high-content image screening; HEK, human embryonic kidney; HPLC, high-performance liquid chromatography; IAPP, islet amyloid polypeptide; ICC, immunocytochemistry; IDE, insulin-degrading enzyme; hiPSC, human induced pluripotent stem cell line; Ket, ketoconazole; LC−MS, liquid chromatography coupled to mass spectrometry; log *D*, distribution coefficient; log *P*, partition coefficient; log P_e, effective permeability; mAβ, monomeric Aβ; MeCN, acetonitrile; MTT, 3-(4,5-dimethylthiazol-2-yl)-2,5-diphenyl-2*H*-tetrazolium bromide; NFT, neurofibrillary tangles; NPC, neural progenitor cell; PAINS, pan-assay interference compounds; PAMPA, parallel artificial membrane permeability assay; PBS, phosphate-buffered saline; PFA, paraformaldehyde; pFyn, Src family kinase; PHF, paired helical filaments; PMF, potential of mean force; PLC, phospholipase C; POPC, 1-palmitoyl-2-oleoyl-*sn*-glycero-3-phosphocholine; PP1, protein phosphatase 1; PrP^C, cellular prion protein; pTau, phosphorylated Tau; Quer, quercetin; SGLT, sodium glucose-linked transporter; siRNA, small interfering RNA; SFK, Src family kinases; STD, saturation-transfer difference; T2D, type 2 diabetes; TfOH, trifluoromethanesulfonic acid; ThT, thioflavin-T; TMSOTf, trimethylsilyl trifluoromethanesulfonate; UV, ultraviolet; Vis, visible

■ REFERENCES

(1) Williams, R.; Colagiuri, S.; Chan, J.; Gregg, E. W.; Ke, C.; Lim, L. L.; Yang, X. *IDF Diabetes Atlas*; 9th ed., eds. Karuranga, S.; Malanda, B.; Saeedi, P.; Salpea, P., International Diabetes Federation: United kingdom, 2019, p.35.

(2) de Matos, A. M.; de Macedo, M. P.; Rauter, A. P. Bridging type 2 diabetes and Alzheimer's disease: assembling the puzzle pieces in the quest for the molecules with therapeutic and preventive potential. *Med. Res. Rev.* **2018**, *38*, 261−324.

(3) Nygaard, H. B. Targeting Fyn kinase in Alzheimer's disease. *Biol. Psychiatry.* **2018**, *83*, 369−376.

(4) Um, J. W.; Strittmatter, S. M. Amyloid-β induced signaling by cellular prion protein and Fyn kinase in Alzheimer disease. *Prion* **2013**, *7*, 37−41.

(5) Smith, L. M.; Zhu, R.; Strittmatter, S. M. Disease-modifying benefit of Fyn blockade persists after washout in mouse Alzheimer's model. *Neuropharmacology* **2018**, *130*, 54−61.

(6) Kaufman, A. C.; Salazar, S. V.; Haas, L. T.; Yang, J.; Kostylev, M. A.; Jeng, A. T.; Robinson, S. A.; Gunther, E. C.; van Dyck, C. H.; Nygaard, H. B.; Strittmatter, S. M. Fyn inhibition rescues established memory and synapse loss in Alzheimer mice. *Ann. Neurol.* **2015**, *77*, 953−971.

(7) Lambert, M. P.; Barlow, A. K.; Chromy, B. A.; Edwards, C.; Freed, R.; Liosatos, M.; Morgan, T. E.; Rozovsky, I.; Trommer, B.; Viola, K. L.; Wals, P.; Zhang, C.; Finch, C. E.; Krafft, G. A.; Klein, W. L. Diffusible, nonfibrillar ligands derived from Abeta(1-42) are potent central nervous system neurotoxins. *Proc. Natl. Acad. Sci. U. S. A.* **1998**, *95*, 6448−6453.

(8) Yamada, E.; Pessin, J. E.; Kurland, I. J.; Schwartz, G. J.; Bastie, C. C. Fyn-dependent regulation of energy expenditure and body weight is mediated by tyrosine phosphorylation of LKB1. *Cell Metab.* **2010**, *11*, 113−124.

(9) Lee, T.-W. A.; Kwon, H.; Zong, H.; Yamada, E.; Vatish, M.; Pessin, J. E.; Bastie, C. C. Fyn deficiency promotes a preferential increase in subcutaneous adipose tissue mass and decreased visceral adipose tissue inflammation. *Diabetes* **2013**, *62*, 1537−1546.

(10) Yang, Y.; Tarabra, E.; Yang, G. S.; Vaitheesvaran, B.; Palacios, G.; Kurland, I. J.; Pessin, J. E.; Bastie, C. C. Alteration of de novo glucose production contributes to fasting hypoglycaemia in Fyn deficient mice. *PLoS One* **2013**, *8*, No. e81866.

(11) Oskarsson, M. E.; Paulsson, J. F.; Schultz, S. W.; Ingelsson, M.; Westermark, P.; Westermark, G. T. In vivo seeding and cross-seeding of localized amyloidosis: a molecular link between type 2 diabetes and Alzheimer's disease. *Am. J. Pathol.* **2015**, *185*, 834−846.

(12) Baram, M.; Atsmon-Raz, Y.; Ma, B.; Nussinov, R.; Miller, Y. Amylin-Aβ oligomers at atomic resolution using molecular dynamics simulations: a link between Type 2 diabetes and Alzheimer's disease. *Phys. Chem. Chem. Phys.* **2016**, *18*, 2330−2338.

(13) Nabavi, S. F.; Sureda, A.; Dehpour, A. R.; Shirooie, S.; Silva, A. S.; Devi, K. P.; Ahmed, T.; Ishaq, N.; Hashim, R.; Sobarzo-Sánchez, E.; Daglia, M.; Braidy, N.; Volpicella, M.; Vacca, R. A.; Nabavi, S. M. Regulation of autophagy by polyphenols: Paving the road for treatment of neurodegeneration. *Biotechnol. Adv.* **2017**, *36*, 1768−1778.

(14) Jia, J. J.; Zeng, X. S.; Song, X. Q.; Zhang, P. P.; Chen, L. Diabetes mellitus and Alzheimer's disease: The protection of epigallocatechin-3-

gallate in streptozotocin injection-induced models. *Front. Pharmacol.* **2017**, *8*, 834.
(15) Guo, Y.; Zhao, Y.; Nan, Y.; Wang, X.; Chen, Y.; Wang, S. (−)-Epigallocatechin-3-gallate ameliorates memory impairment and rescues the abnormal synaptic protein levels in the frontal cortex and hippocampus in a mouse model of Alzheimer's disease. *Neuroreport.* **2017**, *28*, 590−597.
(16) Chen, S.; Nimick, M.; Cridge, A. G.; Hawkins, B. C.; Rosengren, R. J. Anticancer potential of novel curcumin analogs towards castrate-resistant prostate cancer. *Int. J. Oncol.* **2018**, *52*, 579−588.
(17) Rauter, A. P.; Ennis, M.; Hellwich, K. H.; Herold, B. J.; Horton, D.; Moss, G. P.; Schomburg, I. Nomenclature of flavonoids (IUPAC recommendations 2017). *Pure Appl. Chem.* **2018**, 1429−1486.
(18) Biasutto, L.; Marotta, E.; Bradaschia, A.; Fallica, M.; Mattarei, A.; Garbisa, S.; Zoratti, M.; Paradisi, C. Soluble polyphenols: synthesis and bioavailability of 3,4′,5-tri(alpha-D-glucose-3-*O*-succinyl) resveratrol. *Bioorg. Med. Chem. Lett.* **2009**, *19*, 6721−6724.
(19) Hollman, P. C. H. Absorption, bioavailability, and metabolism of flavonoids. *Pharm. Biol.* **2004**, *42*, 74−83.
(20) Xiao, J. Dietary flavonoid aglycones and their glycosides: Which show better biological significance? *Crit. Rev. Food Sci. Nutr.* **2017**, *57*, 1874−1905.
(21) Ladiwala, A. R. A.; Mora-Pale, M.; Lin, J. C.; Bale, S. S.; Fishman, Z. S.; Dordick, J. S.; Tessier, P. M. Polyphenolic glycosides and aglycones utilize opposing pathways to selectively remodel and inactivate toxic oligomers of amyloid *β*. *ChemBioChem* **2011**, *12*, 1749−1758.
(22) Xiao, J.; Capanoglu, E.; Jassbi, A. R.; Miron, A. Advance on the flavonoid *C*-glycosides and health benefits. *Crit. Ver. Food Sci. Nutr.* **2016**, *56*, S29−S45.
(23) Jesus, A. R.; Vila-Viçosa, D.; Machuqueiro, M.; Marques, A. P.; Dore, T. M.; Rauter, A. P. Targeting type 2 diabetes with *C*-glucosyl dihydrochalcones as selective sodium glucose co-transporter 2 (SGLT2) inhibitors: Synthesis and biological evaluation. *J. Med. Chem.* **2017**, *60*, 568−579.
(24) de Matos, A. M.; Calado, P.; Rauter, A. P. Recent Advances on SGLT2 Inhibitors: Synthetic Approaches, Therapeutic Benefits and Adverse Events. In *Successful Drug Discovery*; Volume 5, Eds Fischer, J.; Klein, C.; Childers, W. E., Wiley-VCH: Weinheim, in press, 2020. DOI: DOI: 10.1002/9783527826872.ch4
(25) Jesus, A. R.; Dias, C.; Matos, A. M.; de Almeida, R. F. M.; Viana, A. S.; Marcelo, F.; Ribeiro, R. T.; Macedo, M. P.; Airoldi, C.; Nicotra, F.; Martins, A.; Cabrita, E. J.; Jiménez-Barbero, J.; Rauter, A. P. Exploiting the therapeutic potential of 8-*β*-D-glucopyranosylgenistein: Synthesis, antidiabetic activity, and molecular interaction with islet amyloid polypeptide and amyloid *β*-peptide (1-42). *J. Med. Chem.* **2014**, *57*, 9463−9472.
(26) Rawat, P.; Kumar, M.; Rahuja, N.; Lal Srivastava, D. S.; Srivastava, A. K.; Maurya, R. Synthesis and antihyperglycemic activity of phenolic *C*-glycosides. *Bioorg. Med. Chem. Lett.* **2011**, *21*, 228−233.
(27) He, L.; Zhang, Y. Z.; Tanoh, M.; Chen, G.-R.; Praly, J.-P.; Chrysina, E. D.; Tiraidis, C.; Kosmopoulou, M.; Leonidas, D. D.; Oikonomakos, N. G. In the search of glycogen phosphorylase inhibitors: Synthesis of *C*-D-glycopyranosylbenzo(hydro)quinones − Inhibition of and binding to glycogenphosphorylase in the crystal. *Eur. J. Org. Chem.* **2007**, *2007*, 596−606.
(28) Jaramillo, C.; Knapp, S. Synthesis of *C*-aryl glycosides. *Synthesis* **1994**, *1994*, 1−20.
(29) Nomura, S.; Sakamaki, S.; Hongu, M.; Kawanishi, E.; Koga, Y.; Sakamoto, T.; Yamamoto, Y.; Ueta, K.; Kimata, H.; Nakayama, K.; Tsuda-Tsukimoto, M. Discovery of canagliflozin, a novel *C*-glucoside with thiophene ring, as sodium-dependent glucose cotransporter 2 inhibitor for the treatment of type 2 diabetes mellitus. *J. Med. Chem.* **2010**, *53*, 6355−6360.
(30) Liao, H.; Leng, W.-L.; Hoang, K. L. M.; Yao, H.; He, J.; Voo, A. Y. H.; Liu, X.-W. Asymmetric syntheses of 8-oxabicyclo[3,2,1]octane and 11-oxatricyclo[5.3.1.0]undecane from glycals. *Chem. Sci.* **2017**, *8*, 6656−6661.
(31) Jarreton, O.; Skrydstrup, T.; Espinosa, J.-F.; Jiménez-Barbero, J.; Beau, J.-M. Samarium diiodide promoted *C*-glycosylation: An application to the stereospecific synthesis of *α*-1,2-*C*-mannobioside and its derivatives. *Chem. − Eur. J.* **1999**, *5*, 430−441.
(32) Yuan, X.; Linhardt, R. Recent Advances in the synthesis of *C*-oligosaccharides. *Curr. Top. Med. Chem.* **2005**, *5*, 1393−1430.
(33) dos Santos, R. G.; Jesus, A. R.; Caio, J. M.; Rauter, A. P. Fries-type reactions for the *C*-glycosylation of phenols. *Curr. Org. Chem.* **2011**, *15*, 128−148.
(34) Matsumoto, T.; Katsuki, M.; Suzuki, K. New approach to *C*-aryl glycosides starting from phenol and glycosyl fluoride. Lewis acid-catalyzed rearrangement of *O*-glycoside to *C*-glycoside. *Tetrahedron Lett.* **1988**, *29*, 6935−6938.
(35) Kometani, T.; Kondo, H.; Fujimori, Y. Boron trifluoride-catalyzed rearrangement of 2-aryloxytetrahydropyrans: a new entry to *C*-arylglycosidation. *Synthesis-Stuttgart.* **1988**, *12*, 1005−1007.
(36) Furuta, T.; Kimura, T.; Kondo, S.; Mihara, H.; Wakimoto, T.; Nukaya, H.; Tsuji, K.; Tanaka, K. Concise total synthesis of flavone *C*-glycoside having potent anti-inflammatory activity. *Tetrahedron* **2004**, *60*, 9375−9379.
(37) Kumazawa, T.; Kimura, T.; Matsuba, S.; Sato, S.; Onodera, J. Synthesis of 8-*C*-glucosylflavones. *Carbohydr. Res.* **2011**, *334*, 183−193.
(38) Mahling, J.-A.; Jung, K.-H.; Schmidt, R. R. Synthesis of flavone *C*-glycosides vitexin, isovitexin and isoembigenin. *Leibigs Ann. Chem.* **1995**, *1995*, 461−466.
(39) Haverkamp, J.; van Dongen, J. P. C. M.; Vliegenthart, J. F. G. PMR and CMR spectroscopy of methyl 2,3,4,6-tetra-*O*-methyl-*α*- and -*β*-D-glucopyranoside : An application to the identification of partially methylated glucoses. *Tetrahedron* **1973**, *29*, 3431−3439.
(40) Wegmann, B.; Schmidt, R. R. The application of the trichloroacetimidate method to the synthesis of *α*-D-gluco- and *α*-D-galactopyranosides. *J. Carbohydr. Chem.* **1987**, *6*, 357−375. and references cited therein
(41) Cai, X.; Ng, K.; Panesar, H.; Moon, S.-J.; Paredes, M.; Ishida, K.; Hertweck, C.; Minehan, T. G. Total synthesis of the antitumor natural product polycarcin V and evaluation of its DNA binding profile. *Org. Lett.* **2014**, *16*, 2962−2965.
(42) Wei, X.; Liang, D.; Wang, Q.; Meng, X.; Li, Z. Total synthesis of mangiferin, homomangiferin, and neomangiferin. *Org. Biomol. Chem.* **2016**, *14*, 8821−8831.
(43) Wu, Z.; Wei, G.; Lian, G.; Yu, B. Synthesis of mangiferin, isomangiferin, and homomangiferin. *J. Org. Chem.* **2010**, *75*, 5725−5728.
(44) Morris, G. P.; Clark, I. A.; Vissel, B. Inconsistencies and controversies surrounding the amyloid hypothesis of Alzheimer's disease. *Acta Neuropathol. Commun.* **2014**, *2*, 135.
(45) Hardy, J.; Selkoe, D. J. The amyloid hypothesis of Alzheimer's disease: Progress and problems on the road to therapeutics. *Science* **2002**, *297*, 353−356.
(46) Kittelberger, K. A.; Piazza, F.; Tesco, G.; Reijmers, L. G. Natural amyloid-beta oligomers acutely impair the formation of a contextual fear memory in mice. *PLoS One* **2012**, *7*, No. e29940.
(47) Matrone, C.; Petrillo, F.; Nasso, R.; Ferreti, G. Fyn tyrosine kinase as harmonizing factor in neuronal functions and dysfunctions. *Int. J. Mol. Sci.* **2020**, *21*, 4444.
(48) Sato, M.; Murakami, K.; Uno, M.; Nakagawa, Y.; Katayama, S.; Akagi, K.; Masuda, Y.; Takegoshi, K.; Irie, K. Site-specific inhibitory mechanism for amyloid *β*42 aggregation by catechol-type flavonoids targeting the Lys residues. *J. Biol. Chem.* **2013**, *288*, 23212−23224.
(49) Ingólfsson, H. I.; Thakur, P.; Herold, K. F.; Hobart, E. A.; Ramsey, N. B.; Periole, X.; de Jong, D. H.; Zwama, M.; Yilmaz, D.; Hall, K.; Maretzky, T.; Hemmings, H. C., Jr.; Blobel, C.; Marrink, S. J.; Koçer, A.; Sack, J. T.; Andersen, O. S. Phytochemicals perturb membranes and promiscuously alter protein function. *ACS Chem. Biol.* **2014**, *9*, 1788−1798.
(50) Yang, J. J.; Ursu, O.; Lipinski, C. A.; Sklar, L. A.; Oprea, T. I.; Bologa, C. G. Badapple: promiscuity patterns from noisy evidence. *Aust. J. Chem.* **2016**, *8*, 29.

(51) Shoichet, B. K. Screening in a spirit haunted world. *Drug Discovery Today* **2006**, *11*, 607−615.
(52) Vallverdú-Queralt, A.; Biler, M.; Meudec, E.; Le Guernevé, C.; Vernhet, A.; Jean-Paul Mazauric, J.-P.; Legras, J. L.; Loonis, M.; Trouillas, P.; Cheynier, V.; Dangles, O. *p*-Hydroxyphenyl-pyranoanthocyanins: An experimental and theoretical investigation of their acid-base properties and molecular interactions. *Int. J. Mol. Sci.* **2016**, *17*, 1842.
(53) McGovern, S. L.; Shoichet, B. K. Kinase inhibitors: not just for kinases anymore. *J. Med. Chem.* **2003**, *46*, 1478−1483.
(54) Seidler, J.; McGovern, S. L.; Doman, T. N.; Shoichet, B. K. Identification and prediction of promiscuous aggregating inhibitors among known drugs. *J. Med. Chem.* **2003**, *46*, 4477−4486.
(55) Coan, K. E. D.; Shoichet, B. K. Stoichiometry and physical chemistry of promiscuous aggregate-based inhibitors. *J. Am. Chem. Soc.* **2008**, *130*, 9606−9612.
(56) Bruno, F. F.; Trotta, A.; Fossey, S.; Nagarajan, S.; Nagarajan, R.; Samuelson, L. A.; Kumar, J. Enzymatic synthesis and characterization of polyQuercetin. *J. Macromol. Sci. A* **2010**, *47*, 1191−1196.
(57) Momić, T.; Savić, J.; Černigoj, U.; Trebše, P.; Vasić, V. Protolytic equilibria and photodegradation of quercetin in aqueous solution. *Collect. Czech. Chem. Commun.* **2007**, *72*, 1447−1460.
(58) Mezzetti, A.; Protti, S.; Lapouge, C.; Cornard, J.-P. Protic equilibria as the key factor of quercetin emission in solution. Relevance to biochemical and analytical studies. *Phys. Chem. Chem. Phys.* **2011**, *13*, 6858−6864.
(59) de Granada-Flor, A.; Sousa, C.; Filipe, H. A. L.; Santos, M. S. C. S.; de Almeida, R. F. M. Quercetin dual interaction at the membrane level. *Chem. Commun.* **2019**, *55*, 1750−1753.
(60) Zupancic, E.; Carreira, A. C.; de Almeida, R. F. M.; Silva, L. C. Biophysical implications of sphingosine accumulation in membrane properties at neutral and acidic pH. *J. Phys. Chem. B* **2014**, *118*, 4858−4866.
(61) Zhou, Y.; Shi, J.; Chu, D.; Hu, W.; Guan, Z.; Gong, C.-X.; Iqbal, K.; Liu, F. Relevance of phosphorylation and truncation of Tau to the etiopathogenesis of Alzheimer's disease. *Front Aging Neurosci.* **2018**, *10*, 27.
(62) Iqbal, K.; Liu, F.; Gong, C. X.; Grundke-Iqbal, I. Tau in Alzheimer disease and related tauopathies. *Curr. Alzheimer Res.* **2010**, *7*, 656−664.
(63) Liu, F.; Shi, J.; Tanimukai, H.; Gu, J.; Gu, J.; Grundke-Iqbal, I.; Iqbal, K.; Gong, C. X. Reduced *O*-GlcNAcylation links lower brain glucose metabolism and tau pathology in Alzheimer's disease. *Brain* **2009**, *132*, 1820−1832.
(64) Kópke, E.; Tung, Y. C.; Shaikh, S.; Alonso, A. C.; Iqbal, K.; Grundke-Iqbal, I. Microtubule-associated protein tau. Abnormal phosphorylation of a non-paired helical filament pool in Alzheimer disease. *J. Biol. Chem.* **1993**, *268*, 24374−22384.
(65) Desmarais, J. A.; Unger, C.; Damjanov, I.; Meuth, M.; Andrews, P. Apoptosis and failure of checkpoint kinase 1 activation in human induced pluripotent stem cells under replication stress. *Stem Cell Res. Ther.* **2016**, *7*, 17.
(66) Bischoff, H. The mechanism of alpha-glucosidase inhibition in the management of diabetes. *Clin. Invest. Med.* **1995**, *18*, 303−311.
(67) de Melo, E. B.; da Silveira Gomes, A.; Carvalho, I. α- and β-Glucosidase inhibitors: chemical structure and biological activity. *Tetrahedron* **2006**, *62*, 10277−10302.
(68) Rauter, A. P.; Jesus, A.; Martins, A.; Dias, C.; Ribeiro, R.; Macedo, M. P.; Justino, J.; Mota-Filipe, H.; Pinto, R.; Sepodes, B.; Medeiros, M.; Jiménez Barbero, J.; Airoldi, C.; Nicotra, F. New C-glycosylpolyphenol Antidiabetic Agents, Effect on Glucose Tolerance and Interaction with Beta-Amyloid. Therapeutic Applications of the Synthesized Agent(s) and of *Genista tenera* Ethyl Acetate Extracts Containing Some of Those Agents. US20,150,031,639A1, Oct 03, 2017.
(69) Jean, L.; Thomas, B.; Tahiri-Alaoui, A.; Shaw, M.; Vaux, D. J. Heterologous amyloid seeding: Revisiting the role of acetylcholinesterase in Alzheimer's disease. *PLoS One* **2007**, *2*, No. e652.
(70) Greig, N. H.; Utsuki, T.; Ingram, D. K.; Wang, Y.; Pepeu, G.; Scali, C.; Yu, Q.-S.; Mamczarz, J.; Holloway, H. W.; Giordano, T.; Chen, D.; Furukawa, K.; Sambamurti, K.; Brossi, A.; Lahiri, D. K. Selective butyrylcholinesterase inhibition elevates brain acetylcholine, augments learning and lowers Alzheimer β-amyloid peptide in rodent. *Proc. Natl. Acad. Sci. U. S. A.* **2005**, *102*, 17213−17218.
(71) Diamant, S.; Podoly, E.; Friedler, A.; Ligumsky, H.; Livnah, O.; Soreq, H. Butyrylcholinesterase attenuates amyloid fibril formation *in vitro*. *Proc. Natl. Acad. Sci. U. S. A.* **2006**, *103*, 8628−8633.
(72) Araujo, J. A.; Greig, N. H.; Ingram, D. K.; Sandin, J.; de Rivera, C.; Milgram, N. W. Cholinesterase inhibitors improve both memory and complex learning in aged beagle dogs. *J. Alzheimers Dis.* **2011**, *26*, 143−155.
(73) Greig, N. H.; Lahiri, D. K.; Sambamurti, K. Butyrylcholinesterase: an important new target in Alzheimer's disease therapy. *Int Psychogeriatr.* **2002**, *14*, 77−91.
(74) Mushtaq, G.; Greig, N. H.; Khan, J. A.; Kamal, M. A. Status of acetylcholinesterase and butyrylcholinesterase in Alzheimer's disease and type 2 diabetes mellitus. *C.N.S. Neurol. Disord. Drug Targets* **2014**, *13*, 1432−1439.
(75) Rao, A. A.; Sridhar, G. R.; Das, U. N. Elevated butyrylcholinesterase and acetylcholinesterase may predict the development of type 2 diabetes mellitus and Alzheimer's disease. *Med. Hypotheses* **2007**, *69*, 1272−1276.
(76) Sato, K. K.; Hayashi, T.; Maeda, I.; Koh, H.; Harita, N.; Uehara, S.; Onishi, Y.; Oue, K.; Nakamura, Y.; Endo, G.; Kambe, H.; Fukuda, K. Serum butyrylcholinesterase and the risk of future type 2 diabetes: the Kansai Healthcare Study. *Clin. Endocrinol. (Oxf).* **2014**, *80*, 362−367.
(77) Iwasaki, T.; Yoneda, M.; Nakajima, A.; Terauchi, Y. Serum butyrylcholinesterase is strongly associated with adiposity, the serum lipid profile and insulin resistance. *Intern. Med.* **2007**, *46*, 1633−1639.
(78) Zhang, Y.; Zhang, T.; Wang, F.; Xie, J. Brain tissue distribution of spinosin in rats determined by a new high-performance liquid chromatography-electrospray ionization-mass/mass spectrometry method. *J. Chromatogr. Sci.* **2015**, *53*, 97−103.
(79) Di, L.; Kerns, E. H. Profiling drug-like properties in discovery research. *Curr. Opin. Chem. Biol.* **2003**, *7*, 402−408.
(80) Bols, M.; Hazell, R. G.; Thomsen, I. B. 1-Azafagomine: A hydroxyhexahydropyridazine that potently inhibits enzymatic glycoside cleavage. *Chem. Eur. J.* **1997**, *3*, 940−947.
(81) Cornish-Bowden, A. A simple graphical method for determining the inhibition constants of mixed, uncompetitive and non-competitive inhibitors. *Biochem. J.* **1974**, *137*, 143−144.
(82) Ellman, G. L.; Courtney, K. D.; Andres, V., Jr.; Featherstone, R. M. A new and rapid colorimetric determination of acetylcholinesterase activity. *Biochem. Pharmacol.* **1961**, *7*, 88−95.
(83) Walsh, D. M.; Klyubin, I.; Fadeeva, J. V.; Cullen, W. K.; Anwyl, R.; Wolfe, M. S.; Rowan, M. J.; Selkoe, D. J. Naturally secreted oligomers of amyloid beta protein potently inhibit hippocampal long-term potentiation in vivo. *Nature* **2002**, *416*, 535−539.
(84) Shankar, G. M.; Welzel, A. T.; McDonald, J. M.; Selkoe, D. J.; Walsh, D. M. Isolation of low-n amyloid β-protein oligomers from cultured cells, CSF, and brain. *Methods Mol. Biol.* **2011**, *670*, 33−44.
(85) Shi, Y.; Kirwan, P.; Livesey, F. J. Directed differentiation of human pluripotent stem cells to cerebral cortex neurons and neural networks. *Nat. Protoc.* **2012**, *7*, 1836−1846.
(86) VCCLAB. *Virtual Computational Chemistry Laboratory*; http://www.vcclab.org, accessed April 23, 2019.
(87) Kansy, M.; Senner, F.; Gubernator, K. Physicochemical high throughput screening: parallel artificial membrane permeation assay in the description of passive absorption processes. *J. Med. Chem.* **1998**, *41*, 1007−1010.

https://dx.doi.org/10.1021/acs.jmedchem.0c00841
J. Med. Chem. 2020, 63, 11663−11690